Analysis of the instantaneous Bethe-Salpeter equation and its application to $q\bar{q}$ bound states

Inaugural-Dissertation
zur Erlangung des Doktorgrades
der hohen Mathematisch-Naturwissenschaftlichen Fakultät
der Rheinischen Friedrich-Wilhelms-Universität zu Bonn

vorgelegt von
Jörg Resag
aus Gießen

1994

Abstract

The instantaneous Bethe-Salpeter equation (Salpeter equation) for bound quark-antiquark states is analysed and its relation to the RPA equations well-known from nuclear theory is established. A numerical method to solve the Salpeter equation is formulated and applied to a detailed study of light, heavy and heavy-light meson mass spectra as well as electroweak decay widths. We find that the results for the mass spectra are comparable to nonrelativistic results, whereas the relativistic treatment leads to a striking improvement for the decay observables.

Contents

Chapter 1

Introduction and overview

The quantitative description of hadronic states (mesons and baryons) is one of the challenging tasks in todays physics research. Allthough the underlying quantum field theory (i.e. quantum chromodynamics, QCD) is generally accepted to be well established, up to now it is not possible to calculate hadronic properties from this theory in an unambiguous and straightforward way, as in the case of QED. This is mainly due to the fact that the high value of the QCD coupling constant at low and intermediate energies prevents the use of perturbation theory. The use of nonperturbative methods (e.g. lattice calculations), however, is very involved and easily exceeds the available computer capacities.

An alternative approach to gain insight into the substructure of hadrons is provided by the use of quark models. These models emphasize certain features of the underlying field theory such as chiral symmetry, or they try to reproduce experimental data and observations (such as confinement) which usually can be motivated, but not strictly derived from QCD. To achieve a quantitative description it is neccessary to use different simplifications leading to the various quark models with their specific merits and limitations. Generally these simplifications are not easy to justify and limit the range where the models can be applied.

The most successfull model in describing the mass spectra of light and heavy mesons and baryons is the nonrelativistic constituent quark model (see e.g. refs.[8, 5, 10, 53]). This model assumes nonrelativistic dynamics for the quarks and describes confinement with a linearly rizing potential. Despite its ability to give a good description for the hadron masses, the model fails to describe certain decay observables such as weak decay constants and two-photon decay widths of light mesons (see chapter 4). As shown in refs.[5, 53] the incorporation of relativistic effects in the decay formulas already leads to some improvement for these decays. This fact indicates that a relativistic treatment of the quark dynamics is neccessary in order to obtain a better description of hadronic properties beyond the mere reproduction of the mass spectra.

Unfortunately many relativistic quark models loose the ability to give a reasonable overall fit for the meson and baryon mass spectra. E.g. the Nambu-Jona-

Lasinio model completely ignores confinement and thus is not able to describe excited states, whereas in the bag model (which is especially designed to keep the quarks confined) the problem of identifying spurious states spoils a reasonable fit of hadron masses. One of the aims of this thesis is to formulate a relativistic quark model that basically still has the advantages present in the nonrelativistic treatment.

One of the first steps into this direction was made by Isgur and co-workers [19]. In their work the nonrelativistic kinetic energy is 'relativized' by replacing $m+p^2/(2m) \;\rightarrow\; \omega = \sqrt{p^2+m^2}$ in the hamiltonian, and various relativistic effects in the decay widths are parametrized by nonlocalities of the form m/ω. Their results are quite satisfying and show the importance of a relativistic description especially for decay widths and form factors. However, this approach does not have a clear field theoretical background and still parametrizes relativistic effects within a nonrelativistic framework.

The basic equation to describe bound states in quantum field theory is the Bethe-Salpeter (BS) equation which was first formulated in 1951 by Bethe and Salpeter [58] and by Gell-Mann and Low [18]. In the following we will restrict the discussion to $q\bar{q}$ bound states. In momentum space the BS equation for these states reads

$$\begin{aligned} \chi_P(p) &= S_1^F(p_1) \int \frac{d^4p'}{(2\pi)^4} \left[-i\, K(P,p,p')\, \chi_P(p')\right] S_2^F(-p_2) \\ &=: S(p_1,p_2) \int \frac{d^4p'}{(2\pi)^4} \left[-i\, K(P,p,p')\, \chi_P(p')\right] \end{aligned} \tag{1.1}$$

where P is the 4-momentum of the bound state, p is the relative momentum of the $q\bar{q}$-pair and $p_1 = \eta_1 P + p,\;\; p_2 = \eta_2 P - p$ are the momenta of the quark and the antiquark with $\eta_1,\; \eta_2$ being two arbitrary real numbers satisfying $\eta_1 + \eta_2 = 1$. For a given quark propagator S^F and interaction kernel K the solution of this equation yields BS amplitudes χ_P and masses $P^2 = M^2$ for the bound states (note that for this purpose one also has to discuss the boundary conditions that have to be respected by χ_P). The BS equation differs from the nonrelativistic Schrödinger equation given in momentum space by

$$E\,\psi(\vec{p}) = \frac{\vec{p}^{\,2}}{2m}\,\psi(\vec{p}) + \int \frac{d^3p'}{(2\pi)^3}\, V(\vec{p}-\vec{p}\,')\,\psi(\vec{p}\,') \tag{1.2}$$

in two ways.

- The BS equation depends on the relative energy p^0 of the quarks. In coordinate space this corresponds to a dependence on two time variables $t_1,\; t_2$ for the quark and the antiquark which are neccessary to describe retardation effects of the interaction.

- Because of relativistic covariance the full Dirac structure is present in the BS equation. This implies the existence of positive and negative energy components for the quark and the antiquark in the BS amplitude.

The use of the exact BS equation given above is of rather limited practical value in QCD. Firstly the quark propagator S^F and the interaction kernel K are themselves unknown functions in QCD (given by an infinite number of Feynman diagrams). Secondly the dependence on p^0 leads to difficult principle and technical problems concerning the analytic pole structure in p^0 and the highly nontrivial numerical effort connected with these poles. Furthermore there is still the problem to formulate appropriate boundary conditions for χ_P.

There is basically one case known (the so-called Wick-model [70, 13]) where the BS equation can be reduced to a simple one-dimensional differential equation which can be solved numerically. The Wick-model describes the interaction of two massive scalar particles by the exchange of a scalar massless particle in the ladder approximation. Already in this simple model some difficulties arize, e.g. there exist solutions of the BS equation which in the nonrelativistic limit do not converge to the corresponding solutions of the Schrödinger equation.

For these reasons we will not treat the full BS equation as given above. Instead we will apply the following approximations to avoid the problems stated above, i.e.

- the full quark propagator will be replaced by the bare propagator with an effective constituent quark mass,

- retardation effects in the interaction will be neglected (instantaneous approximation), so that the interaction kernel becomes independent of p^0 in the CMS and can be written formally as a potential

$$K(P,p,p')\Big|_{P=(M,\vec{0})} = V(\vec{p},\vec{p}\,') \tag{1.3}$$

The first approximation is consistent with the picture of a hadron mainly built out of constituent quarks, analogously to the nonrelativistic ansatz. In a more involved approach one could determine the quark propagators by solving the Dyson-Schwinger equation with the same (instantaneous) interaction as in the BS equation. This approach would allow to incorporate the spontaneous breaking of chiral symmetry in the model, as shown in ref.[26].

The second approximation is motivated by the fact that very little is known about the dynamical origin of the confinement in QCD, so that introducing noninstantaneous confinement corrections into the formalism would be highly model dependent. Therefore if an ad-hoc modelling of retardation must be done, ignoring it altogether is probably the best choice at the moment [48]. It should be noted that naive noninstantaneous extensions fail as has been shown by S.N.Biswas et al. [6] for the harmonic oscillator BS-kernel $V(x) = -bx^2 = b\,(\vec{x}^{\,2} - (x^0)^2)$ that

yields only a continuous spectrum. Similar results are to be expected for other kernels like $1/q^4$. A more technical motivation for an instantaneous interaction is the fact that the BS equation simplifies considerably in this case since the p^0-dependence can be eliminated in the CMS, i.e.

$$\begin{aligned} \int dp^0\, \chi_P(p) &= \left(\int dp^0\, S(\eta_1 P + p,\, \eta_2 P - p)\right) \\ &\cdot \int \frac{d^3q}{(2\pi)^4} \left[-i\, V(\vec{p},\vec{q}) \left(\int dq^0\, \chi_P(q)\right)\right] \end{aligned} \tag{1.4}$$

with $P = (M, \vec{0})$. The integral $\int dp^0\, S(\eta_1 P + p,\, \eta_2 P - p)$ over the quark propagators can be computed analytically with the help of the residue theorem. Defining the Salpeter amplitude as $\Phi(\vec{p}) := \int dp^0\, \chi_{(M,\vec{0})}(p)$ one thus obtains the Salpeter equation [61]

$$\begin{aligned} \Phi(\vec{p}) &= \int \frac{d^3p'}{(2\pi)^3} \frac{\Lambda_1^-(\vec{p})\,\gamma^0\,[(V(\vec{p},\vec{p}\,')\,\Phi(\vec{p}\,')]\,\gamma^0\,\Lambda_2^+(-\vec{p})}{M+\omega_1+\omega_2} \\ &- \int \frac{d^3p'}{(2\pi)^3} \frac{\Lambda_1^+(\vec{p})\,\gamma^0\,[(V(\vec{p},\vec{p}\,')\,\Phi(\vec{p}\,')]\,\gamma^0\,\Lambda_2^-(-\vec{p})}{M-\omega_1-\omega_2} \end{aligned} \tag{1.5}$$

with $\omega_i = \sqrt{\vec{p}^{\,2} + m_i^2}$ and the projection operators $\Lambda_i^{\pm}(\vec{p}) = (\omega_i \pm H_i(\vec{p}))/(2\omega_i)$ on positive and negative energies. Here $H_i(\vec{p}) = \gamma^0(\vec{\gamma}\vec{p} + m_i)$ is the standard Dirac hamiltonian and m_i are the constituent quark masses.

The Salpeter equation is independent of p^0, but still has the full Dirac structure including positive and negative energies for the quark and the antiquark. It should be noted that the instantaneous ansatz for the interaction kernel can also be formulated covariantly, as shown in chapter 2.

In the language of time-ordered perturbation theory an instantaneous interaction implies that quark and antiquark both move forward or backward in time simultaneously, where the second possibility leads to the so-called Z-graphs [48], see fig.1.1. The single Z-graphs, where only one particle moves back in time, do not appear. Mathematically this leads to certain projection properties for the Salpeter amplitudes which reduce the number of independant functions neccessary to describe a meson state. On the other hand the lack of single Z-graphs prevents the Salpeter equation to approach the Dirac equation in the limit of one very heavy and one light quark. However, it is not clear if this fact is relevant for the case of $q\bar{q}$-states, since both equations neglect most of the influence of virtual particle-hole pairs, and it remains an open question which equation gives the better approximation.

Because of the presence of double Z-graphs one cannot interprete the eigenstates of the Salpeter equation as pure $q\bar{q}$-states. Instead the Salpeter equation still permits any number of $q\bar{q}$-pairs to be present simultaneously in these states (see ref.[15] where this is discussed in the context of the RPA equations). This is

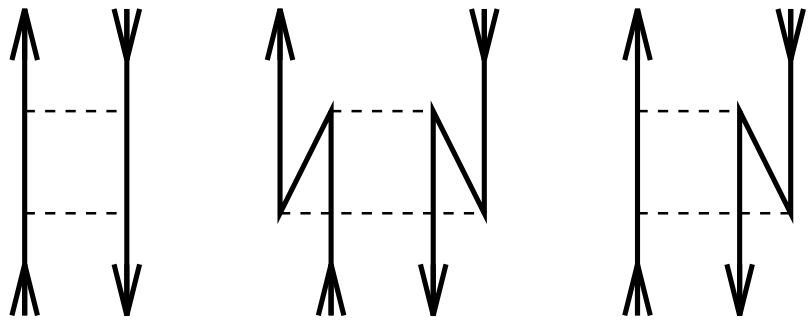

Figure 1.1: Time ordered diagrams with an instantaneous interaction represented by the dashed lines. The first and the second diagram (double Z-graph) are taken into account in the Salpeter equation, whereas the third diagram (single Z-graph) is neglected.

in contrast to the reduced Salpeter equation (see chapter 2) and the Schrödinger equation where these graphs are neglected.

The Salpeter equation represents a step in between the full BS equation and the nonrelativistic Schrödinger equation. There exist some other ansatzes in the literature to eliminate the p^0-dependence in the BS equation. The resulting p^0-independent equations are usually called quasipotential equations. Examples are the Blankenbecler-Sugar equation [7] which has been used as a basis for a quark model by P.C.Tiemeijer and J.A.Tjon [66], the null-plane ansatz investigated by A.N.Mitra et.al. [36] or the half-shell approach proposed by F.Gross [21]. The Salpeter equation has the advantage that the instantaneous approximation used there has an easy form and a clear physical interpretation, i.e. retardation effects are neglected in the interaction.

The thesis is organized in the following way:

In chapter 2 it is shown that the Salpeter equation can be reformulated into an eigenvalue equation for the mass M of the bound state, i.e.

$$\mathcal{H}\psi = M\,\psi \tag{1.6}$$

with $\psi = \Phi\,\gamma^0$ and an operator $\mathcal{H}$ which is given explicitely in eq.(2.19). The BS normalization condition for χ motivates the definition of a scalar product $\langle\psi,\psi\rangle$ (or more precisely a bilinear form, since $\langle\psi,\psi\rangle$ is not positive definit). It is shown that $\mathcal{H}$ is hermitian with respect to this scalar product, which implies that M is real if $\langle\psi,\psi\rangle \neq 0$, and that eigenfunctions for different eigenvalues are orthogonal. The detailed investigation of the structure of the Salpeter equation in chapter 2 shows that the solutions come in pairs ψ_1, M and ψ_2, $-M$, i.e. if ψ_1 is a solution with eigenvalue M, then there exists a solution ψ_2 with eigenvalue $-M$, where ψ_1 and ψ_2 can be related to each other by charge conjugation. Equivalently

exchanging the partial amplitudes for positive and negative energies turns ψ_1 into ψ_2 and M into $-M$. With the help of this structure one can expand ψ in a complete set of basis functions and rewrite the Salpeter equation into a matrix equation which for a finite basis can be solved numerically, where the variational principle is used to optimize the basis functions.

Since a relativistic treatment is especially important for the calculation of decay widths, it is briefly outlined in chapter 2 how some decay widths of special interest (i.e. weak decay constants, leptonic and two-photon decay widths) can be calculated within the present framework. The corresponding formulas are taken from the PhD thesis of Claus Münz [37], where the calculation of decay widths and form factors within the Salpeter approach is investigated in detail. The calculated decay observables given in the present work have been obtained using the formalism outlined there.

The structure for the Salpeter equation found in chapter 2 is well-known from the RPA (random phase approximation) equations in many body theory. In chapter 3 it is explicitely shown that the Salpeter equation and the RPA equations have the same form. This is not surprising since the RPA equations can be derived under the same assumptions that lead to the Salpeter equation, i.e. free propagators and an instantantaneous interaction, as shown in detail in chapter 3. The RPA equations show a typical doubling of the physical eigenvalues, so that only half of the RPA eigenvalues can be identified with the spectrum of the underlying hamiltonian. Analogously only the positive mass solutions of the Salpeter equation are of physical interest.

In chapter 4 an explicit quark model based on the Salpeter equation is presented and applied to calculate mass spectra and decay widths for light mesons. Analogously to the nonrelativistic case confinement is parametrized by a linearly rizing potential with scalar or alternatively vector Dirac spin structure. In order to describe the pseudoscalar mesons a residual interaction has to be added to the confining potential. The usual choice for this residual interaction is the one-gluon-exchange (OGE) as done e.g. by P.C.Tiemeijer and J.A.Tjon [66]. We do not apply the OGE to the light mesons in this work, since it leads to degenerate π and η meson masses in clear contradiction to experiment. Instead we will apply an instanton induced interaction ('t Hooft interaction) as computed by 't Hooft and others [24, 62, 49] which has the appropriate structure to describe the π and the η masses simultaneously. A nonrelativistic version of this interaction has already led to good results for the meson and baryon mass spectra [8, 53, 10]. We therefore feel encouraged to test this ansatz in the relativistic Salpeter framework.

It turns out that for a vector confinement the parameters can be chosen such that an excellent description of the light pseudoscalar and vector ground state mesons is achieved including weak decay constants, leptonic and two photon widths. The slope of the Regge trajectories comes out too small for this parameter set (model V1 in chapter 4), but can be readjusted by changing the parameters (model V2) with still moderate changes for the weak decay constants and the

two-photon widths. The leptonic widths, however, come out too large in this case. A comparision with nonrelativistic results shows the striking improvement for the weak decay constants and the two-photon widths due to the incorporation of the full relativistic Dirac structure and the negative energy components. The leptonic decay widths can already be described in the nonrelativistic approach.

A scalar confinement does not give satisfying results. Instead it turns out that for light mesons our numerical method does not lead to converging results with positive meson masses, if the number of basis states is increased. This is in agreement with recent results of J.Parramore and J.Piekarewic [48] who carried out a detailed stability analysis for the Salpeter equation with a scalar confinement. Their investigation reveals the existence of imaginary eigenvalues, which we expect to persist even for large values of the constituent quark mass. Nevertheless for large enough quark masses this instability is in fact spurious since in the nonrelativistic limit the Salpeter equation leads to the Schrödinger equation where such an instability does not exist. Consequently for higher quark masses this instability will be relevant only for a dramatically increasing number of basis states. Numerical solutions obtained with a smaller number of basis states aquire a quasistable character, i.e. are almost independent of the exact number of basis states taken into account.

In chapter 5 the heavy quarkonia ($c\bar{c}$ and $b\bar{b}$) are investigated, where confinement is parametrized in the same way as for the light mesons, and the OGE interaction replaces the 't Hooft interaction. The OGE is the natural candidate for heavy quarkonia, as is already motivated from the observed similarities of the charmonium and bottomonium mass spectra with the spectrum of positronium (for a more detailed discussion see the chapters 5 and 6). Reasonable fits to the experimental data can be obtained with a scalar as well as with a vector confinement, which is in contrast to the nonrelativistic quark model where a scalar confinement is prefered. Some moderate deviations in the mass spectra and especially in the leptonic decay widths, however, indicate the relevance of retardation effects and higher order gluon diagrams in the interaction. It should be noted that the instability of the Salpeter equation with a scalar confinement as discussed above is completely invisible here for any reasonable number of basis states. We therefore think that it is legitimate to compare these (quasistable) solutions to the experimental meson masses.

Finally the heavy-light (D and B -) mesons are investigated in chapter 6. To achieve this aim a simultaneous fit of light and heavy mesons is obtained, where the interaction kernel consists of a scalar plus vector confinement and a residual interaction, i.e. the 't Hooft interaction for light mesons and the OGE for heavy and heavy-light mesons. The combination of a scalar plus vector spin structure for the confinement is enforced by the fact that a pure vector confinement does not give appropriate spin-orbit splittings in the mass spectra (especially for the D-mesons), whereas a pure scalar confinement leads to the discussed instability of the solutions, especially for the light mesons. The obtained mass spectra have

a quality similar to results found within the nonrelativistic quark model, whereas the results for the weak decay constants and the two-photon widths are much better than the corresponding nonrelativistic results.

Chapter 2

Analysis of the instantaneous Bethe-Salpeter equation

We investigate the structure of the instantaneous Bethe-Salpeter equation for $q\bar{q}$-bound states in the general case of unequal quark masses and develop a numerical scheme for the calculation of mass spectra and Bethe-Salpeter amplitudes. In order to appreciate the merits of the various competing models beyond the reproduction of the mass spectra, explicit formulas are given to calculate electroweak decays [37]. This chapter is a slightly extended version of ref.[54]. The results for an explicit quark model will be compared to experimental data in chapters 4, 5 and 6.

2.1 Introduction

Despite many efforts the bound state problem of QCD is still far from being well understood. One of the main tasks is to investigate the relevance of quarks as dynamical degrees of freedom in hadronic bound states. Since a relativistic treatment for the quarks in deeply bound states is essential, the Bethe-Salpeter(BS)-equation [58, 18] provides a suitable starting point. Unlike in QED one cannot use perturbation theory to obtain usefull approximations for the interaction kernel in QCD. Therefore our knowledge of the interaction between quarks is still quite fragmentary and various phenomenological alternatives have to be tested. In the present work we will discuss to $q\bar{q}$-states. The use of general $q\bar{q}$-interaction kernels depending on the relative time variable leads to serious conceptional and practical problems [42, 43]. Furthermore a parametrization of confinement including retardation effects is still lacking. Therefore it is very usefull at this point to make the simplifying assumption that the BS-kernel can be approximated by an effective interaction that is instantaneous in the rest frame of the bound state. The BS-equation then reduces to the (full) Salpeter equation [61] that has been investigated for $q\bar{q}$-states e.g. by Llewellyn Smith [31], Le Yaouanc

and coworkers [71] and recently by Lagaë [29]. However, a detailed analysis of the mathematical structure of this equation and its application to a comprehensive study of mesonic states appears to be missing in the literature up to now.

The Salpeter equation represents a step in between the full four-dimensional BS-equation and the Schrödinger equation used in the nonrelativistic quark model (see Fig.2.1). As will be shown in chapter 3 it corresponds to the random phase approximation (RPA) equations known in many body physics. For low binding energies compared to the quark masses a further approximation would lead from the Salpeter equation to the reduced Salpeter equation (compare Sec.2.3.1) which corresponds to the Tamm-Dancoff approximation (TDA). Applying the nonrelativistic limit $p/m \ll 1$ to the reduced Salpeter equation finally gives the Schrödinger equation. It is known [15] that the RPA still permits any number of particle-hole pairs to be present simultaneously in the ground state and the excited states, whereas the TDA has only one particle-hole pair present at any instant of time. In that sense the Salpeter equation goes beyond the description of a meson as a pure quark-antiquark state.

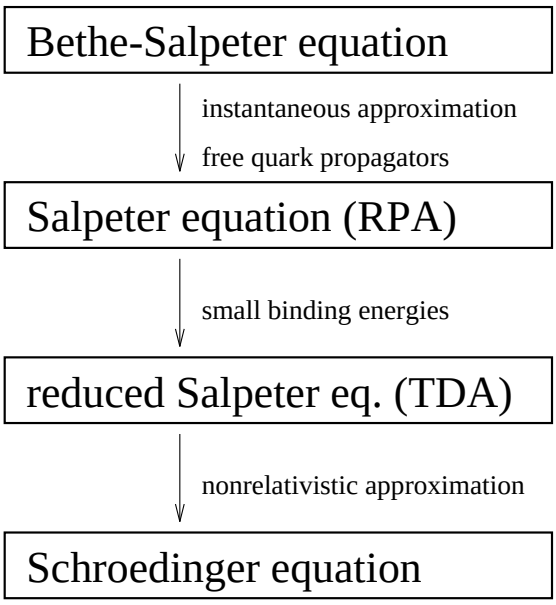

Figure 2.1: The various approximations leading from the Bethe-Salpeter equation to the Schrödinger equation

In this chapter we analyze the properties of the Salpeter equation for the general case of unequal quark masses in Sec.2.3. In Sec.2.4 we present a flexible numerical treatment of this equation based on the variational principle of ref.[29]. We use the block structure of the Salpeter amplitude to derive an expansion in terms of a complete set of basis functions which leads to a matrix equation

analogous to the RPA equation. Our numerical method can be applied to a wide class of phenomenological interaction kernels. In Sec.2.5 we show how to reconstruct the full BS-amplitudes from the Salpeter amplitudes and present formulas for the calculation of some decay observables within the Mandelstam formalism including the decay $\pi^0 \to 2\gamma$ (see ref.[37]). Concluding remarks are given in Sec.2.6.

2.2 The Bethe-Salpeter equation

The BS-amplitude χ for a fermion-antifermion bound state $|P\rangle$ is defined by

$$[\chi_P(x_1,x_2)]_{\alpha\beta} = \left\langle 0 \left| T\,\Psi_\alpha(x_1)\,\bar\Psi_\beta(x_2) \right| P \right\rangle \tag{2.1}$$

where P is the four-momentum of the bound state, T denotes the time ordering for the fermion operators Ψ, $\bar\Psi$, and α, β stand for spinor, flavor and color indices. The BS-equation for $\chi_P(x_1,x_2)$ reads

$$\begin{aligned}\chi_P(x_1,x_2) = &\int d^4x_5\, d^4x_6\, d^4x_7\, d^4x_8 \\ &S_1^F(x_1-x_5)\,[-i\,K(x_5,x_6,x_7,x_8)\,\chi_P(x_7,x_8)]\,S_2^F(x_6-x_2)\end{aligned} \tag{2.2}$$

also shown in graphical form in Fig.2.2. The interaction kernel K is given by the sum of all $q\bar q$-irreducible Feynman diagrams and acts on χ as

$$[K(x_5,x_6,x_7,x_8)\,\chi_P(x_7,x_8)]_{\alpha\beta} = \sum_{\alpha'\,\beta'} K(x_5,x_6,x_7,x_8)_{\alpha\alpha',\beta\beta'}\chi_P(x_7,x_8)_{\alpha'\,\beta'} \tag{2.3}$$

The BS-equation has first been derived by Bethe and Salpeter in 1951 [58], where the propagator formalism of Feynman has been used. A more rigorous derivation based on the operator formalism of quantum field theory has been given by Gell-Mann and Low [18] in the same year (see also the text book of Lurie [33]).

For our purpose it is usefull to transform the BS-equation into momentum space. Due to translational invariance the Fourier transformation of χ and K can be written as

$$\begin{aligned}\chi_P(x_1,x_2) &= e^{-iPX}\int\frac{d^4p}{(2\pi)^4}\,e^{-ipx}\,\chi_P(p) \\ K(x_1,x_2,x_1',x_2') &= \int\frac{d^4P}{(2\pi)^4}\int\frac{d^4p}{(2\pi)^4}\int\frac{d^4p'}{(2\pi)^4} \\ &\qquad e^{-iP(X-X')}\,e^{-ipx}\,e^{ip'x'}\,K(P,p,p')\end{aligned} \tag{2.4}$$

where $x_1 = X+\eta_2 x,\ x_2 = X-\eta_1 x$ with the conjugate momenta $p_1 = \eta_1 P+p,\ p_2 = \eta_2 P - p$. Here η_1, η_2 are two arbitrary real numbers satisfying $\eta_1+\eta_2 = 1$. The BS-equation for $\chi_P(p)$ then reads

$$\chi_P(p) = S_1^F(p_1)\int\frac{d^4p'}{(2\pi)^4}\,[-i\,K(P,p,p')\,\chi_P(p')]\,S_2^F(-p_2) \tag{2.5}$$

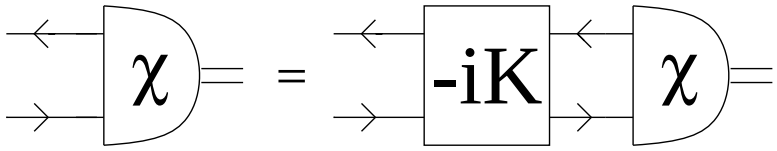

Figure 2.2: Graphical representation of the BS equation

Mathematically this equation is a homogeneous integral equation for the 4×4 matrix function $\chi_P(p)$ in the four variables $p = (p^0, \vec{p})$. Furthermore the equation depends on four parameters $P = (P^0, \vec{P})$. In order to obtain a discrete mass spectrum $P^2 = M^2$ for the bound states one has to formulate boundary conditions for χ_P such as the normalization condition given in sec.2.3.2.

If K is approximated by its lowest order contribution (ladder approximation) the kernel is of the form

$$\begin{aligned} K(x_1, x_2, x_3, x_4) &= K_L(x_3 - x_4)\, \delta(x_1 - x_3)\, \delta(x_2 - x_4) \\ \Longleftrightarrow \quad K(P, p, p') &= K_L(p - p') \end{aligned} \tag{2.6}$$

with $K_L(x_3 - x_4) = \int d^4q/(2\pi)^4\, e^{-iq(x_3 - x_4)}\, K_L(q)$. In the present work the ladder approximation (together with the subsequent instantaneous approximation) will be used to incorporate the residual $q\bar{q}$-interactions, i.e. the one-gluon exchange (OGE) for heavy quarkonia and D-mesons, and the 't Hooft interaction for the light mesons.

2.3 General properties of the Salpeter equation

2.3.1 Formulating the Salpeter equation

For an interaction that is instantaneous in the rest frame of the bound state with momentum $P = (M, \vec{0})$ the BS-kernel can be written in momentum space as

$$K(P, p, p')\,\Big|_{P=(M,\vec{0})} = V(\vec{p}, \vec{p}\,') \tag{2.7}$$

which can also be formulated in a covariant way [68] as

$$K(P, p, p') = V(p_\perp,\, p'_\perp) \tag{2.8}$$

where $p_\perp = p - (Pp/P^2)\, P$ is perpendicular to P. In practical calculations one has to justify this ansatz a posteriori by investigating its consequences in the framework of explicit models.

Furthermore we will approximate the full quark propagators by free propagators, i.e. $S_i^F(p_i) \approx i\,(\gamma p_i - m_i + i\epsilon)^{-1}$ where m_1 and m_2 are interpreted as effective masses for the quark and the antiquark. This approximation has been criticized [9] because free propagators might be incompatible with a confining kernel. On the other hand one can argue that this choice naturally leads to non-relativistic potential models that have been applied successfully to heavy quarkonia (a recent model calculation is presented in [5], for an extensive review see [32]). We thus feel that free propagators should be a reasonable effective parameterization at least for heavy quarks. It is still an open question whether free propagators can also be applied to light quarks, and one has to investigate this problem within explicit models.

With an instantaneous BS-kernel and free propagators with effective quark masses one can perform the p^0 integrals in the BS-equation in the rest frame of the bound state with mass M (see appendix A) and thus arrives at the (full) Salpeter equation

$$\begin{aligned}\Phi(\vec{p}) &= \int\frac{d^3p'}{(2\pi)^3}\,\frac{\Lambda_1^-(\vec{p})\,\gamma^0\,[(V(\vec{p},\vec{p}\,')\,\Phi(\vec{p}\,')]\,\gamma^0\,\Lambda_2^+(-\vec{p})}{M+\omega_1+\omega_2}\\ &- \int\frac{d^3p'}{(2\pi)^3}\,\frac{\Lambda_1^+(\vec{p})\,\gamma^0\,[(V(\vec{p},\vec{p}\,')\,\Phi(\vec{p}\,')]\,\gamma^0\,\Lambda_2^-(-\vec{p})}{M-\omega_1-\omega_2}\end{aligned} \tag{2.9}$$

with $\omega_i = \sqrt{\vec{p}^{\,2}+m_i^2}$ and the projection operators $\Lambda_i^{\pm}(\vec{p}) = (\omega_i \pm H_i(\vec{p}))/(2\omega_i)$ on positive and negative energies. Here $H_i(\vec{p}) = \gamma^0(\vec{\gamma}\vec{p}+m_i)$ is the standard Dirac hamiltonian. We also have introduced the Salpeter amplitude Φ by

$$\begin{aligned}\Phi(\vec{p}) &= \int dp^0\,\chi_P(p^0,\vec{p})\,\Big|_{P=(M,\vec{0})}\\ &= \int d^3x\,e^{-i\vec{p}\vec{x}}\,\langle 0|\Psi(0,\eta_2\vec{x})\,\bar{\Psi}(0,-\eta_1\vec{x})|P\rangle\,\Big|_{P=(M,\vec{0})}\end{aligned} \tag{2.10}$$

For weakly bound states with $|\vec{p}|/m_i \ll 1$ and $M \approx m_1+m_2$ one has

$$\frac{1}{M+\omega_1+\omega_2} \ll \frac{1}{M-\omega_1-\omega_2} \tag{2.11}$$

so that the first term in eq.(2.9) can be dropped. This leads to the so called reduced Salpeter equation, which has been used in various studies of relativistic bound states (see e.g. the work of Gara et al. [17] and references therein). In the case of light quarks, however, the use of the reduced Salpeter equation is dubious, especially for deeply bound states like the pion. Quark models for light quarks should therefore be based on the full Salpeter equation eq.(2.9).

Let α, β in eq.(2.1) refer to Dirac indices in the standard Dirac representation of ref.[25]. Then Φ is a 4×4-matrix in spinor space that can be written in block matrix form as

$$\Phi = \begin{pmatrix}\Phi^{+-} & \Phi^{++}\\ \Phi^{--} & \Phi^{-+}\end{pmatrix} \tag{2.12}$$

where each component is a 2×2-matrix. Applying $\Lambda_1^{\pm}(\vec{p})$ from the left hand side and $\Lambda_2^{\pm}(-\vec{p})$ from the right hand side to the Salpeter equation leads to

$$\begin{aligned} \Lambda_1^+(\vec{p})\,\Phi(\vec{p})\,\Lambda_2^+(-\vec{p}) &= 0 \\ \Lambda_1^-(\vec{p})\,\Phi(\vec{p})\,\Lambda_2^-(-\vec{p}) &= 0 \end{aligned} \tag{2.13}$$

These relations allow us to express Φ^{+-}, Φ^{-+} in terms of Φ^{++}, Φ^{--} as

$$\begin{aligned} \Phi^{+-} &= +c_1\Phi^{++}s - c_2 s\Phi^{--} \\ \Phi^{-+} &= -c_1\Phi^{--}s + c_2 s\Phi^{++} \end{aligned} \tag{2.14}$$

with the shorthand notation $s = \vec{\sigma}\vec{p}$, $c_i = \omega_i/(\omega_1 m_2 + \omega_2 m_1)$. We thus find that Φ can be written as

$$\Phi = \hat{\Phi}\,(\Phi^{++}, \Phi^{--}) \tag{2.15}$$

with $\hat{\Phi}$ being a bilinear function. One can interpret Φ^{++} as the upper component and Φ^{--} as the lower component of Φ, as can be seen in the nonrelativistic limit where Φ^{--} vanishes for solutions that fulfill $M \approx m_1 + m_2$ and where $\Phi^{++}\,i\sigma_2$ becomes the usual Schrödinger wave function.

For further discussion it is usefull to rewrite the Salpeter equation in the form of an eigenvalue problem for the bound state mass M. We follow the treatment of Lagaë [29] and define

$$\psi(\vec{p}) := \Phi(\vec{p})\,\gamma^0 \tag{2.16}$$

$$[W(\vec{p},\vec{p}\,')\,\psi(\vec{p}\,')] := \gamma^0\,[V(\vec{p},\vec{p}\,')\,\Phi(\vec{p}\,')] \tag{2.17}$$

The Salpeter equation can now be written as

$$(\mathcal{H}\psi)(\vec{p}) = M\,\psi(\vec{p}) \tag{2.18}$$

where

$$\begin{aligned} (\mathcal{H}\psi)(\vec{p}) &= H_1(\vec{p})\psi(\vec{p}) - \psi(\vec{p})H_2(\vec{p}) \\ &- \int \frac{d^3p'}{(2\pi)^3}\,\Lambda_1^+(\vec{p})\,[W(\vec{p},\vec{p}\,')\,\psi(\vec{p}\,')]\,\Lambda_2^-(\vec{p}) \\ &+ \int \frac{d^3p'}{(2\pi)^3}\,\Lambda_1^-(\vec{p})\,[W(\vec{p},\vec{p}\,')\,\psi(\vec{p}\,')]\,\Lambda_2^+(\vec{p}) \end{aligned} \tag{2.19}$$

The equivalence of eq.(2.18) and eq.(2.9) can be shown by applying the projectors $\Lambda_i^{\pm}$ to both equations from both sides. From eq.(2.18) one obtains e.g.

$$\begin{aligned} \Lambda_1^+(\vec{p})\,\psi(\vec{p})\,\Lambda_2^+(\vec{p}) &= 0 \\ \Lambda_1^-(\vec{p})\,\psi(\vec{p})\,\Lambda_2^-(\vec{p}) &= 0 \end{aligned} \tag{2.20}$$

as in eq.(2.13) due to the relation $\Lambda_i^{\pm}(\vec{p})\,\gamma^0 = \gamma^0\,\Lambda_i^{\pm}(-\vec{p})$. Note that eq.(2.20) can also be written in the concise form

$$\frac{H_1}{\omega_1}\psi + \psi\frac{H_2}{\omega_2} = 0 \tag{2.21}$$

2.3.2 Normalization condition and scalar product

The normalization for general BS-amplitudes has been given for bound states with conserved quantum numbers by Nishijima [46] and Mandelstam [35]. We follow Cutkosky [14], who treated the more general case where no current has to be conserved. As this has already been treated within textbooks (e.g. [33]), we will only give the result for the normalization. A more detailed discussion is given in ref.[37].

Let the bound state be normalized as $\langle P\,|P'\rangle = (2\pi)^3\,2P^0\,\delta^3(\vec{P}-\vec{P}')$. Then the normalization condition in graphical representation is given by Fig.2.3 (compare e.g. [30]). Contracting with the momentum of the bound state, this reads explicitly:

$$\int \frac{d^4p}{(2\pi)^4}\frac{d^4p'}{(2\pi)^4}\,tr\left[\bar{\chi}_P(p)P^\mu\frac{d}{dP^\mu}\Big(I(P,p,p')+\,i\,K(P,p,p')\Big)\chi_P(p')\right] = 2iM^2 \tag{2.22}$$

The summation over color indices is suppressed here. I denotes the product of the inverse quark-propagators:

$$I(P,p,p')_{\alpha\alpha',\beta\beta'} = \delta^{(4)}(p-p')\,(2\pi)^4 S_{1\;\alpha\alpha'}^{F\,-1}(\eta_1 P+p)\,S_{2\;\beta'\beta}^{F\,-1}(-\eta_2 P+p) \tag{2.23}$$

Note that the vectorial condition of Fig.(2.3) and the scalar normalization (2.22) are in fact equivalent which follows from: (a) the formal covariance of the equation and (b) the fact that in the rest frame the time component of Fig.(2.3) gives

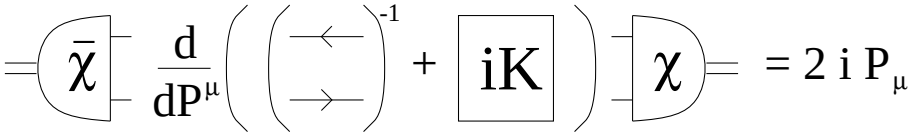

Figure 2.3: The normalization condition

eq.(2.22) and the space components vanish, as the derivative $d/(dP^i)[I+K]$ is proportional to p^i, p'^i or γ^i so that the integrals or the trace on the rhs. of eq.(2.22) give zero. For an interaction-kernel, which is instantaneous in the rest frame, i.e. of the type of eq.(2.8), we have:

$$P^\mu\frac{d}{dP^\mu}V\,(p_\perp,p'_\perp) = 0 \tag{2.24}$$

so that the contributions of the interaction kernel to the normalization vanish. At this point we would like to mention that the BS-equation and the normalization condition for an instantaneous interaction may be formulated covariantly, so that the corresponding amplitudes χ are correctly normalized in any frame. The

explicit normalization for the corresponding Salpeter amplitudes Φ [35, 61] will be performed in the rest frame. First we define the vertex functions:

$$\begin{aligned} \Gamma_P(p) &:= [S_1^F(p_1)]^{-1}\,\chi_P(p)\,[S_2^F(-p_2)]^{-1} \\ \bar{\Gamma}_P(p) &:= [S_2^F(-p_2)]^{-1}\,\bar{\chi}_P(p)\,[S_1^F(p_1)]^{-1} \end{aligned} \tag{2.25}$$

With the BS equation (2.5) we then obtain the following important result:

$$\Gamma_P(p)\Big|_{P=(M,\vec{0})} = \Gamma(\vec{p}\,) = -i\int\frac{d^3p}{(2\pi)^4}\,[V(\vec{p},\vec{p}\,')\Phi(\vec{p}\,')] \tag{2.26}$$

i.e. the vertex-function depends only on the relative three-momentum $\vec{p}$. This formula allows the reconstruction of the vertex function Γ and therefore of the full BS-amplitude χ from the Salpeter amplitude Φ. Inserting eq.(2.25) into the normalization condition (2.22) the dependence on p^0 is completely determined by the quark-propagators, so that the p^0-integration may be performed analytically.

We use the general relation between the BS-amplitude χ and it's adjoint $\bar{\chi}$ for spin-1/2-fermions (see e.g. [25] for the scalar case):

$$\begin{aligned} \chi(p) &= -\frac{1}{2\pi i}\int dq^0\left(\frac{f(q^0,\vec{p}\,)}{p^0-q^0+i\epsilon}+\frac{g(q^0,\vec{p}\,)}{p^0-q^0-i\epsilon}\right) \\ \bar{\chi}(p) &= -\frac{1}{2\pi i}\gamma^0\int dq^0\left(\frac{f^\dagger(q^0,\vec{p}\,)}{p^0-q^0+i\epsilon}+\frac{g^\dagger(q^0,\vec{p}\,)}{p^0-q^0-i\epsilon}\right)\gamma^0 \end{aligned} \tag{2.27}$$

with matrix valued functions f and g. From this we derive the following relations in the special case of an instantaneous interaction:

$$\bar{\Gamma}(\vec{p}\,) = -\gamma_0\,\Gamma^\dagger(\vec{p}\,)\,\gamma_0 \qquad \bar{\Phi}(\vec{p}\,) = \gamma_0\,\Phi^\dagger(\vec{p}\,)\,\gamma_0 \tag{2.28}$$

This leads to the normalization condition for the Salpeter-amplitudes in the rest frame:

$$\int\frac{d^3p}{(2\pi)^3}\,tr\left\{\Phi^\dagger(\vec{p}\,)\Lambda_1^+(\vec{p}\,)\Phi(\vec{p}\,)\Lambda_2^-(-\vec{p}\,)-\Phi^\dagger(\vec{p}\,)\Lambda_1^-(\vec{p}\,)\Phi(\vec{p}\,)\Lambda_2^+(-\vec{p}\,)\right\} = (2\pi)^2\,2M \tag{2.29}$$

It also may be expressed in terms of the 2×2 amplitudes Φ^{++} and Φ^{--} defined in eq.(2.12) as:

$$\int\frac{d^3p}{(2\pi)^3}\frac{2\omega_1\omega_2}{\omega_1 m_2+\omega_2 m_1}\,tr\left\{\,(\Phi^{++}(\vec{p}\,))^\dagger\,\Phi^{++}(\vec{p}\,)-(\Phi^{--}(\vec{p}\,))^\dagger\,\Phi^{--}(\vec{p}\,)\,\right\} = (2\pi)^2\,2M \tag{2.30}$$

This form also shows the connection to the nonrelativistic norm: in the NR limit $\Phi^{++}(\vec{p}\,)\,i\sigma_2$ becomes the usual Schrödinger wave function and $\Phi^{--}(\vec{p}\,)$ goes to zero as $\vec{p}^{\,2}/m^2\cdot\Phi^{++}(\vec{p}\,)$. Furthermore the weight function becomes equal to unity so that we obtain the usual Schrödinger normalization. For deeply bound states

however we have appreciable deviations from this norm, as the lower amplitude Φ^{--} is of the same order as the upper component Φ^{++} (see Sec.2.3.3).

Eq.(2.29) motivates the definition of a scalar product for amplitudes $\psi_1 = \Phi_1\gamma^0$ and $\psi_2 = \Phi_2\gamma^0$ as

$$\begin{aligned} \langle\psi_1\,|\psi_2\rangle &= \int \mathrm{tr}\,\left(\psi_1^\dagger\,\Lambda_1^+\,\psi_2\,\Lambda_2^- - \psi_1^\dagger\,\Lambda_1^-\,\psi_2\,\Lambda_2^+\right) \\ &= \frac{1}{2}\int \mathrm{tr}\,\left[\psi_1^\dagger\,\left(\frac{H_1}{\omega_1}\,\psi_2 - \psi_2\,\frac{H_2}{\omega_2}\right)\right] \end{aligned} \tag{2.31}$$

with all quantities depending on $\vec{p}$ and the notation $\int = \int d^3p/(2\pi)^3$. Note that this scalar product is not positive definite. The normalization condition (2.29) for solutions of the Salpeter equation is then given as

$$\langle\psi\,|\psi\rangle = (2\pi)^2\,2M \tag{2.32}$$

The following discussion will be restricted to amplitudes satisfying eq.(2.21). In that case one has

$$\langle\psi_1\,|\,\mathcal{H}\,\psi_2\rangle = \int(\omega_1+\omega_2)\,\mathrm{tr}\,\left(\psi_1^\dagger\,\psi_2\right) - \int\int'\,\mathrm{tr}\,\left(\psi_1^\dagger\,W\psi_2'\right) \tag{2.33}$$

where the prime indicates the dependence of ψ_2 on $\vec{p}\,'$. If one considers kernels that fulfill $\int\int'\mathrm{tr}\,(\psi_1^\dagger\,W\psi_2') = \int\int'\mathrm{tr}\,(\psi_2^\dagger\,W\psi_1')^*$, which is valid for a wide class of interactions (e.g. for $W\psi' = f\,((\vec{p}-\vec{p}\,')^2)\;\Gamma_1\,\psi(\vec{p}\,')\,\Gamma_2$ with hermitian matrices Γ_i and a scalar function f), the Salpeter hamiltonian $\mathcal{H}$ is selfadjoint with respect to the scalar product given in eq.(2.31), i.e.

$$\langle\psi_1\,|\,\mathcal{H}\,\psi_2\rangle = \langle\,\mathcal{H}\,\psi_1\,|\,\psi_2\rangle \tag{2.34}$$

This has two important consequences, namely

- bound state masses M are real for eigenfunctions ψ with nonzero norm $\langle\psi\,|\psi\rangle \neq 0$
- amplitudes ψ_1 and ψ_2 corresponding to different eigenvalues $M_1 \neq M_2^*$ are orthogonal, i.e. $\langle\psi_1\,|\,\psi_2\rangle = 0$

The first point can be seen easily from $M\,\langle\psi\,|\psi\rangle = \langle\psi\,|\mathcal{H}\,\psi\rangle = \langle\mathcal{H}\,\psi\,|\psi\rangle = M^*\,\langle\psi\,|\psi\rangle$ and the second follows from $M_2\,\langle\psi_1\,|\,\psi_2\rangle = \langle\psi_1\,|\mathcal{H}\,\psi_2\rangle = \langle\mathcal{H}\,\psi_1\,|\,\psi_2\rangle = M_1^*\,\langle\psi_1\,|\,\psi_2\rangle$.

2.3.3 Structure of the Solutions

The Salpeter equation exhibits some further general structures connecting solutions with positive and negative eigenvalues. For the case of equal quark masses

J.F. Lagaë [29] has shown that for kernels satisfying $(W\psi)^\dagger = W\psi^\dagger$ the eigenvalues will come in pairs of opposite sign, the corresponding eigenfunctions having normalizations with opposite sign. In the following we will extend this result to the general case of unequal quark masses and compare the block structure of the conjugate solutions. We further show that nondegenerate bound states with mass $M = 0$ have zero norm $\langle\psi \mid \psi\rangle = 0$. The discussion of physical acceptable solutions is postponed to the end of this section.

To deal with the unequal mass case we first investigate the structure of the BS-equation under charge conjugation. The details are shown in the appendix with the result that solutions of

$$\begin{aligned}(\mathcal{H}_{f_1f_2}\psi_{f_1f_2})(\vec{p}) &= M\,\psi_{f_1f_2}(\vec{p})\\ (\mathcal{H}_{f_2f_1}\psi_{f_2f_1})(\vec{p}) &= M\,\psi_{f_2f_1}(\vec{p})\end{aligned} \tag{2.35}$$

are related through

$$\psi_{f_1f_2}(\vec{p}) = -S_C\ {}^t\psi_{f_2f_1}(-\vec{p})\,S_C \tag{2.36}$$

with S_C given in eq.(B.25) in the appendix. The indices of $\mathcal{H}$ denote the flavor dependence of H_i and $\Lambda_i^\pm$ in eq.(2.19). For simplicity only the case without flavor mixing is considered, the generalization being straightforward.

In the following discussion we will assume that the BS-kernel satisfies the relation $(W_{f_1f_2}\psi'_{f_1f_2})^\dagger = W_{f_2f_1}(\psi'_{f_1f_2})^\dagger$, which is fulfilled e.g. for kernels of the form

$$W_{f_1f_2}\psi'_{f_1f_2} = f\left((\vec{p}-\vec{p}\,')^2\right)\,\Gamma\,\psi_{f_1f_2}(\vec{p}\,')\,\Gamma \tag{2.37}$$

with a hermitian matrix Γ. The hermitian conjugate of eq.(2.18) thus leads to

$$-\,(\mathcal{H}_{f_1f_2}\psi_{f_1f_2})^\dagger = \mathcal{H}_{f_2f_1}\psi^\dagger_{f_1f_2} = -M^*\,\psi^\dagger_{f_1f_2} \tag{2.38}$$

Renaming $f_1 \leftrightarrow f_2$ and comparing this equation to eq.(2.35) we thus have shown that

- solutions of the Salpeter equation come in pairs $(\psi_{f_1f_2},\ M)$ and $(\psi^\dagger_{f_2f_1},\ -M^*)$ where eq.(2.36) connects the two solutions.

Consider the normalization of $\psi_{f_1f_2}$ and $\psi^\dagger_{f_2f_1}$: With eq.(2.36) and the relation $S_C\,\Lambda_i^\pm(\vec{p})\,S_C = {}^t\Lambda_i^\mp(-\vec{p})$ one finds $\langle\psi_{f_2f_1}\mid\psi_{f_2f_1}\rangle_{f_2f_1} = \langle\psi_{f_1f_2}\mid\psi_{f_1f_2}\rangle_{f_1f_2}$ where the indices of the scalar product determine the flavors of $\Lambda_1^\pm$ and $\Lambda_2^\pm$ in eq.(2.31). On the other hand cyclic permutation under the trace shows that $\langle\psi^A_{f_2f_1}|\,\psi^B_{f_2f_1}\rangle_{f_2f_1} = -\langle(\psi^B_{f_2f_1})^\dagger|\,(\psi^A_{f_2f_1})^\dagger\rangle_{f_1f_2}$ so that we have

$$\langle\psi_{f_1f_2}|\,\psi_{f_1f_2}\rangle_{f_1f_2} = -\langle\psi^\dagger_{f_2f_1}|\,\psi^\dagger_{f_2f_1}\rangle_{f_1f_2} \tag{2.39}$$

and we find that

- the states with eigenvalues M and $-M^*$ have opposite norm.

Let us now compare the block matrix structure of the two conjugated solutions. With the angular momentum decomposition eq.(B.15) (see appendix)

$$\begin{aligned}\Phi^{++}(\vec{p}) &= \sum_{L\,S} \mathcal{R}^{(+)}_{LS}(p)\ [Y_L(\Omega_p)\otimes\varphi_S]^J \\ \Phi^{--}(\vec{p}) &= \sum_{L\,S} \mathcal{R}^{(-)}_{LS}(p)\ [Y_L(\Omega_p)\otimes\varphi_S]^J \end{aligned} \tag{2.40}$$

with the 2×2-matrices $\varphi_{0\,0} = 1/\sqrt{2}$, $\varphi_{1\,q} = \sigma_q/\sqrt{2}$ it is straightforward to show that

$$\left[\left(\Phi^{++}_{f_2f_1}\right)^{JM_J}\right]^\dagger = (-1)^{-J-M_J}\sum_{LS}(-1)^{L+S}\ \left[\mathcal{R}^{(+)}_{LS}(p)\right]_{f_2f_1}\ [Y_L(\Omega_p)\otimes\varphi_S]^J_{-M_J} \tag{2.41}$$

and similarly for Φ^{--}. It is shown in appendix B.4 that

$$[\mathcal{R}^{(+)}_{LS}(p)]_{f_2f_1} = (-1)^{L+S}\,[\mathcal{R}^{(+)}_{LS}(p)]_{f_1f_2} \tag{2.42}$$

Since L and S are integer the phase vanishes and we obtain the result

$$\left[\left(\Phi^{++}_{f_2f_1}\right)^{JM_J}\right]^\dagger = (-1)^{-J-M_J}\left(\Phi^{++}_{f_1f_2}\right)^{J\,-M_J} \tag{2.43}$$

According to eqs.(2.15),(2.16) we write

$$\psi^\dagger_{f_2f_1} = \gamma^0\ \left[\hat{\Phi}_{f_2f_1}(\,\phi^{++}_{f_2f_1},\,\phi^{--}_{f_2f_1})\right]^\dagger \tag{2.44}$$

where the indices of $\hat{\Phi}$ indicate the flavor dependence of c_i in eq.(2.14). The hermitian conjugate of eq.(2.20) with f_1 and f_2 interchanged gives $\Lambda^+_{f_1}\,\psi^\dagger_{f_2f_1}\,\Lambda^+_{f_2} = 0$ and $\Lambda^-_{f_1}\,\psi^\dagger_{f_2f_1}\,\Lambda^-_{f_2} = 0$ so that we can write

$$\psi^\dagger_{f_2f_1} = \hat{\Phi}_{f_1f_2}\left(\xi^{++}_{f_1f_2},\,\xi^{--}_{f_1f_2}\right)\,\gamma^0 \tag{2.45}$$

with some amplitudes ξ^{++}, ξ^{--} that can be determined by comparing eq.(2.45) to eq.(2.44) with the result $(\xi^{++}_{f_1f_2})^{JM_J} = -[(\Phi^{--}_{f_2f_1})^{JM_J}]^\dagger = (-1)^{1-J-M_J}\,(\Phi^{--}_{f_1f_2})^{J\,-M_J}$ and the same expression with $++$ and $--$ interchanged. According to eq.(2.45) we therefore find

$$\left(\psi^{JM_J}_{f_2f_1}\right)^\dagger = (-1)^{1-J-M_J}\hat{\Phi}_{f_1f_2}\left[\left(\Phi^{--}_{f_1f_2}\right)^{J\,-M_J},\left(\Phi^{++}_{f_1f_2}\right)^{J\,-M_J}\right]\,\gamma^0 \tag{2.46}$$

We thus have the result that

- exchanging the functions Φ^{++} and Φ^{--} in $\Phi = \hat{\Phi}\,(\Phi^{++},\Phi^{--})$ turns an amplitude with eigenvalue M into an amplitude with eigenvalue $-M^*$.

With the relations obtained above it is easy to investigate the eigenvalue $M = 0$ which is assumed to be not degenerate apart from the trivial degeneracy in the angular momentum projection M_J. From eqs.(2.35),(2.38) we have

$$\mathcal{H}_{f_1 f_2} \psi_{f_1 f_2} = 0 \qquad \mathcal{H}_{f_1 f_2} \psi^{\dagger}_{f_2 f_1} = 0 \tag{2.47}$$

which through eq.(2.46) implies $(\psi^{JM_J}_{f_2 f_1})^{\dagger} = \lambda \, \psi^{J\,-M_J}_{f_1 f_2}$ with $|\lambda| = 1$. Then eq.(2.39) gives

$$\left\langle \psi^{JM_J}_{f_1 f_2} \,\middle|\, \psi^{JM_J}_{f_1 f_2} \right\rangle_{f_1 f_2} = - \left\langle \left(\psi^{JM_J}_{f_2 f_1}\right)^{\dagger} \,\middle|\, \left(\psi^{JM_J}_{f_2 f_1}\right)^{\dagger} \right\rangle_{f_1 f_2} = - \left\langle \psi^{J\,-M_J}_{f_1 f_2} \,\middle|\, \psi^{J\,-M_J}_{f_1 f_2} \right\rangle_{f_1 f_2} \tag{2.48}$$

Since the scalar product is invariant under rotations one can substitute $-M_J$ by M_J and obtains

$$\left\langle \psi^{JM_J}_{f_1 f_2} \,\middle|\, \psi^{JM_J}_{f_1 f_2} \right\rangle_{f_1 f_2} = 0 \tag{2.49}$$

So we find that

- nondegenerate eigenfunctions with eigenvalue $M = 0$ have zero norm.

From eq.(2.46) it is clear that $(\psi^{JM_J}_{f_2 f_1})^{\dagger} = \lambda \, \psi^{J\,-M_J}_{f_1 f_2}$ is equivalent to setting

$$\Phi^{++} = \pm \Phi^{--} \tag{2.50}$$

This equation illustrates a common aspect of the Salpeter equation: in the nonrelativistic limit with $M \approx m_1 + m_2$ the large component Φ^{++} dominates over the small component Φ^{--}, but if one goes to deeply bound states (e.g. by increasing the coupling constant of an attractive interaction) the two components become more and more equal until finally $\Phi^{++} = \pm \Phi^{--}$ is achieved for $M = 0$.

From the discussion above it has become clear that we have to identify the physically acceptable solutions. There are two criteria making sure that a solution is acceptable:

- The norm of the solution has to be nonzero which automatically implies that M is real.

- The eigenvalue M and the norm have to be positive in order to fulfill the normalization condition $\langle \psi \, | \psi \rangle = (2\pi)^2 \, 2M$.

We would like to mention that the typical doubling of the physical eigenvalues is well known from the RPA equations in nonrelativistic many particle theory [56]. For a hamiltonian H with spectrum E_n the RPA equations have solutions E_n, $-E_n$. This doubling can be traced back to the appearance of the time ordering operator T in the definition of the particle-hole propagator. Therefore neglecting negative mass eigenvalues is consistent with the RPA structure of the Salpeter equation (compare chap.2.4).

The role of the solutions with $M = 0$ and $\langle\psi \mid \psi\rangle = 0$ is not clear. On one hand there is a priori no contradiction with the normalization condition. On the other hand the Salpeter equation has been obtained in the rest frame of the bound state, i.e. one first performs the limit $\vec{P} \to 0$ and then investigates the case $M \to 0$. However, the correct procedure for massless bound states is first to perform the limit $M \to 0$ in the BS-equation. In the resulting equation one then can study the limit $\vec{P} \to 0$. It cannot generally be expected that exchanging the limits for $\vec{P}$ and M leads to equivalent results (compare [31] for a more detailed discussion of this problem). Furthermore the definition of the instantaneous interaction kernel eq.(2.8) becomes dubious since $p_\perp$ is not well defined for $P \to 0$. We therefore prefer to require $M > 0$ and $\langle\psi \mid \psi\rangle > 0$ for physically acceptable solutions.

2.4 Numerical treatment

From the definition of $\hat{\Phi}$ in eq.(2.15) it is easy to derive a basis expansion for $\psi = \Phi\gamma^0$. Let

$$E_i(\vec{p}) = R_{n_i L_i}(p)\ [Y_{L_i}(\Omega_p) \otimes \varphi_{S_i}]^J_{M_J} \tag{2.51}$$

be a complete set of 2×2 basis functions with real radial functions $R_{n_i L_i}(p)$. The basis functions are chosen orthonormal with respect to the usual scalar product given by

$$(E_i \mid E_j) = \int \frac{d^3p}{(2\pi)^3}\,\mathrm{tr}\,\left[E_i^+(\vec{p})\,E_j(\vec{p})\right] = \delta_{ij} \tag{2.52}$$

where the trace just gives the usual scalar product for the spin matrices $\mathrm{tr}\,\varphi^+_{SM_S}\varphi_{S'M'_S} = \delta_{SS'}\delta_{M_S M'_S}$. Note that the angular structure of the basis functions matches the structure of Φ^{++} and Φ^{--} as given in eq.(B.15). We choose $R_{n_i L_i}(p)$ to be real functions. It is now possible to expand

$$\Phi^{++}(\vec{p}) = \sum_{i=1}^{\infty} a_i^{(+)}\,E_i(\vec{p}) \tag{2.53}$$

$$\Phi^{--}(\vec{p}) = \sum_{i=1}^{\infty} a_i^{(-)}\,E_i(\vec{p}) \tag{2.54}$$

which implies $\mathcal{R}^{(\pm)}_{LS}(p) = \sum_{i=1}^{\infty} a_i^{(\pm)}\,R_{n_i L_i}(p)\,\delta_{LL_i}\,\delta_{SS_i}$ for the radial wave function. Since $\mathcal{R}^{(\pm)}_{LS}(p)$ are real functions in most cases of interest, the coefficients $a_i^{(\pm)}$ then also have to be real. Now define the 4×4-amplitudes

$$\begin{aligned} e_i^{(+)} &= \hat{\Phi}\,(E_i, 0)\,\gamma^0 \\ e_i^{(-)} &= \hat{\Phi}\,(0, E_i)\,\gamma^0 \end{aligned} \tag{2.55}$$

Note that these functions are not orthogonal with respect to the scalar product given in eq.(2.31). Since $\hat{\Phi}$ is bilinear we nevertheless can expand ψ as

$$\psi = \sum_{i=1}^{\infty} \left(a_i^{(+)}\,e_i^{(+)} + a_i^{(-)}\,e_i^{(-)}\right) \tag{2.56}$$

so that the constraint $\Lambda_1^+ \psi \Lambda_2^+ = \Lambda_1^- \psi \Lambda_2^- = 0$ is automatically fulfilled. The Salpeter equation $\mathcal{H}\psi = M\psi$ can now be written as the matrix equation

$$\begin{pmatrix} H^{++} & H^{+-} \\ H^{-+} & H^{--} \end{pmatrix} \begin{pmatrix} a^{(+)} \\ a^{(-)} \end{pmatrix} = M \begin{pmatrix} N^{++} & N^{+-} \\ N^{-+} & N^{--} \end{pmatrix} \begin{pmatrix} a^{(+)} \\ a^{(-)} \end{pmatrix} \tag{2.57}$$

with $H_{ij}^{ss'} = \langle e_i^{(s)} | \mathcal{H}\, e_j^{(s')} \rangle$ and $N_{ij}^{ss'} = \langle e_i^{(s)} | e_j^{(s')} \rangle$. From the definition of the scalar product one easily sees that $N^{++} = -N^{--}$ and $N^{+-} = N^{-+} = 0$. Furthermore we find from eqs.(2.46),(2.55) that $e_i^{(+)}$ and $e_i^{(-)}$ are connected by $[(e_i^{(+)})_{f_1 f_2}^{J M_J}]^\dagger = (-1)^{1-J-M_J} (e_i^{(-)})_{f_2 f_2}^{J -M_J}$ so that we can use eqs.(2.38),(2.39) as well as the invariance of the scalar product under flavor exchange and under the replacement $-M_J \to M_J$ to obtain $H_{ij}^{--} = (H_{ij}^{++})^*$ and $H_{ij}^{-+} = (H_{ij}^{+-})^*$. The matrix representation of the Salpeter equation thus takes the form

$$\begin{pmatrix} H^{++} & H^{+-} \\ (H^{+-})^* & (H^{++})^* \end{pmatrix} \begin{pmatrix} a^{(+)} \\ a^{(-)} \end{pmatrix} = M \begin{pmatrix} N^{++} & 0 \\ 0 & -N^{++} \end{pmatrix} \begin{pmatrix} a^{(+)} \\ a^{(-)} \end{pmatrix} \tag{2.58}$$

which is of the same form as the well-known RPA equations in nuclear physics [56]. Let $(a^{(+)}, a^{(-)})$ be an eigenvector with eigenvalue M. Then eq.(2.58) shows that $((a^{(-)})^*, (a^{(+)})^*)$ is an eigenvector with eigenvalue $-M^*$ which is just the result of the previous section. Usually the Salpeter hamiltonian $\mathcal{H}$ has the property that the matrix elements $H_{ij}^{ss'}$ and also the eigenvector coefficients $a_i^{(\pm)}$ are real within the basis given above. In that case and since $N_{ij}^{ss'}$ is real, also M must be real. This result has already been shown before for eigenvectors with nonzero norm.

Furthermore we see that if $M = 0$ is an eigenvalue we expect from eq.(2.58) that the eigenvector fulfills $a^{(+)} = \pm a^{(-)}$ and we reobtain the result that this solution has zero norm.

In a numerical treatment only a finite basis $i \leq i_{max} \approx 10$ can be taken into account. Then eq.(2.58) becomes a finite matrix equation that can be solved with standard numerical methods. One thus obtains an approximate eigenvalue M_β and an approximate eigenfunction ψ_β to the Salpeter equation that exactly fulfill the relation

$$\langle \psi_\beta \, | \mathcal{H}\, \psi_\beta \rangle = M_\beta \, \langle \psi_\beta \, | \psi_\beta \rangle \tag{2.59}$$

The index β indicates that the basis states E_i and thus ψ_β may depend on a (variational) parameter β of dimension MeV^{-1} that sets the absolute scale for the momentum dependence via $E_i^\beta(\vec{p}) = \beta^{3/2}\, E_i^{\beta=1}(\vec{p}\beta)$.

For solutions of nonzero norm we require

$$\delta M[\psi] = \delta \frac{\langle \psi \, | \mathcal{H}\, \psi \rangle}{\langle \psi \, | \psi \rangle} = 0 \tag{2.60}$$

in analogy to the Ritz' variational principle, where the variation δ is taken over all functions ψ with nonzero norm that fulfill $\Lambda_1^+ \psi \Lambda_2^+ = \Lambda_1^- \psi \Lambda_2^- = 0$. According to eq.(2.59) we make the variational ansatz $\psi = \psi_\beta$ implying $M[\psi_\beta] = M_\beta$ and

look for stationary points of M_β as a function of β (which also fixes β for each meson). The calculation of the matrix elements within an explicit model is given in appendix D.2. At this point we would only like to make a few technical comments. The matrix elements of the interaction kernel can be efficiently calculated by inserting two complete sets of basis functions written schematically as

$$\langle i \,|\, f_1(\vec{p})\, V(r)\, f_2(\vec{p}\,') \,|\, j \rangle = \sum_{g,h} \langle i \,|f_1(\vec{p})|\, g \rangle \; \langle g \,|V(r)|\, h \rangle \; \langle h \,|f_2(\vec{p}\,')|\, j \rangle \qquad (2.61)$$

so that $V(r)$ can be parameterized in coordinate space. A suitable choice for the basis functions is given by the functions $R_{nL}(y) = N_{nL}\, y^L\, L_n^{2L+2}(y)\, e^{-y/2}$ with $y = p\beta$ and $L_n^{2L+2}(y)$ being a Laguerre polynomial. We found that about ten basis states are sufficient to solve the Salpeter equation with rather high accuracy. The choice of 3-dimensional harmonic oscillator functions is less favored since their asymptotic behavior $\sim e^{-y^2/2}$ for $y \to \infty$ turns out to be not appropriate for our quark model (especially for deeply bound states like the pion).

2.5 Decay observables

Apart from describing the mass spectrum of mesons, any realistic model must also be able to describe mesonic transitions and decays. The important question arises whether a good description of the extremely deeply bound states as the pion or the kaon can be combined with a reasonable description of confinement, i.e. is compatible with the spectrum of higher excited states and states with higher angular momenta. The Salpeter formalism offers a natural framework, as the role of the lower component of the wave function turns out to be crucial for the correct normalization and calculation of the decays. This can be seen most clearly in the following formulas for the leptonic decays and the weak decay constants. For a detailed derivation of the decay formulas see ref.[37].

2.5.1 Leptonic decay width and weak decay constant

The transition or decay of bound states are calculated from BS amplitudes using the formalism given by Mandelstam [35]. We will merely sketch it by considering first the leptonic decays of vector mesons. The corresponding Feynman diagram is given by Fig.2.4. Considering only graphs of leading order in the electromagnetic coupling constant we obtain the approximation on the right hand side.

The exceptional role of these decays (together with the weak decay constants) is that if the BS kernel would be exact also the decay amplitudes would be correct to any order in the strong interaction. The hadronic part of the transition matrix element is given by [33]:

$$\langle 0 \,|\, j_\mu(0) \,|\, (M,\vec{0})\, 1^- \rangle = -tr\left(\gamma_\mu\, \chi_{(M,\vec{0})}(x=0)\right) = -\int \frac{d^3p}{(2\pi)^4}\, tr\; (\gamma_\mu\, \Phi(\vec{p})) \qquad (2.62)$$

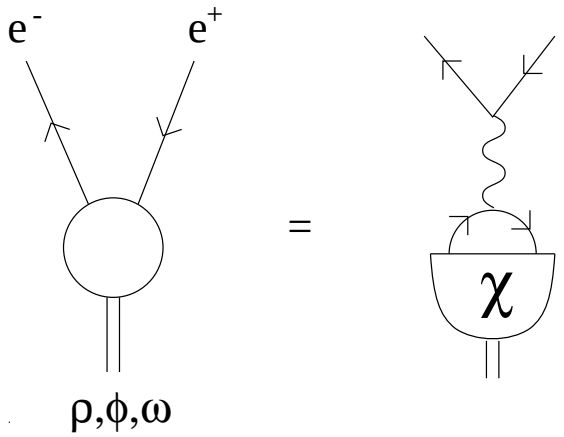

Figure 2.4: Leptonic decays in the Mandelstam formalism up to lowest order in the electromagnetic coupling constant

The instantaneous approximation thus simplyfies this calculation, as one can express the transition in terms of the Salpeter amplitude Φ. The integration and trace in eq.(2.62) for the current pick up only the s-wave amplitude. The usual spin summation and averaging leads to the decay width:

$$\Gamma(1^- \to l^+ l^-) = 24 \frac{\alpha^2 \, \tilde{e}_q^2}{M^3} \left| \int \frac{p^2 dp}{(2\pi)^3} \left(\mathcal{R}_{01}^{(+)}(p) - \mathcal{R}_{01}^{(-)}(p) \right) \right|^2 \tag{2.63}$$

where $\alpha = 1/137$ is the electromagnetic coupling constant and $\tilde{e}_q$ is the quark charge in units of the electron charge. Note that the lower component is evidently very important here (remember that it also influences the absolute values of the decay widths by entering in the normalization eq.(2.30)). For M we use the experimental meson mass to obtain the correct phase space.

The next observables considered are the weak decay constants f_π and f_K. They are defined by the matrix element of the axial current [41] (with this definition $f_\pi^{(exp)} = 132$ MeV):

$$i \, f_\pi P_\mu \;\; = \;\; \left\langle \, 0 \, \left| j_\mu^5(0) \right| \, P \, 0^- \, \right\rangle \tag{2.64}$$

Again for an instantaneous interaction this can be evaluated from the Salpeter amplitude

$$f_\pi \;\; = \;\; \left| \, \frac{\sqrt{3}}{M} \int \frac{d^3 p}{(2\pi)^4} \, tr \; \left(\Phi(\vec{p}\,) \gamma_0 \gamma_5 \right) \right| \tag{2.65}$$

and in terms of the $\Phi^{\pm\pm} = \mathcal{R}_{00}^{(\pm)} \, Y_{00} \, \varphi_{00}$:

$$f_\pi \;\; = \;\; \left| \, \frac{\sqrt{3}}{M} \int \frac{d^3 p}{(2\pi)^4} \, tr \; \left(\Phi^{++}(\vec{p}\,) - \Phi^{--}(\vec{p}\,) \right) \right|$$

$$= \left| \frac{\sqrt{24\pi}}{M} \int \frac{p^2 dp}{(2\pi)^4} \left(\mathcal{R}_{00}^{(+)}(p) - \mathcal{R}_{00}^{(-)} \right) \right| \tag{2.66}$$

2.5.2 The decay $\pi^0, \eta \to 2\gamma$

These decays provide another test for the description of the low lying pseudoscalar mesons. To our knowledge they have not been calculated in the framework of the full Salpeter equation (for a slightly more restricted ansatz see Mitra et al. [36]). The basic idea here is to reconstruct the vertex function Γ from the Salpeter amplitude Φ by means of the BS-eq.(2.26) itself, which gives the full fourdimensional structure of the BS amplitude χ. This has to be taken into account for a correct description of decays. The corresponding Feynman diagrams for the neutral pseudoscalar decay in lowest order of the interaction are given in Fig.2.5. Of course this is not correct to any order in the strong interaction like e.g. in

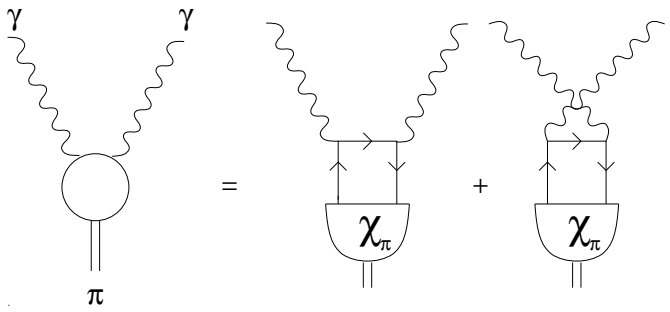

Figure 2.5: The decay $\pi^0, \eta \to 2\gamma$

the case of the pion decay constant, as we obviously neglect the strong interaction of the intermediate quark. Therefore we expect these calculations to be less accurate.

The lengthy calculation of the corresponding decay width can be found in ref.[37] and will therefore not be given here.

2.6 Conclusion

In the present chapter we have investigated the structure of the instantaneous BS-equation (Salpeter equation) for the general case of unequal quark masses. Furthermore we have developed a numerical scheme to solve the Salpeter equation which enables the calculation of mass spectra and Salpeter amplitudes. In order to test various models beyond the mere reproduction of the mass spectra, we have further given explicit formulas for the computation of weak meson decay

constants (f_π, f_K etc.), the decay widths into two photons and into an electron-positron pair.

Because of the relativistic kinematics, the correct relativistic normalization of the amplitudes and the dynamical treatment of the lower component Φ^{--} we expect the Salpeter equation to provide a framework for quark models that is superior to other treatments like the reduced Salpeter equation or the nonrelativistic quark model. After a discussion of its relation to the RPA equations of many body theory in the chapter 3, we will investigate an explicit quark model based on the Salpeter equation in chapters 4, 5 and 6.

Chapter 3

Salpeter equation and RPA equations

We give a derivation of the particle-hole RPA equations for an interacting multi-fermion system by applying the instantaneous approximation to the amputated two-fermion propagator of the system. In relativistic field theory the same approximation leads from the fermion-antifermion Bethe-Salpeter equation to the Salpeter equation. We show that RPA equations and Salpeter equation are indeed equivalent. This chapter is a slightly modified version of ref.[55].

3.1 Introduction

In the study of systems of many interacting fermions one finds that methods used in relativistic field theory usually correspond to approximations well-known in nonrelativistic many-particle theory. An interesting example is the correspondence of the Hartree-Fock approximation and the so-called Gap-equation used e.g. in the Nambu-Jona-Lasinio model [44], which both give the lowest approximation for the interactions in many-body problems. An improvement is obtained by including correlations in the excited states as well as the ground state of the system. In nonrelativistic many-body theory this leads to the particle-hole Random-Phase-Approximation (RPA) equations.

The RPA equations have been derived by various methods (see e.g. ref.[56]). The most systematic approach is the Green's function method, especially in view of possible generalizations. Although the connection of the RPA equations to the Bethe-Salpeter equation is mentioned in the literature [15], a clear and systematic description appears to be missing. It is the purpose of this chapter to close this gap and to establish the relation to the Salpeter equation.

The chapter is organized in the following way: In Sec.3.2 we will give a derivation of the RPA equations based on the Green's function method. The derivation is based on two approximations, i.e.

- we apply the instantaneous approximation to the amputated two-fermion propagator
- we substitute the full one-fermion propagators by free propagators.

In relativistic field theory the same approximations lead from the fermion-antifermion Bethe-Salpeter equation to the Salpeter equation (see chapter 2.3). The structure of this equation shows many similarities with the RPA equations (see also chapter 2.3.3). We will show in Sec.3.3 that the Salpeter equation and the RPA equations are indeed equivalent. Concluding remarks are given in Sec.3.4.

3.2 RPA equations and the instantaneous approximation

3.2.1 Pole structure of the polarization propagator

Let H be the hamiltonian for the dynamics of a (nonrelativistic or relativistic) system of many interacting identical fermions with ground state $|\psi_0\rangle$ and excited states $|\psi_\lambda\rangle$, $\lambda > 0$. The corresponding energies will be denoted as E_0 and E_λ with $E_\lambda \leq E_{\lambda'}$ for $\lambda < \lambda'$. For simplicity we assume a discrete energy spectrum, i.e. free states are considered in a finite space volume. In the relativistic case $|\psi_0\rangle$ is usually the vacuum, so that the excited states are particle-hole excitations of the vacuum, e.g. the mesons for the case of quarks.

For completeness and in order to introduce the notation some well-known definitions and facts will be recalled in the following.

Let a_α, $a_\alpha^\dagger$ be fermion field operators with the anticommutator given by $\left\{a_\alpha^\dagger,\, a_\beta\right\} = \delta_{\alpha\beta}$. They correspond to an orthonormal single particle basis φ_α which will be specified later. The Heisenberg-picture will be used in the following and we define $A_\alpha(t) := e^{iHt}\, a_\alpha\, e^{-iHt}$. The two-fermion propagator is then given by

$$\begin{aligned} i^2\,[G(t,t',u,u')]_{\alpha\alpha'\beta\beta'} &= \\ &= \quad \langle\psi_0|T\, A_\alpha(t)\, A_{\alpha'}(t')\, A_\beta^\dagger(u)\, A_{\beta'}^\dagger(u')\,|\psi_0\rangle \\ &= -\langle\psi_0|T\, A_\beta^\dagger(u)\, A_\alpha(t)\, A_{\beta'}^\dagger(u')\, A_{\alpha'}(t')\,|\psi_0\rangle \end{aligned} \tag{3.1}$$

(compare fig.3.1). Let $u = t + \epsilon$ and $u' = t' + \epsilon$ with $\epsilon > 0$. In the limit $\epsilon \to 0$ one has

$$\begin{aligned} \lim_{\epsilon\to 0}\,[G(t,t',t+\epsilon,t'+\epsilon)]_{\alpha\alpha'\beta\beta'} &= \\ = \quad \Theta(t-t')\,\langle\psi_0|\, A_\beta^\dagger(t)\, A_\alpha(t)\, A_{\beta'}^\dagger(t')\, A_{\alpha'}(t')\,|\psi_0\rangle \,+ & \\ + \quad \Theta(t'-t)\,\langle\psi_0|\, A_{\beta'}^\dagger(t')\, A_{\alpha'}(t')\, A_\beta^\dagger(t)\, A_\alpha(t)\,|\psi_0\rangle & \end{aligned} \tag{3.2}$$

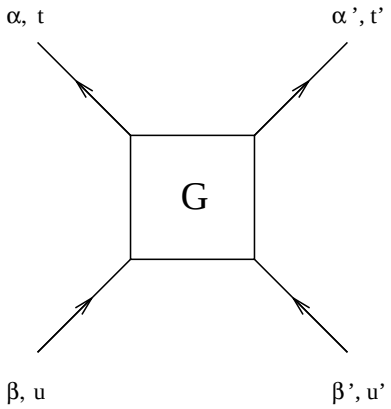

Figure 3.1: The two-fermion propagator G

and with $1 = \sum_\lambda |\psi_\lambda\rangle\langle\psi_\lambda|$ one obtains

$$\begin{aligned}
&\lim_{\epsilon\to 0} \left[G(t,t',t+\epsilon,t'+\epsilon)\right]_{\alpha\alpha'\beta\beta'} = \\
&\quad = \sum_\lambda \Big[\Theta(t-t')\, e^{-i(E_\lambda - E_0)\,(t-t')}\, \langle\psi_0|a^\dagger_\beta a_\alpha|\psi_\lambda\rangle\, \langle\psi_\lambda|a^\dagger_{\beta'} a_{\alpha'}|\psi_0\rangle \; + \\
&\qquad + \Theta(t'-t)\, e^{-i(E_\lambda - E_0)\,(t'-t)}\, \langle\psi_0|a^\dagger_{\beta'} a_{\alpha'}|\psi_\lambda\rangle\, \langle\psi_\lambda|a^\dagger_\beta a_\alpha|\psi_0\rangle\Big]
\end{aligned} \tag{3.3}$$

The term for the ground state ($\lambda = 0$) can be rewritten in terms of the one-fermion propagators $S^F_{\alpha\beta}(t-t') = -i\,\langle\psi_0|T\, A_\alpha(t)\, A^\dagger_\beta(t')|\psi_0\rangle$ as

$$\langle\psi_0|a^\dagger_\beta a_\alpha|\psi_0\rangle\, \langle\psi_0|a^\dagger_{\beta'} a_{\alpha'}|\psi_0\rangle = -\lim_{\epsilon\to 0}\, S^F_{\alpha\beta}(-\epsilon)\, S^F_{\alpha'\beta'}(-\epsilon) \tag{3.4}$$

The polarization propagator $\Pi(t-t')$ is now defined as

$$\begin{aligned}
&\lim_{\epsilon\to 0} \left[G(t,t',t+\epsilon,t'+\epsilon)\right]_{\alpha\alpha'\beta\beta'} = \\
&\quad = \; -\lim_{\epsilon\to 0}\, S^F_{\alpha\beta}(-\epsilon)\, S^F_{\alpha'\beta'}(-\epsilon) + i\,\left[\Pi(t-t')\right]_{\alpha\alpha'\beta\beta'}
\end{aligned} \tag{3.5}$$

so that

$$\begin{aligned}
&i\,\left[\Pi(t-t')\right]_{\alpha\alpha'\beta\beta'} = \\
&\quad = \sum_{\lambda\neq 0} \Big[\Theta(t-t')\, e^{-i(E_\lambda - E_0)\,(t-t')}\, \langle\psi_0|a^\dagger_\beta a_\alpha|\psi_\lambda\rangle\, \langle\psi_\lambda|a^\dagger_{\beta'} a_{\alpha'}|\psi_0\rangle \; + \\
&\qquad + \Theta(t'-t)\, e^{-i(E_\lambda - E_0)\,(t'-t)}\, \langle\psi_0|a^\dagger_{\beta'} a_{\alpha'}|\psi_\lambda\rangle\, \langle\psi_\lambda|a^\dagger_\beta a_\alpha|\psi_0\rangle\Big]
\end{aligned} \tag{3.6}$$

Since

$$\Theta(t)\, e^{-iEt} = \frac{1}{2\pi i} \int \frac{e^{-i\nu t}\, d\nu}{E - \nu - i\epsilon} \tag{3.7}$$

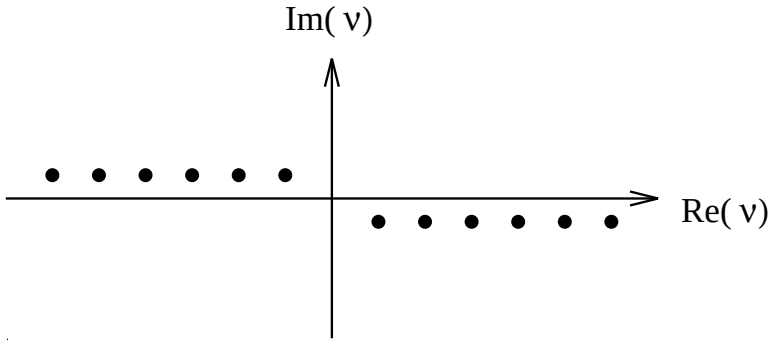

Figure 3.2: Location of the poles of $\Pi(\nu)$

one can write the fourier transform $\Pi(\nu) = \int dt\, e^{i\nu t}\, \Pi(t)$ as

$$[\Pi(\nu)]_{\alpha\alpha'\beta\beta'} = \sum_{\lambda\neq 0} \left[\frac{\langle\psi_0|a^\dagger_\beta a_\alpha|\psi_\lambda\rangle \langle\psi_\lambda|a^\dagger_{\beta'} a_{\alpha'}|\psi_0\rangle}{\nu - (E_\lambda - E_0 - i\epsilon)} - \frac{\langle\psi_0|a^\dagger_{\beta'} a_{\alpha'}|\psi_\lambda\rangle \langle\psi_\lambda|a^\dagger_\beta a_\alpha|\psi_0\rangle}{\nu + (E_\lambda - E_0 - i\epsilon)} \right] \tag{3.8}$$

Thus the energy levels of the excited states appear as a doubled system of poles in the polarization propagator $\Pi(\nu)$ at $\nu = \pm(E_\lambda - E_0 - i\epsilon)$ as shown in fig.3.2. This doubling of the spectrum can be traced back to the appearence of the time ordering operator T in the definition of the two-fermion propagator G. From any equation that determines the poles of Π we will therefore obtain a doubled eigenvalue spectrum. This statement holds for relativistic as well as nonrelativistic calculations. It is clear that the appearence of the second set of poles does not yield any further physical information, since only half of the poles can be identified with the eigenvalues of the hamiltonian H.

3.2.2 The instantaneous approximation

The amputated two-fermion propagator M is defined as (see also fig.3.3)

$$\begin{aligned}
&[G(t,t',u,u')]_{\alpha\alpha'\beta\beta'} = \\
&\quad -S^F_{\alpha\beta}(t-u)\, S^F_{\alpha'\beta'}(t'-u') + S^F_{\alpha\beta'}(t-u')\, S^F_{\alpha'\beta}(t'-u) + \\
&\quad + \sum_{\alpha_1\alpha_2} \sum_{\alpha_3\alpha_4} \int dt_1 dt_2 dt_3 dt_4\, S^F_{\alpha\alpha_1}(t-t_1)\, S^F_{\alpha'\alpha_2}(t'-t_2) \cdot \\
&\quad \cdot [M(t_1,t_2,t_3,t_4)]_{\alpha_1\alpha_2\alpha_3\alpha_4}\, S^F_{\alpha_3\beta}(t_3-u)\, S^F_{\alpha_4\beta'}(t_4-u')
\end{aligned} \tag{3.9}$$

The instantaneous approximation of M used for the investigation of one-particle – one-hole propagation is given by the ansatz

$$M \;\rightarrow\; M^{inst} = \delta(t_1 - t_3)\, \delta(t_2 - t_4)\, \Gamma(t_1 - t_2) \tag{3.10}$$

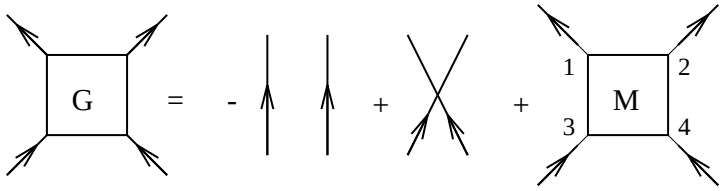

Figure 3.3: Definition of the amputated two-fermion propagator M

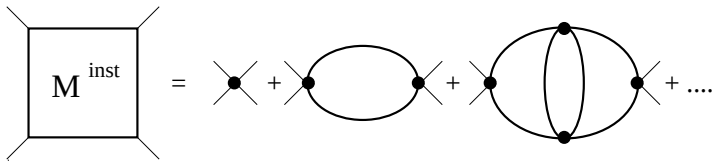

Figure 3.4: Diagrams that contribute to M^{inst} for a 4-point-interaction

i.e. it is assumed that particles and holes interact instantaneously with each other.

In nonrelativistic many-body theory this ansatz is equivalent to taking into account only diagrams that have the appropriate instantaneous structure, as shown in fig.3.4. The same statement also holds for a relativistic 4-point-interaction. In more general relativistic field theories like QCD, however, the instantaneous approximation cannot easily be interpreted in terms of Feynman diagrams.

With the relations of the previous section (using $t' = 0$) the instantaneous approximation yields for the polarization propagator

$$\begin{aligned} i\,[\Pi^{inst}(t)]_{\alpha\alpha'\beta\beta'} &= S^F_{\alpha\beta'}(t)\, S^F_{\alpha'\beta}(-t) + \\ &+ \sum_{\alpha_1\alpha_2} \sum_{\alpha_3\alpha_4} \int dt_1 dt_2\, S^F_{\alpha\alpha_1}(t-t_1)\, S^F_{\alpha'\alpha_2}(-t_2) \cdot \\ &\cdot\, [\Gamma(t_1-t_2)]_{\alpha_1\alpha_2\alpha_3\alpha_4}\, S^F_{\alpha_3\beta}(t_1-t)\, S^F_{\alpha_4\beta'}(t_2) \end{aligned} \tag{3.11}$$

To simplify the notation we define

$$[g(t)]_{\alpha\alpha'\beta\beta'} := S^F_{\alpha\beta'}(t)\, S^F_{\alpha'\beta}(-t) \tag{3.12}$$

Furthermore let

$$(A\,B)_{\alpha\beta\gamma\delta} := \sum_{\alpha'\beta'} A_{\alpha\alpha'\gamma\beta'}\, B_{\beta'\beta\alpha'\delta} \tag{3.13}$$

An easy way to represent this definition is to define multi-indices as $A_{\alpha\beta\gamma\delta} =: A_{(\alpha\gamma)(\delta\beta)} =: A_{ij}$ so that the usual matrix multiplication can be applied to A_{ij}.

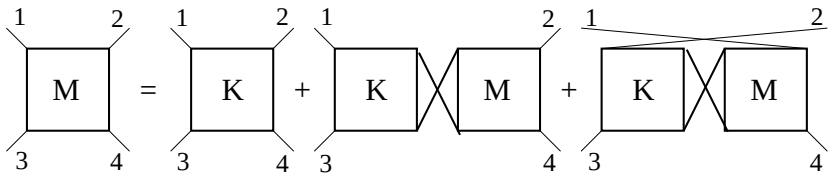

Figure 3.5: The Bethe-Salpeter equation for the amputated two-fermion propagator M

With these definitions the Fourier transform of eq.(3.11) can be written as

$$i\,\Pi^{inst}(\nu) = g(\nu) + g(\nu)\,\Gamma(\nu)\,g(\nu) \tag{3.14}$$

The exact Bethe-Salpeter equation for the amputated two-fermion propagator M reads

$$\begin{aligned} M_{1234} \;&=\; K_{1234} + \sum_{\alpha_5\alpha_6}\sum_{\alpha_7\alpha_8}\int dt_5\,dt_6\,dt_7\,dt_8 \\ &\quad \Big[K_{1537}\,S^F_{58}\,S^F_{67}\,M_{6284} + K_{2537}\,S^F_{58}\,S^F_{67}\,M_{6184}\Big] \end{aligned} \tag{3.15}$$

(compare fig.3.5) with an appropriate particle-hole kernel K and the notation $[K(t_a,t_b,t_c,t_d)]_{\alpha_a\alpha_b\alpha_c\alpha_d} =: K_{abcd}$ and analogously for M and S^F.

In a first step one neglects the last (exchange) term. The second step is to substitute M^{inst} for M which implies that also K must have this instantaneous structure, i.e.

$$K \;\rightarrow\; K^{inst} = \delta(t_1-t_3)\,\delta(t_2-t_4)\,iV(t_1-t_2) \tag{3.16}$$

After applying the Fourier transformation the instantaneous Bethe-Salpeter equation reads

$$\Gamma(\nu) = iV(\nu) + iV(\nu)\,g(\nu)\,\Gamma(\nu) \tag{3.17}$$

Together with $i\,\Pi^{inst} = g + g\,\Gamma\,g$ one obtains $i\,\Pi^{inst} = g - g\,V\,\Pi^{inst}$ or

$$i\,\Pi^{inst}(\nu) = \Big([g(\nu)]^{-1} - i\,V(\nu)\Big)^{-1} \tag{3.18}$$

3.2.3 The RPA-equations

From eq.(3.8) we know that $\Pi(\nu)$ has poles at $\nu = \pm(E_\lambda - E_0 - i\epsilon)$. On the other hand we can use eq.(3.18) to obtain a spectral decomposition for $\Pi^{inst}(\nu)$ in order to calculate the pole positions and matrix elements in the instantaneous approximation. In the following we therefore look for solutions $F(\nu)$ of the equation

$$\Big([g(\nu)]^{-1} - i\,V(\nu)\Big)\;F(\nu) = 0 \tag{3.19}$$

To proceed further we approximate the full propagators S^F in g by the free propagators $[S_0^F(t)]_{\alpha\beta} = -i\,\langle\chi_0|T\,A_\alpha^0(t)\,[A_\beta^0(0)]^\dagger|\chi_0\rangle$ with $A_\alpha^0(t) = e^{iH_0t}\,a_\alpha\,e^{-iH_0t}$, where $H_0 = \sum_\alpha \epsilon_\alpha\,a_\alpha^\dagger a_\alpha$ is some 'free' hamiltonian with ground state $|\chi_0\rangle$. The basis states φ_α have thus been chosen as eigenstates of H_0, i.e. $H_0\,\varphi_\alpha = \epsilon_\alpha\,\varphi_\alpha$. In the nonrelativistic case an appropriate choice for H_0 is the Hartree-Fock hamiltonian, whereas in the relativistic case one can use the free Dirac hamiltonian with some effective fermion mass m.

For a system of n fermions, the ground state $|\chi_0\rangle$ of H_0 is a product wavefunction where the lowest n eigenstates are occupied, i.e. $a_\alpha\,|\chi_0\rangle = 0$ for $\alpha > n$ and $a_\alpha^\dagger\,|\chi_0\rangle = 0$ for $\alpha \le n$. In the relativistic case $|\chi_0\rangle$ is the filled Dirac sea. With

$$\begin{aligned} H_0\,a_\alpha^\dagger\,|\chi_0\rangle &= (\epsilon_\alpha + \epsilon_0)\,a_\alpha^\dagger\,|\chi_0\rangle && (3.20)\\ H_0\,a_\alpha\,|\chi_0\rangle &= (-\epsilon_\alpha + \epsilon_0)\,a_\alpha\,|\chi_0\rangle && (3.21)\end{aligned}$$

one finds

$$[iS_0^F(t)]_{\alpha\beta} = e^{-i\epsilon_\alpha t}\,\delta_{\alpha\beta}\,[\Theta(t)\,\Theta(\alpha-n) - \Theta(-t)\,\Theta(n-\alpha)] \qquad (3.22)$$

and therefore

$$\begin{aligned} [g^0(t)]_{\alpha\alpha'\beta\beta'} &= [S_0^F(t)]_{\alpha\beta'}\,[S_0^F(-t)]_{\alpha'\beta} = \\ &= -e^{-(\epsilon_\alpha-\epsilon_\beta)t}\,\delta_{\alpha\beta'}\,\delta_{\alpha'\beta}\,\cdot \\ &\quad \cdot[\Theta(t)\,\Theta(\alpha-n)\,\Theta(n-\beta) + \\ &\quad +\Theta(-t)\,\Theta(\beta-n)\,\Theta(n-\alpha)] \qquad (3.23)\end{aligned}$$

In the following we will use capital letters like $\alpha = A$ for $\alpha > n$ and small letters like $\alpha = a$ for $\alpha \le n$. Using eq.(3.7) for the Θ-functions and the multi-index notation of the previous section we find for the fourier transform of g^0

$$\begin{aligned} \left[\left(g^0(\nu)\right)^{-1}\right]_{(Ab)\,(B'a')} &= -i\,(\epsilon_A - \epsilon_b - \nu)\,\delta_{(Ab)\,(B'a')} && (3.24)\\ \left[\left(g^0(\nu)\right)^{-1}\right]_{(aB)\,(b'A')} &= -i\,(\epsilon_B - \epsilon_a + \nu)\,\delta_{(aB)\,(b'A')} && (3.25)\end{aligned}$$

Note that the matrix elements of g are zero if one of the multi-indices equals (ab) or (AB). Because of $i\Pi^{inst} = g + g\Gamma g$ the same holds for Π^{inst} and because of $i\Pi^{inst} = g - gV\Pi^{inst}$ also the matrix elements of V with these indices are not relevant. It is therefore sufficient to consider only the index combinations (Ab) and (bA). This simplification is a consequence of approximating the full fermion propagators by the free ones. Write

$$F = \begin{pmatrix} X \\ Y \end{pmatrix} \qquad (3.26)$$

with $X_k = F_{(Ab)}$ and $Y_k = F_{(bA)}$. In the following we will assume that X, Y are vectors of dimension D, i.e. $k = 1 \ldots D$. Define $2D \times 2D$ -matrices Ω and N by $[g^0(\nu)]^{-1} =: -i\,(\Omega - \nu\, N)$ so that

$$\begin{aligned} \Omega_{(Ab)(B'a')} &= (\epsilon_A - \epsilon_b)\,\delta_{(Ab)(B'a')} \\ \Omega_{(aB)(b'A')} &= (\epsilon_B - \epsilon_a)\,\delta_{(aB)(b'A')} \\ N_{(Ab)(B'a')} &= \delta_{(Ab)(B'a')} \\ N_{(aB)(b'A')} &= -\delta_{(aB)(b'A')} \end{aligned} \tag{3.27}$$

which we will write in matrix notation as

$$\Omega = \begin{pmatrix} (\epsilon_A - \epsilon_b) & 0 \\ 0 & (\epsilon_B - \epsilon_a) \end{pmatrix} \quad , \quad N = \begin{pmatrix} 1 & 0 \\ 0 & -1 \end{pmatrix} \tag{3.28}$$

Setting $h := \Omega + V$ we find that eq.(3.19) (multiplied with i) can be written as

$$h\, F^\rho = \nu_\rho\, N\, F^\rho \tag{3.29}$$

where ρ labels the different solutions and $F^\rho := F(\nu_\rho)$. In the nonrelativistic case one usually approximates the kernel V by its lowest order contribution, i.e. the two-fermion potential. Then this equation is exactly the RPA-equation of e.g. ref.[56].

Up to now it is not clear how to connect ν_ρ and F^ρ with the eigenvalues and eigenstates of the full Hamiltonian H. It is usefull at this point to recall some of the properties of the RPA-equation [15, 56]:

- h is a hermitian matrix and has the structure

$$h = \begin{pmatrix} A & B \\ B^* & A^* \end{pmatrix} \tag{3.30}$$

- Let

$$F^\sigma = \begin{pmatrix} X^\sigma \\ Y^\sigma \end{pmatrix} \tag{3.31}$$

  be a solution with eigenvalue ν_σ. Then

$$F^\tau = \begin{pmatrix} X^\tau \\ Y^\tau \end{pmatrix} = \begin{pmatrix} (Y^\sigma)^* \\ (X^\sigma)^* \end{pmatrix} \tag{3.32}$$

  is a solution with eigenvalue $\nu_\tau = -\nu_\sigma$ (we assume that ν_σ is real). For the components of the eigenvectors this means that $F^\tau_{(Ab)} = [F^\sigma_{(bA)}]^*$ and $F^\tau_{(bA)} = [F^\sigma_{(Ab)}]^*$.

- If F^{ρ_1} and F^{ρ_2} are solutions with $\nu_{\rho_1} \neq \nu_{\rho_2}$ then

$$\langle F^{\rho_1} | N |\, F^{\rho_2} \rangle := (F^{\rho_1})^\dagger\, N\, F^{\rho_2} = 0 \tag{3.33}$$

- If B is 'small enough' the $2D$ eigenvalues ν_ρ are real and nonzero. We will use the index convention $\sigma = 1 \ \ldots \ D$ for $\nu_\sigma > 0$ and $\tau = D+1 \ \ldots \ 2D$ for $\nu_\tau < 0$ with $\nu_\tau = -\nu_\sigma$. The solutions can then be normalized as

$$\langle F^{\rho'} | N | \, F^\rho \rangle = N_\rho \, \delta_{\rho'\rho} \tag{3.34}$$

with $N_\sigma = 1$ and $N_\tau = -1$. They form a $2D$-dimensional basis, i.e. one can expand a vector F as $F = \sum_\rho \, c_\rho \, F^\rho$ with $c_\rho = N_\rho^{-1} \, \langle F^\rho | N | \, F \rangle$ so that

$$1 = \sum_\rho \, N_\rho^{-1} \, | F^\rho \rangle \, \langle F^\rho | N |$$ (3.35)

The following calculation

$$\begin{aligned} (N\nu - h)^{-1} \, N | F^{\rho'} \rangle &= (\nu - N^{-1} h)^{-1} \, | F^{\rho'} \rangle = \frac{1}{\nu - \nu_{\rho'}} \, | F^{\rho'} \rangle = \\ &= \sum_\rho \, \frac{1}{\nu - \nu_\rho} \, N_\rho^{-1} \, | F^\rho \rangle \, \langle F^\rho | N | F^{\rho'} \rangle \end{aligned} \tag{3.36}$$

now showes that the spectral decomposition of $(N\nu - h)^{-1}$ is given by

$$(N\nu - h)^{-1} = \sum_{\rho=1}^{2D} \, \frac{1}{\nu - \nu_\rho} \, N_\rho^{-1} \, | F^\rho \rangle \, \langle F^\rho |$$ (3.37)

Let $(\alpha\beta)$ stand for (Ab) or (aB). Since $F^\tau_{(\alpha\beta)} = [F^\sigma_{(\beta\alpha)}]^*$ the spectral decomposition for the matrix elements of $\Pi^{inst}(\nu)$ can be written as

$$\begin{aligned} [\Pi^{inst}(\nu)]_{\alpha\delta\beta\gamma} &= (N\nu - h)^{-1}_{(\alpha\beta)\,(\gamma\delta)} = \\ &= \sum_{\sigma=1}^{M} \, \left[\frac{1}{\nu - \nu_\sigma} \, F^\sigma_{(\alpha\beta)} \, [F^\sigma_{(\gamma\delta)}]^* - \frac{1}{\nu + \nu_\sigma} \, [F^\sigma_{(\beta\alpha)}]^* \, F^\sigma_{(\delta\gamma)} \right] \end{aligned} \tag{3.38}$$

Comparing this equation with the exact pole structure given in eq.(3.8) we can identify

$$F^\sigma_{\alpha\beta} = \langle \psi_0 | a^\dagger_\beta a_\alpha | \psi_\sigma \rangle$$ (3.39)

$$\nu_\sigma = E_\sigma - E_0$$ (3.40)

3.3 From the Salpeter equation to the RPA-equations

In relativistic field theory particle-hole excitations of the fermionic vacuum are described by the fermion-antifermion Bethe-Salpeter equation (see chapter 2.2). In the instantaneous approximation this equation reduces to the Salpeter equation

(see chapter 2.3). From the considerations of the previous section we expect the Salpeter equation to be equivalent to the RPA equations (3.29). We will show in this section that this is indeed the case.

As shown in chapter 2.3 eq.(2.18) the Salpeter equation for one fermion flavor can be written in the form

$$(\mathcal{H}\psi)(\vec{p}) = M\,\psi(\vec{p}) \tag{3.41}$$

where

$$\begin{aligned}(\mathcal{H}\psi)(\vec{p}) &= H(\vec{p})\psi(\vec{p}) - \psi(\vec{p})H(\vec{p}) \\ &- \int \frac{d^3p'}{(2\pi)^3}\,\Lambda^+(\vec{p})\,[W(\vec{p},\vec{p}\,')\,\psi(\vec{p}\,')]\,\Lambda^-(\vec{p}) \\ &+ \int \frac{d^3p'}{(2\pi)^3}\,\Lambda^-(\vec{p})\,[W(\vec{p},\vec{p}\,')\,\psi(\vec{p}\,')]\,\Lambda^+(\vec{p})\end{aligned} \tag{3.42}$$

with the free Dirac hamiltonian $H(\vec{p}) = \gamma^0(\vec{\gamma}\vec{p} + m)$, the projection operators $\Lambda^{\pm} = (\omega \pm H(\vec{p}))/(2\omega)$ and $\omega = \sqrt{\vec{p}^{\,2} + m^2}$ (don't confuse $H(\vec{p})$ with the full hamiltonian of the previous section). Here M is the mass of the bound state, m is the effective fermion mass and W is the instantaneous interaction kernel. The scalar product was given by (see eq.(2.31))

$$\langle\psi_1\,|\psi_2\rangle = \int \mathrm{tr}\,\left(\psi_1^\dagger\,\Lambda^+\,\psi_2\,\Lambda^- - \psi_1^\dagger\,\Lambda^-\,\psi_2\,\Lambda^+\right) \tag{3.43}$$

with all quantities depending on $\vec{p}$ and the notation $\int = \int d^3p/(2\pi)^3$.

Let $u(\vec{p})$, $v(\vec{p})$ be free Dirac spinors (we use the conventions of [25] in the following). Define the 4×4 -matrices

$$\begin{aligned} w_{rs}^{(+)}(\vec{p}) &:= u_r(\vec{p}) \otimes v_s^\dagger(-\vec{p}) \\ w_{rs}^{(-)}(\vec{p}) &:= v_s(-\vec{p}) \otimes u_r^\dagger(\vec{p}) \end{aligned} \tag{3.44}$$

Note that in the notation of chapter 2.3.1 eq.(2.15) this definition corresponds to

$$\begin{aligned} w_{rs}^{(+)}(\vec{p}) &= \sqrt{\frac{(\omega_1+m_1)\,(\omega_2+m_2)}{2m_1\,2m_2}}\;\hat{\Phi}\left[-\varphi_{rs}\,,\; -\frac{\vec{\sigma}\vec{p}}{\omega_1+m_1}\,\varphi_{rs}\,\frac{\vec{\sigma}\vec{p}}{\omega_2+m_2}\right]\;\gamma^0 \\ w_{rs}^{(-)}(\vec{p}) &= \sqrt{\frac{(\omega_1+m_1)\,(\omega_2+m_2)}{2m_1\,2m_2}}\;\hat{\Phi}\left[\frac{\vec{\sigma}\vec{p}}{\omega_1+m_1}\,\varphi_{sr}\,\frac{\vec{\sigma}\vec{p}}{\omega_2+m_2}\,,\; \varphi_{sr}\right]\;\gamma^0 \end{aligned}$$

where $\varphi_{rs} = \chi_r \otimes \chi_s^+$ and χ_r is the Pauli-spinor of the fermion with spin projection $r = \pm 1/2$.

We will use the box normalization in the following, i.e. we substitute

$$\int \frac{d^3p}{(2\pi)^3} \;\longrightarrow\; \frac{1}{V}\sum_{\vec{p}} \tag{3.45}$$

Since $\Lambda^+ \psi \, \Lambda^+ = \Lambda^- \psi \, \Lambda^- = 0$ we can expand

$$\psi(\vec{p}) = \sqrt{V} \, \frac{m}{\omega} \sum_{r,s=\pm 1/2} \left(b^{(+)}_{\vec{p},rs} \, w^{(+)}_{rs}(\vec{p}) + b^{(-)}_{\vec{p},rs} \, w^{(-)}_{rs}(\vec{p}) \right) \tag{3.46}$$

with some suitable coefficients b. The factors in front of the summation sign have been choosen to simplify the notation in the following.

Solving the Salpeter equation $\mathcal{H}\psi = M \, \psi$ is equivalent to solving

$$\langle \psi_1 | \mathcal{H} \, \psi_2 \rangle = M \, \langle \psi_1 | \psi_2 \rangle \tag{3.47}$$

for all given ψ_1.

With eq.(3.46) and the relations for u, v of ref.[25] we compute

$$\begin{aligned}
\mathrm{tr} \left[[w^{(+)}_{rs}]^\dagger \, \Lambda^+ \, w^{(+)}_{r's'} \, \Lambda^- - [w^{(+)}_{rs}]^\dagger \, \Lambda^- \, w^{(+)}_{r's'} \, \Lambda^+ \right] &= + \frac{\omega^2}{m^2} \, \delta_{rr'} \, \delta_{ss'} & (3.48) \\
\mathrm{tr} \left[[w^{(-)}_{rs}]^\dagger \, \Lambda^+ \, w^{(-)}_{r's'} \, \Lambda^- - [w^{(-)}_{rs}]^\dagger \, \Lambda^- \, w^{(-)}_{r's'} \, \Lambda^+ \right] &= - \frac{\omega^2}{m^2} \, \delta_{rr'} \, \delta_{ss'} & (3.49) \\
\mathrm{tr} \left[[w^{(+)}_{rs}]^\dagger \, \Lambda^+ \, w^{(-)}_{r's'} \, \Lambda^- - [w^{(+)}_{rs}]^\dagger \, \Lambda^- \, w^{(-)}_{r's'} \, \Lambda^+ \right] &= 0 & (3.50) \\
\mathrm{tr} \left[[w^{(-)}_{rs}]^\dagger \, \Lambda^+ \, w^{(+)}_{r's'} \, \Lambda^- - [w^{(-)}_{rs}]^\dagger \, \Lambda^- \, w^{(+)}_{r's'} \, \Lambda^+ \right] &= 0 & (3.51)
\end{aligned}$$

where all quantities depend on $\vec{p}$. Using the multiindex $i = (\vec{p}, r, s)$ the scalar product in the box normalization can therefore be written as

$$\begin{aligned}
\langle \psi_1 | \psi_2 \rangle &= \sum_i \left[(b^{(+)}_1)^*_i \, (b^{(+)}_2)_i - (b^{(-)}_1)^*_i \, (b^{(-)}_2)_i \right] = \\
&= \begin{pmatrix} b^{(+)}_1 \\ b^{(-)}_1 \end{pmatrix}^\dagger \begin{pmatrix} 1 & 0 \\ 0 & -1 \end{pmatrix} \begin{pmatrix} b^{(+)}_2 \\ b^{(-)}_2 \end{pmatrix} & (3.52)
\end{aligned}$$

We further have

$$\begin{aligned}
\langle \psi_1 | \mathcal{H} \, \psi_2 \rangle &= \langle \psi_1 | \mathcal{T} \, \psi_2 \rangle + \langle \psi_1 | \mathcal{V} \, \psi_2 \rangle \quad \text{with} & (3.53) \\
\langle \psi_1 | \mathcal{T} \, \psi_2 \rangle &= \frac{1}{V} \sum_{\vec{p}} 2\omega \, \mathrm{tr} \left(\psi_1^\dagger(\vec{p}) \, \psi_2(\vec{p}) \right) & (3.54) \\
\langle \psi_1 | \mathcal{V} \, \psi_2 \rangle &= - \frac{1}{V^2} \sum_{\vec{p}} \sum_{\vec{p}'} \mathrm{tr} \left(\psi_1^\dagger(\vec{p}) \, W(\vec{p}, \vec{p}\,') \, \psi_2(\vec{p}\,') \right) & (3.55)
\end{aligned}$$

We proceed analogously for the kinetic energy term and compute

$$\mathrm{tr} \left[[w^{(a)}_{rs}(\vec{p})]^\dagger \, [w^{(a')}_{r's'}(\vec{p})] \right] = \frac{\omega^2}{m^2} \, \delta_{rr'} \, \delta_{ss'} \, \delta_{aa'} \tag{3.56}$$

(where $a, a' = \pm$) so that with $\omega_i = \omega(\vec{p})$

$$\begin{aligned}
\langle \psi_1 | \mathcal{T} \, \psi_2 \rangle &= \sum_i 2\omega_i \left[(b^{(+)}_1)^*_i \, (b^{(+)}_2)_i + (b^{(-)}_1)^*_i \, (b^{(-)}_2)_i \right] = \\
&=: \begin{pmatrix} b^{(+)}_1 \\ b^{(-)}_1 \end{pmatrix}^\dagger \begin{pmatrix} 2\omega & 0 \\ 0 & 2\omega \end{pmatrix} \begin{pmatrix} b^{(+)}_2 \\ b^{(-)}_2 \end{pmatrix} & (3.57)
\end{aligned}$$

For the interaction term we define

$$V_{ij}^{a_1 a_2} := -\frac{1}{V}\,\frac{m}{\omega}\,\frac{m}{\omega'}\,\mathrm{tr}\,\Big([w_{r_1 s_1}^{(a_1)}(\vec{p})]^\dagger\, W(\vec{p},\vec{p}')\, w_{r_2 s_2}^{(a_2)}(\vec{p}')\Big) \tag{3.58}$$

with $a_1, a_2 = \pm$ and the multiindices $i = (\vec{p}, r_1, s_1)$, $j = (\vec{p}', r_2, s_2)$. Consider interaction kernels that fulfill the relation $[W(\vec{p},\vec{p}')\,\psi(\vec{p}')]^\dagger = W(\vec{p},\vec{p}')\,[\psi(\vec{p}')]^\dagger$ (this is usually the case for kernels of physical interest): Since $[w_{rs}^{(+)}(\vec{p})]^\dagger = w_{rs}^{(-)}(\vec{p})$ we have $V_{ij}^{--} = (V_{ij}^{++})^*$ and $V_{ij}^{-+} = (V_{ij}^{+-})^*$ so that we can write

$$\begin{aligned}\langle\psi_1|\mathcal{V}\,\psi_2\rangle &= \sum_{i,j}\sum_{a_1,a_2=\pm} (b_1^{(a_1)})_i^*\, V_{ij}^{a_1 a_2}\, (b_2^{(a_2)})_j \\ &= \begin{pmatrix} b_1^{(+)} \\ b_1^{(-)} \end{pmatrix}^\dagger \begin{pmatrix} V^{++} & V^{+-} \\ (V^{+-})^* & (V^{++})^* \end{pmatrix} \begin{pmatrix} b_2^{(+)} \\ b_2^{(-)} \end{pmatrix}\end{aligned} \tag{3.59}$$

Since $b_1^{(\pm)}$ are arbitrary the Salpeter equation can now be written in matrix form as

$$\begin{aligned}&\left[\begin{pmatrix} 2\omega & 0 \\ 0 & 2\omega \end{pmatrix} + \begin{pmatrix} V^{++} & V^{+-} \\ (V^{+-})^* & (V^{++})^* \end{pmatrix}\right] \begin{pmatrix} b^{(+)} \\ b^{(-)} \end{pmatrix} = \\ = \; & M \begin{pmatrix} 1 & 0 \\ 0 & -1 \end{pmatrix} \begin{pmatrix} b^{(+)} \\ b^{(-)} \end{pmatrix}\end{aligned} \tag{3.60}$$

We identify the eigenvalues of the free hamiltonian with the kinetic energies of the free fermions as $\epsilon_A = -\epsilon_a = \omega_i$ and $\epsilon_B = -\epsilon_b = \omega_i$. Further we identify the positive eigenvalues M with $\nu_\sigma = E_\sigma - E_0$ and

$$\begin{pmatrix} b^{(+)} \\ b^{(-)} \end{pmatrix} = F^\sigma = \begin{pmatrix} X^\sigma \\ Y^\sigma \end{pmatrix} \tag{3.61}$$

Therefore we find that the Salpeter equation (3.60) has exactly the form of the RPA-equations (3.29).

In this context we would like to mention a work of J.Piekarewicz [48, 50] which gives a direct derivation of the Salpeter equation using a method similar to our derivation of the RPA equations given in section 3.2.

3.4 Conclusion

It has been shown that the RPA equations can be derived by applying the instantaneous approximation to the amputated two-fermion propagator and by approximating the full fermion propagators by the free ones. Our derivation holds for nonrelativistic as well as relativistic fermionic systems. Since in relativistic field theory the same approximations lead from the fermion-antifermion Bethe-Salpeter equation to the Salpeter equation, this equation should be equivalent to the RPA equations. We have shown explicitely that this is indeed the case.

The RPA equations have been carefully analysed by many authors, especially in the context of nuclear physics (compare e.g. the references given in [56]; the mathematical structure of the RPA equations has been investigated in refs.[11, 67]). It is interesting that these results can be transfered to the Salpeter equation, as has been done recently by J.Parramore and J.Piekarewicz [48]. These authors employed the techniques developed by Thouless in the context of nuclear collective excitations [65] to test the stability of solutions of the Salpeter equation with a scalar confinement. As discussed in more detail in chapter 4 they find an instability for this case, which is in agreement to our results presented in the following chapters.

Chapter 4

Spectra and decays for light mesons

The spectra and electroweak decay properties of light mesons are analyzed within the framework of the instantaneous Bethe-Salpeter equation. The interaction kernel comprises alternative spin-structures for a parameterization of confinement and a residual quark-antiquark interaction based on instanton effects. It is shown that only with a vector confinement the parameters can be chosen such as to yield a good description of the light pseudoscalar and vector mesons including weak and two photon decays. However it is found that it is not possible to reconcile this with the Regge behavior of higher lying meson states with the same parameter set. For the Salpeter equation with a scalar confinement we find an instability, i.e. for an increasing number of basis states the numerically obtained eigenvalues do not converge to real positive numbers, which is in agreement with results recently obtained by J.Parramore and J.Piekarewicz [48].

4.1 Introduction

In chapter 2 we analyzed the Bethe-Salpeter(BS) equation with an instantaneous interaction (Salpeter equation). We will now use this formalism as a basis for a quark model of light mesons. In spite of the intrinsic difficulties connected with the instantaneous treatment, we feel that an application to light meson systems is worthwhile, mainly because a parametrization of confinement including retardation effects is still lacking. The present treatment has a number of advantages compared to others, i.e.

- The relativistic kinematics of the quarks is treated correctly;
- The amplitudes have the correct relativistic normalization;
- The lower component Φ^{--} of the Salpeter amplitude is determined dynamically.

On the other hand the practical advantages of a nonrelativistic treatment are also present, i.e.

- The Salpeter equation can be formulated as an eigenvalue problem $\mathcal{H}\psi = M\psi$ for the mass M of the bound state.
- One can define a (not positive definite) scalar product $\langle\psi_a|\psi_b\rangle$ for the Salpeter amplitudes.
- The Salpeter operator $\mathcal{H}$ is selfadjoint with respect to this scalar product.

The numerical method developed in chapter 2 enables the calculation of meson mass spectra and the corresponding BS-amplitudes. In this chapter we have also given formulas to compute some important electroweak meson decay widths.

In this section we shall apply this method to an explicit quark model for light mesons. Our main concern in this context will be whether a realistic description of deeply bound states like the pion is compatible with a reasonable description of confinement.

Let us first give a list of the main features of light mesons that will be considered in the following:

- the low masses of π and K
- the weak decay constants f_π and f_K
- the decays π^0, η, $\eta' \to 2\,\gamma$
- the masses and the flavor mixing coefficients of η and η'
- the masses and the leptonic decay widths for the ρ, ω and ϕ mesons
- the Regge behavior $M^2 \sim J$

As far as we know there presently is no model that can describe all these features in a consistent way. On the one hand there is the nonrelativistic quark model that gives a reasonable description of the mass spectra [8, 53, 10], but that completely fails in describing the decay widths of the deeply bound states like the pion (see Sec.4.3.4). On the other hand there are models like the Nambu Jona-Lasinio model [44, 27, 69] that are based on the chiral symmetry of QCD for vanishing current quark masses. This model leads to a good description for the π, K, η and η' mesons, but higher angular momenta states or radial excitations cannot be described since confinement is ignored.

Attempts to arrive at a more complete description based on the Salpeter equation or related quasipotential equations have recently been given by J.F.Lagaë [29] and by P.C.Tiemeijer and J.Tjon [66]. Their results show the difficulty of finding a suitable ansatz for the confining interaction kernel.

The model we present in the following is based on a linear scalar or alternatively vector confining kernel combined with an effective interaction computed by 't Hooft from instanton effects in QCD [24, 62, 49]. A nonrelativistic version of this interaction has already lead to good results for the meson and baryon mass spectra [8, 53, 10]. We therefore feel encouraged to test this ansatz in the relativistic Bethe-Salpeter framework.

The chapter is organized as follows: The explicit form of the confining BS-kernel and of the 't Hooft kernel is given in Sec.4.2. In Sec.4.3 we present the calculated meson mass spectra and obtain the pion and kaon decay constants f_π, f_K, the decay width into two photons for the π^0, η and η' mesons and the leptonic widths for the vector mesons ρ, ω and ϕ. We will compare these decay widths to corresponding nonrelativistic results in Sec.4.3.4 using the wave function of ref.[8], which shows the impressive improvement due to the relativistic treatment of the quarks compared to the nonrelativistic potential model. Finally we give some concluding remarks in Sec.4.4.

4.2 The Bethe-Salpeter kernel

4.2.1 Confinement

Up to now the confining interaction of QCD is only known in the static limit of heavy quarks. In this limit it has been shown [32, 20] that the static potential between quarks is of the form $V_C(r) = a_c + b_c r + W$ where W denotes the relativistic corrections of the order p^2/m^2. As stated by Gromes [32] it is still an open question whether an additional $1/r$ term should also be included into the static confining potential. Usually one concludes from the sign of the spin-orbit coupling term in W that the confining $q\bar{q}$-interaction behaves like a Lorentz scalar.

The problem for the case of light quarks is that up to now there is no unambiguous extension of the confining potential beyond the static limit. Especially there is no prescription on how to extend it to a noninstantaneous form. Naive noninstantaneous extensions fail as has been shown by S.N.Biswas et al. [6] for the harmonic oscillator BS-kernel $V(x) = -bx^2 = b\,(\vec{x}^{\,2} - (x^0)^2)$ that yields only a continuous spectrum. Similar results are to be expected for other kernels like $1/q^4$. Because of these difficulties the only way we see at the moment is to parameterize confinement as an instantaneous interaction kernel.

The sign of the LS-term in the static limit would be compatible with a scalar confinement kernel. However some authors [17, 29] have shown that the linear Regge behavior $M^2 \sim J$ is lost for this choice, since their calculated bound state masses come out too small for higher angular momenta. This is due to the relativistic corrections to the static potential and becomes more problematic with decreasing quark masses. Recently J.Parramore and J.Piekarewicz [48] gave

an analytical argument that the Salpeter equation with a scalar confinement even leads to an instability, i.e. purely imaginary eigenvalues. In our framework this is reflected by the fact that for an increasing number of basis states the obtained eigenvalues do not converge to real positive numbers, but finally become imaginary [38].

In the context of nuclear collective excitations treated in the RPA approach this signals the instability of the ground state against the formation of particle-hole pairs. However, it is not clear if this interpretation can be reasonably transfered to the Salpeter equation. It is interesting to note that for relativistic quasipotential approaches, which converge to the Dirac equation in the case of a heavy-light $q\bar{q}$ state, the instability occures for a vector confinement, whereas a scalar confinement leads to stable results [66]. The same holds for the Dirac equation itsself [39]. This indicates that the observed instability of the Salpeter equation with a scalar confinement might be a defect of the instantaneous approximation.

J.Parramore and J.Piekarewicz [48] further suggest that the instability will persist even for large values of the constituent quark mass. Nevertheless the numerical solutions aquire a quasistable character in this case, as will be shown in detail in the following sections.

For a vector confining kernel the instability problem is not present, but in the static limit a vector kernel leads to an LS-term which has the wrong sign.

To our knowledge there presently is no convincing parameterization for the confining kernel that exhibits both features, i.e. leads to linear Regge trajectories and yields a spin-orbit term with the correct sign.

In the following we will analyze both spin structures for the confinement, i.e. a scalar $1 \otimes 1$ and a vector $\gamma^0 \otimes \gamma^0$ interaction. In the rest frame of the bound state the corresponding BS-kernels in eq.(2.9) are parameterized as

$$\left[V_C^V(\vec{p},\vec{p}\,')\,\Phi(\vec{p}\,')\right] = -\mathcal{V}_C((\vec{p}-\vec{p}\,')^2)\,\gamma^0\,\Phi(\vec{p}\,')\,\gamma^0 \tag{4.1}$$

$$\left[V_C^S(\vec{p},\vec{p}\,')\,\Phi(\vec{p}\,')\right] = \mathcal{V}_C((\vec{p}-\vec{p}\,')^2)\,\Phi(\vec{p}\,') \tag{4.2}$$

where $\mathcal{V}_C$ is a scalar function which has the fourier transform $\mathcal{V}_C^F(r) = a_c + b_c r$ in analogy to nonrelativistic quark models (note that in the nonrelativistic limit $\mathcal{V}_C^F(r)$ becomes the potential in the Schrödinger equation).

4.2.2 't Hooft interaction

The 't Hooft lagrangian

It is already known from nonrelativistic potential models that the masses of the scalar and pseudoscalar mesons π, K, η, η' cannot be described with a confining potential alone. The usual extension would be to add another contribution to the interaction kernel that comes from One Gluon Exchange (OGE). This works

quite well for heavy quarkonia [5, 17] (see also chapter 5). For light mesons, however, the flavor independent OGE leads to degenerate π and η meson masses in clear contradiction to the experimental mass values $m_\pi = 140\,MeV$ and $m_\eta = 549\,MeV$. In order to cure this discrepancy one would have to take into account higher order diagrams.

There is another QCD based candidate for a residual $q\bar{q}$-interaction computed by 't Hooft and others from instanton effects [24, 62, 49] which has the appropriate flavor dependence to solve this problem. This has been shown within a nonrelativistic potential model [8], where a good description of the meson and baryon mass spectra has been obtained.

Instantons are special solutions of the classical nonabelian Yang-Mills equations in Euclidian space. They are peaked both in space and imaginary time having a finite extension ρ. Since they cannot be deformed continuously into classical solutions corresponding to gluon fields they lead to an effective interaction between quarks that is not covered by perturbative gluon diagrams. This interaction leads to spontaneous breaking of chiral symmetry as can be seen by normal ordering of the underlying Lagrangian (see appendix C). The normal ordered Lagrangian takes the form

$$\mathcal{L} = k + \sum_{j=1}^{3} :(i\bar{q}_j\gamma^\mu\partial_\mu q_j - m_j\,\bar{q}q): + \Delta\mathcal{L}(2) + \Delta\mathcal{L}(3) \tag{4.3}$$

where k is an inessential constant that renormalizes the vacuum energy. $\Delta\mathcal{L}(2)$ and $\Delta\mathcal{L}(3)$ are two and three body terms and $m_j = m_j^0 + \Delta m_j$ is the effective constituent quark mass. In the following we will consider these terms.

The constituent quark mass

The contribution Δm_j to the effective constituent quark mass $m_j = m_j^0 + \Delta m_j$ is given by

$$\begin{aligned}
\Delta m_n &= \int_0^{\rho_c} d\rho \frac{d_0(\rho)}{\rho^5}\frac{4}{3}\pi^2\rho^3\left(m_n^0\rho - \frac{2}{3}\pi^2\rho^3\langle\bar{q}_n q_n\rangle\right)\left(m_s^0\rho - \frac{2}{3}\pi^2\rho^3\langle\bar{q}_s q_s\rangle\right) \\
\Delta m_s &= \int_0^{\rho_c} d\rho \frac{d_0(\rho)}{\rho^5}\frac{4}{3}\pi^2\rho^3\left(m_n^0\rho - \frac{2}{3}\pi^2\rho^3\langle\bar{q}_n q_n\rangle\right)^2
\end{aligned} \tag{4.4}$$

where the instanton density for three colors and three flavors reads [63]

$$d_0(\rho) = (3.63\cdot 10^{-3})\left(\frac{8\pi^2}{g^2(\rho)}\right)^6 \exp\left(-\frac{8\pi^2}{g^2(\rho)}\right) \tag{4.5}$$

with

$$\left(\frac{8\pi^2}{g^2(\rho)}\right) = 9\ln\left(\frac{1}{\Lambda_{QCD}\,\rho}\right) + \frac{32}{9}\ln\ln\left(\frac{1}{\Lambda_{QCD}\,\rho}\right) \tag{4.6}$$

within two loop accuracy [64]. Here $\Lambda_{_{QCD}}$ is the QCD scale parameter. The integration over the instanton size ρ has to be carried out up to a cutoff value ρ_c where the $ln\,ln$ term from the two loop correction is still small compared to the ln term.

Equations of type (4.4) are usually called Gap equations. They describe the generation of a dynamical quark mass due to the interaction with the negative Dirac see. In our model the constituent quark masses m_j will be used as free parameters that are fitted to the experimental data. It will be checked in the end (see Sec.4.3.5) whether the obtained quark masses are compatible with common values for the quark condensates present in Δm_j assuming that the confinement interaction does not contribute essentially to the process of chiral symmetry breaking.

The two body interaction

The two body term reads (see appendix C)

$$\Delta\mathcal{L}(2) = -\frac{3}{16}\sum_i\sum_{kl}\sum_{mn} g_{\rm eff}(i)\,\varepsilon_{ikl}\varepsilon_{imn} \\ \Big\{ : q_k^\dagger q_l^\dagger \left[\gamma_0\cdot\gamma_0 + \gamma_0\gamma_5\cdot\gamma_0\gamma_5\right](2\mathcal{P}_{\bar{3}}^C + \mathcal{P}_6^C)\, q_m q_n : \Big\} \tag{4.7}$$

where the effective coupling constants are given as

$$g_{\rm eff}(i) = \int_0^{\rho_c} d\rho \frac{d_0(\rho)}{\rho^5}\left(\frac{4}{3}\pi^2\rho^3\right)^2\left(m_i^0\rho - \frac{2}{3}\pi^2\rho^3\langle\bar{q}_i q_i\rangle\right) \tag{4.8}$$

and the tensor notation

$$q^\dagger q^\dagger\,(A\cdot B)\,q\,q := \sum_{i,j}\sum_{k,l} q_i^\dagger q_j^\dagger\, A_{ik}\cdot B_{jl}\, q_k q_l \tag{4.9}$$

has been used for Dirac and color indices. This representation explicitly shows the antisymmetric flavor dependence of the interaction. The color sextett and antitriplett projection matrices are given by

$$\mathcal{P}_6^C = \frac{1}{2}(1^C + \Pi^C) = \frac{2}{3}1^C + \frac{1}{4}\vec{\lambda}\cdot\vec{\lambda} \tag{4.10}$$

$$\mathcal{P}_{\bar{3}}^C = \frac{1}{2}(1^C - \Pi^C) = \frac{1}{3}1^C - \frac{1}{4}\vec{\lambda}\cdot\vec{\lambda} \tag{4.11}$$

so that

$$2\mathcal{P}_{\bar{3}}^C + \mathcal{P}_6^C = \frac{1}{2}(3\,1^C - \Pi^C) = \frac{4}{3}1^C - \frac{1}{4}\vec{\lambda}\cdot\vec{\lambda} \tag{4.12}$$

where Π^C is a color exchange matrix defined as $\Pi^C_{ij,kl} = \delta_{il}\,\delta_{jk}$ and λ^a $(a = 1,\ldots,8)$ are the $SU(3)$ color matrices. Just like the quark masses also the coupling constants will be treated as free parameters in our model.

The three body interaction

After a lengthy calculation the three body force can finally be written in the form

$$\begin{aligned}\Delta\mathcal{L}(3) &= \frac{27}{80} g_{\rm eff}^{(3)} \Big\{ : \, q^\dagger q^\dagger q^\dagger \\ &\quad [\gamma_0 \cdot \gamma_0 \cdot \gamma_0 + \gamma_0\gamma_5 \cdot \gamma_0\gamma_5 \cdot \gamma_0 \\ &\quad + \gamma_0\gamma_5 \cdot \gamma_0 \cdot \gamma_0\gamma_5 + \gamma_0 \cdot \gamma_0\gamma_5 \cdot \gamma_0\gamma_5] \\ &\quad \mathcal{P}_1^F (2\mathcal{P}_{10}^C + 5\mathcal{P}_8^C)\, qqq \, : \Big\} \end{aligned} \tag{4.13}$$

where $\mathcal{P}_1^F$ is the projector onto a three-particle flavor singulett state, $\mathcal{P}_{10}^C$ and $\mathcal{P}_8^C$ are projectors onto the color decuplett and the color octett. The effective three-body coupling constant is given by

$$g_{\rm eff}^{(3)} = \int_0^{\rho_c} d\rho \, \frac{d_0(\rho)}{\rho^5} \, \left(\frac{4}{3} \pi^2 \rho^3 \right)^3 \tag{4.14}$$

Obviously this three body force does not contribute to $q\bar{q}$-states and to colorfree qqq-states.

The 't Hooft kernel

In order to distinguish different indices in the following we will use the notation s_i for Dirac indices, c_i for color indices and f_i for flavor indices. The vertex corresponding to $\Delta\mathcal{L}_2$ is shown in Fig.4.1. As shown in appendix C.3 the vertex

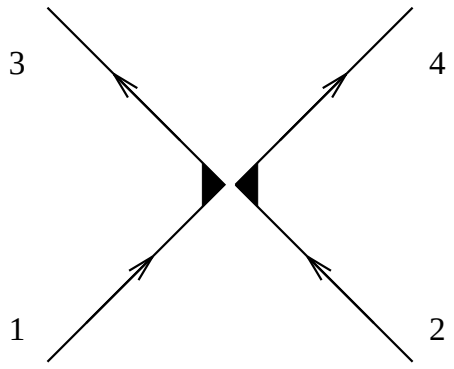

Figure 4.1: Instanton induced interaction vertex corresponding to $\Delta\mathcal{L}_2$.

reads

$$\begin{aligned}&(-i)\, G_{f_3 f_4, f_1 f_2} \, (1_{s_3 s_1} 1_{s_4 s_2} + \gamma^5_{s_3 s_1} \gamma^5_{s_4 s_2}) \\ &(4/3 \; 1_{c_3 c_1} \, 1_{c_4 c_2} - 1/4 \; \vec{\lambda}_{c_3 c_1} \vec{\lambda}_{c_4 c_2}) \end{aligned} \tag{4.15}$$

with the definition

$$G_{f_3f_4,f_1f_2} := \frac{3}{8}\sum_{f_5} g_{\rm eff}(f_5)\,\epsilon_{f_5f_3f_4}\,\epsilon_{f_5f_1f_2} \tag{4.16}$$

For the $q\bar{q} \to q\bar{q}$ amplitude we have to consider the two diagrams given in Fig.4.2. In a meson the quark and the antiquark are in a color singulett state represented

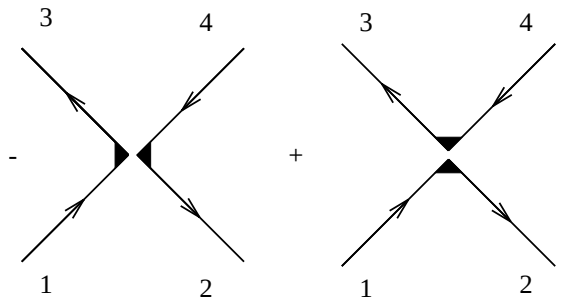

Figure 4.2: Instanton induced interaction vertices for $q\bar{q} \to q\bar{q}$.

by the matrix $\chi^C_{c_1c_2} = \delta_{c_1c_2}/\sqrt{3}$. The color matrix elements for the two vertices are then given by

$$\sum_{c_1c_2}\sum_{c_3c_4} (\chi^C_{c_3c_4})^* \frac{1}{2}\left(3\,1_{c_3c_1}1_{c_2c_4} - \Pi_{c_3c_2,c_1c_4}\right)\chi^C_{c_1c_2} \;=\; 0 \tag{4.17}$$

$$\sum_{c_1c_2}\sum_{c_3c_4} (\chi^C_{c_3c_4})^* \frac{1}{2}\left(3\,1_{c_3c_4}1_{c_2c_1} - \Pi_{c_3c_2,c_4c_1}\right)\chi^C_{c_1c_2} \;=\; 4 \tag{4.18}$$

so that only the second vertex in Fig.4.2 contributes to the interaction kernel. The effective 't Hooft interaction vertex between $q\bar{q}$ color singulett states is then given by

$$(-4i)\,G_{f_2f_3,f_1f_4}(1_{s_3s_4}1_{s_2s_1} + \gamma^5_{s_3s_4}\gamma^5_{s_2s_1}) \tag{4.19}$$

Since we assume $SU(2)$-flavor invariance of the interaction we set

$$g := \frac{3}{8}g_{\rm eff}(s) \quad , \quad g' := \frac{3}{8}g_{\rm eff}(n) \tag{4.20}$$

Table 4.1: Flavor matrix elements of $G_{f_2f_3,f_1f_4}$ for pseudoscalar mesons

	π^0	η_n	η_s
π^0	-g	0	0
η_n	0	g	$\sqrt{2}$ g'
η_s	0	$\sqrt{2}$ g'	0

Table 4.2: Flavor dependence of the instanton induced interaction $G_{f_2f_3,f_1f_4}$ (see eq.(4.16))

$f_1f_2 \rightarrow$ $f_3f_4 \downarrow$	ud	$d\bar{u}$	$u\bar{s}$	$d\bar{s}$	sd	$s\bar{u}$	$u\bar{u}$	dd	$s\bar{s}$
ud	-g	0							
$d\bar{u}$	0	-g							
$u\bar{s}$			-g'	0	0	0			
$d\bar{s}$			0	-g'	0	0			
$s\bar{d}$			0	0	-g'	0			
$s\bar{u}$			0	0	0	-g'			
$u\bar{u}$							0	g	g'
$d\bar{d}$							g	0	g'
$s\bar{s}$							g'	g'	0

where s stands for strange and n stands for nonstrange (u,d) flavor. The results for $G_{f_2f_3,f_1f_4}$ are given in Tab.4.2. Tab.4.1 shows the matrix elements of $G_{f_2f_3,f_1f_4}$ for the flavor functions

$$\pi^0 = (u\bar{u} - d\bar{d})/\sqrt{2} \tag{4.21}$$

$$\eta_n = (u\bar{u} + d\bar{d})/\sqrt{2} \tag{4.22}$$

$$\eta_s = s\bar{s} \tag{4.23}$$

From the vertex we can extract the lowest order contribution of the 't Hooft interaction to the BS-kernel as

$$[V_T(\vec{p},\vec{p}\,')\,\Phi(\vec{p}\,')]_{f_1f_2} = 4\sum_{f_1'f_2'} G_{f_2f_1',f_1f_2'} \left[1\,\mathrm{tr}\left(\Phi_{f_1'f_2'}(\vec{p}\,')\right) + \gamma^5\,\mathrm{tr}\left(\Phi_{f_1'f_2'}(\vec{p}\,')\,\gamma^5\right)\right] \tag{4.24}$$

As shown in the appendix this interaction only acts on the scalar and pseudoscalar mesons $J^{\pi_P} = 0^{\pm}$. For the pseudoscalar mesons it is attractive for the π meson with a coupling constant g and for the K meson with a coupling constant g'. For the η and η' mesons the interaction leads to mixing of nonstrange and strange flavor amplitudes. The effective sign of the interaction is reversed for the scalar mesons thus being repulsive for the a_0. Note that in the nonrelativistic limit the 't Hooft interaction only acts on the pseudoscalar states $J^{\pi_P} = 0^-$. The 't Hooft kernel as it stands represents a pointlike interaction that has to be regularized. Following ref.[8] we do this by multiplying the kernel with a regularizing Gaussian function

$$\mathcal{V}_{\mathrm{reg}}(q) = e^{-\frac{1}{4}\Lambda^2 q^2} \tag{4.25}$$

with $\vec{q} = \vec{p} - \vec{p}'$ and $q = |\vec{q}|$. In coordinate space this choice corresponds to replacing the $\delta(\vec{r})$ function by

$$\mathcal{V}^F_{\rm reg}(r) = \frac{1}{(\Lambda\sqrt{\pi})^3}\, e^{-\frac{r^2}{\Lambda^2}} \tag{4.26}$$

which introduces a finite effective range Λ.

4.3 Results and discussion

4.3.1 Models and Parameters

The main concern of this chapter was to see whether we can obtain a consistent description of a) the masses and decays of the low lying pseudoscalar and vector mesons and b) confinement reflected e.g. by the Regge trajectories.

For this purpose we investigate two different models of the confinement kernel: 1) a vector $\gamma^0 \otimes \gamma^0$- and 2) a scalar $1 \otimes 1$-structure.

The parameters used are the nonstrange and strange quark masses m_n and m_s, the offset a_c and slope b_c of the confinement interaction, the two coupling constants g, g' and the effective range Λ of the residual instanton induced interaction. So the total number of parameters amounts to seven.

We used two sets of parameters in the vector confinement case: Model V1 was tuned to reproduce the masses and decays of the low lying mesons. We therefore used a small nonstrange quark mass m_n, as the correct description of the pseudoscalar decays depends essentially on this quantity. Given this mass we had to take a moderate confinement slope to reproduce the decays of the vector mesons. The offset a_c was fixed by the ρ-mass and m_s by the K^*-mass. Finally g and g' were fixed by the masses of the pseudoscalars π, η and K. In Model V2 we used a larger nonstrange mass of m_n of about 1/3 of the nucleon mass, which is a value common to Nonrelativistic Quark Models. The aim of this parameter set was to obtain a good description of the Regge trajectories and the higher lying resonances. Note that the slope of the confining potential comes out larger than in nonrelativistic models, where a typical value is $b_c \approx 850$ MeV/fm [8].

Finally in Model S we investigated a scalar confinement provided with the same quark mass m_n as in V2. As shown in fig.4.5 the obtained eigenvalues do not converge to real positive numbers for an increasing number of basis states, but finally become purely imaginary. However for higher quark masses this instability quickly becomes less visible, and the eigenvalue aquires a quasistable character.

It is clear that for large enough quark masses the instability should become rather spurious, since in the nonrelativistic limit the Salpeter equation leads to the Schrödinger equation, where such an instability does not exist. As shown by J.Parramore and J.Piekarewicz [48] the reason for the instability can be traced back to the existence of negative energy amplitudes in the Salpeter equation.

Table 4.3: Parameters of the different models (see Sec.4.3.1)

Parameter	V1	V2	S
m_n[MeV]	170	340	340
m_s [MeV]	390	568	487
a_c [MeV]	-552	-1340	-998
b_c [MeV/fm]	570	1400	1000
g [MeV fm^3]	51.67	34.65	44.79
g' [MeV fm^3]	46.92	30.84	41.01
Λ [fm]	0.42	0.42	0.42

The coupling of positive and negative energy components induced by the scalar confinement implies that for momenta larger than the constituent quark mass the confining potential shifts from an effectively rizing into a sliding regime.

By solving the Salpeter equation within a small number of basis states one effectively introduces a momentum cutoff, i.e. the sliding regime will be missed — and so will the instability — whenever the constituent mass exceeds the value of the cutoff. Consequently for higher quark masses only for a dramatically increasing number of basis states this instability will be relevant, whereas numerical solutions obtained with a smaller number of basis states aquire a quasistable character, i.e. are almost independant of the exact number of basis states taken into account. Since for high momenta the instantaneous approximation should be less valid anyway, a quasistable numerical solution ψ can be considered as a physically reasonable approximate solution to the Salpeter equation in the sense that $\langle e_i | \mathcal{H} \psi \rangle = M \langle e_i | \psi \rangle$ is fullfilled exactly, where $i = 1 \ldots i_{max}$ labels the basis functions e_i taken into account (compare chapter 2.4 for the notation).

In the following these quasistable masses will be given for model S provided the quasistable character is indeed present. This is the case for small angular momenta and as long as the fraction of the confinement slope b_c and the quark mass m_q is sufficiently small.

The parameters for the three models are listed in Tab.4.3.

4.3.2 Mass spectra

The quality of the mass spectra is different for the three models, as different priorities led us to the parameters. Common to all three models is an overall agreement of the masses of the pseudoscalars π, K, η, η' and the vector mesons ρ, ω, ϕ, K^*. The spectra for these mesons are compared to experimental data in Figs. 4.3, 4.4. The 't Hooft interaction leads to the correct splitting of π, η and η' mass. In contrast to experiment, where the a_0 and f_0 mesons are nearly degenerate, we obtain a large splitting due to the instanton induced interaction of several hundred MeV (compare Tab.4.4). For a vector type kernel with positive spin orbit splitting this leads an enormous attraction in the f_0 channel: allthough there is a scalar state at roughly 1GeV, we also find a state with imaginary mass and zero norm. The physical interpretation of this phenomenon however is not clear. For a scalar confinement this effect is compensated by the negative spin orbit splitting. In the following we will discuss the differences of the three parameter sets.

Since in model V1 we used a small confinement slope to reproduce the decays of the vector mesons, the calculated Regge trajectory is too flat (see Fig.4.6). The spin-orbit splitting between the 1^{++} and 2^{++} mesons in our model is purely due to the confining interaction. In both models with a vector kernel this splitting is about 200 MeV and thus exceeds the experimental mass difference, which is in fact rather small (see Tab.4.4).

In model V2 with large quark masses and large confinement slope b_c we obtain a good description of the masses of all mesons comparable to results of nonrelativistic calculations. However b_c has to be much larger in the BS framework, as the kinetic energy is obviously overestimated in nonrelativistic calculations. The Regge trajectories representing the confinement property are well reproduced (Fig.4.6). For the spin-orbit splitting the same remarks as for V1 apply.

Finally the quasistable solutions of model S give a reasonable description of the ground states of the pseudoscalar and vector mesons. For the states with large angular momentum the quasistable character of the solutions is less prominent. As mentioned above the method of solving the BS equation by a basis expansion does not lead to convergent solutions with positive norm. With increasing dimension of the basis the smallest positive eigenvalue decreases until it becomes imaginary (see fig.4.5; a similar problem arises if one studies a $\gamma_\mu \otimes \gamma^\mu$ interaction). For these reasons we also omitted in the Regge plot the state with angular momentum j=4. The f_1 meson mass is larger than the mass of the f_2 meson. Taken together with the results for the vector case this indicates that the spin-orbit splitting can only be explained by a mixture of scalar and vector type interaction, as will be investigated in chapter 6.

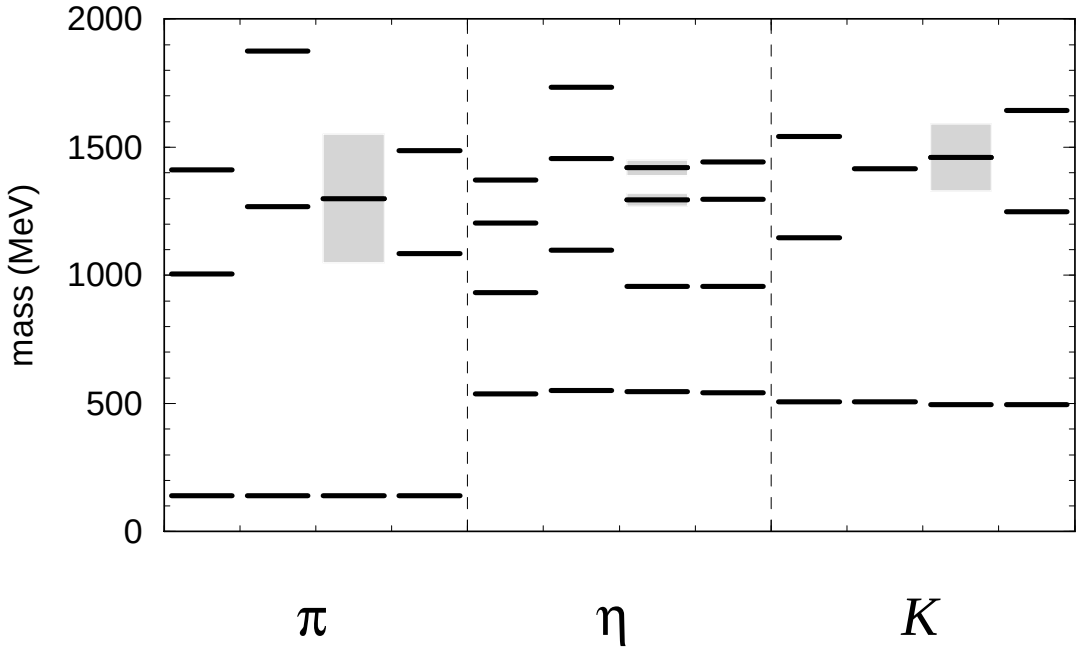

Figure 4.3: Mass spectra of the pseudoscalar mesons. The columns for each meson correspond (from the left) to model V1, model V2, experiment [47] and model S. The shaded areas (3rd column) indicate the experimental full width of the meson.

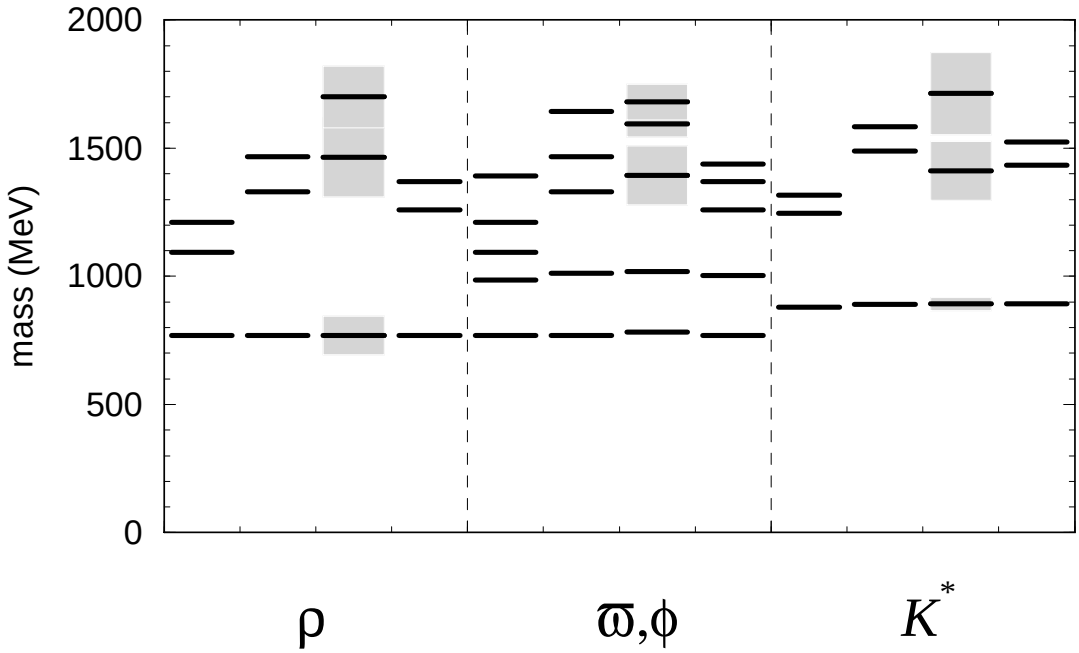

Figure 4.4: Mass spectra of the vector mesons (see also caption to Fig. 4.3).

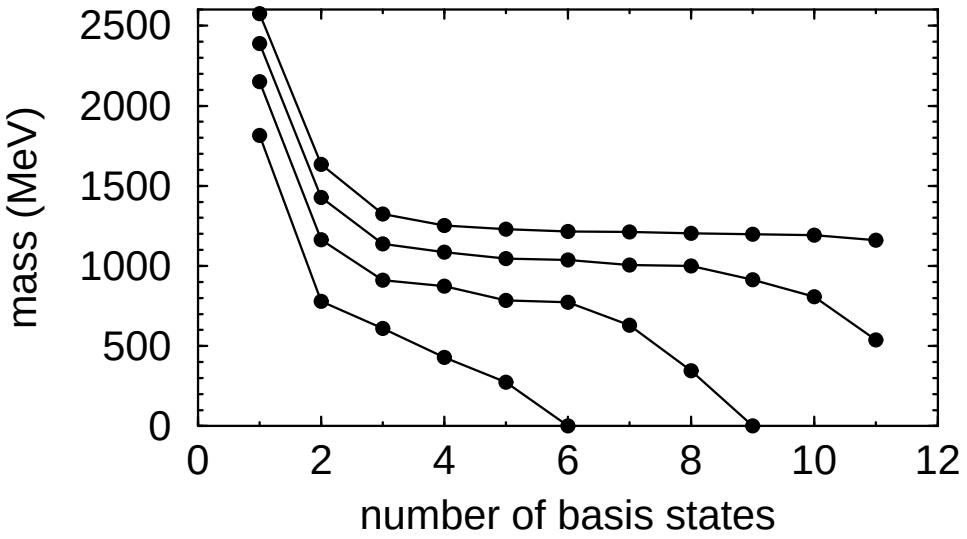

Figure 4.5: Dependence of the calculated Salpeter eigenvalues for a state with $J^{PC} = 0^{-+}$ on the number of basis states taken into account. The four curves correspond to the quark masses $m_q = 200\,MeV$ (lowest curve), 250, 300 and $350\,MeV$ (upper curve). For the interaction kernel a pure scalar confinement (i.e. without 't Hooft interaction) with $a_c = 0$ and $b_c = 1000$ MeV/fm has been used. The radial part of the basis states in momentum space is given by $R_{nL}(y) = N_{nL}\, y^L\, L_n^{2L+2}(y)\, e^{-y/2}$ with $y = p\beta$ and $L_n^{2L+2}(y)$ being a Laguerre polynomial. We used $\beta = 5.0\,fm$ here.

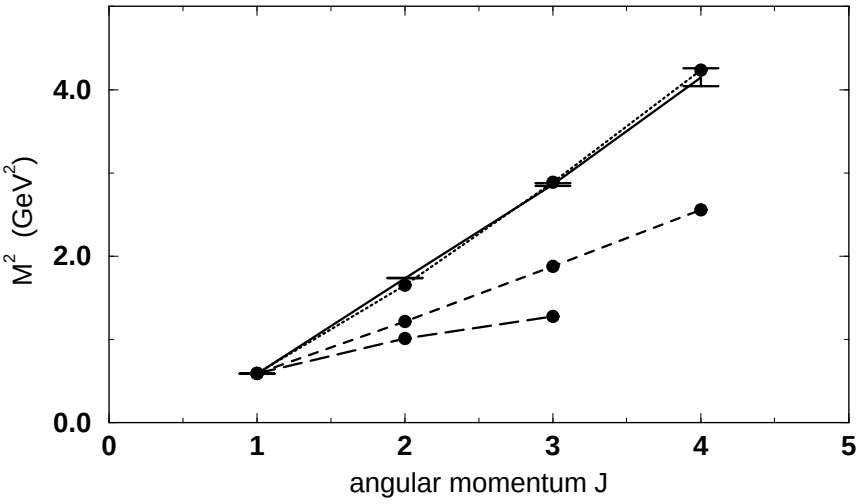

Figure 4.6: Regge trajectory for the isovector mesons with $S = 1$. The solid line shows the experimental masses for ρ, a_2, ρ_3, a_4 [47] where the errorbar gives the experimental error for the resonance position. The short dashed line corresponds to the calculated masses of model V1, the dotted line to model V2 and the long dashed line to the scalar confinement (model S).

Table 4.4: Spin orbit splitting for the first positive parity mesons and the effect of the instanton induced interaction on the 0^{++} mesons, where a * denotes the existence of an additional state with imaginary mass and zero norm, see Sec.4.3.2 (all Masses in MeV).

Meson	J^{PC} I	V1	V2	S
$a_0(980)$	0^{++} 1	960	1130	1260
$f_0(975)$	0^{++} 0	950*	1270*	950
$f_1(1285)$	1^{++} 0	930	1060	1150
$f_2(1270)$	2^{++} 0	1100	1280	1010

4.3.3 Decay Observables

In this section we will discuss the influence of the parameters on the decay observables of the pseudoscalar and vector mesons.

The parameters of Model V1 have been chosen in order to give a good description of the masses and the decays of the pseudoscalar and vector ground states. Tab.4.5 shows that we obtain an almost quantitative agreement. As an important result we consider the fact that the π and η can be described within the present framework, albeit with relatively small quark masses. This is reflected in the simultaneous agreement we obtain for the pion decay constant f_π and the decay width $\pi^0 \to \gamma\gamma$, which in the Goldstone picture are related to the Adler Bell Jackiv anomaly [1]. It becomes clear that a relativistic treatment of the decay formula and of the normalization are important for a correct understanding of the pion as deeply bound quark antiquark state. This can also be seen in Fig.4.7 showing the upper and lower component Φ^{++}, Φ^{--} of the pion amplitude. In contrast to the wave function for the ρ meson (Fig.4.8) the upper pion amplitude is only about 10% larger than the lower one in the region of small relative momenta. For higher momenta the amplitudes even become equal. This fact obviously leads to important cancellations for the normalization and for the decay constant. This was already emphasized in an earlier quark model [31], where the effects of different estimates for the relation between the upper and lower component on weak decay constants for pion and kaon were analyzed. For a comparison with nonrelativistic decay formulas compare Sec.4.3.4. Although the pion amplitude has significant contributions up to momenta of about 4GeV/c, the main part e.g. of the integral for the π^0 decay width comes from momenta of about 150 MeV/c (as this is the scale of nonstrange and pion mass).

For the $\eta \to \gamma\gamma$ decay we also find excellent agreement with experiment, whereas the process for the η' is underestimated. The results depend strongly on the correct $n\bar{n}$- $s\bar{s}$ mixing, as e.g. for the η we obtain a negative interference. The mixing (due to the instanton induced interaction) can be compared to a simple

Table 4.5: Comparison of experimental and calculated meson decay observables for the Salpeter models V1, V2, S and nonrelativistic results NR

Mesonic decay	experimental [47]	V1	V2	S	NR
f_π [MeV]	131.7± 0.2	130	260	200	1440
f_K [MeV]	160.6 ± 1.4	180	300	210	730
$\Gamma(\pi^0 \to \gamma\gamma)$ [eV]	7.8 ± 0.5	7.6	4.0	4.4	30000
$\Gamma(\eta \to \gamma\gamma)$ [eV]	460 ± 5	440	220	220	18500
$\Gamma(\eta' \to \gamma\gamma)$ [eV]	4510 ± 260	2900	2030	1390	750
$\Gamma(\rho \to e^+e^-)$ [keV]	6.8 ± 0.3	6.8	28	8.1	8.95
$\Gamma(\omega \to e^+e^-)$ [keV]	0.60 ± 0.02	0.73	3.1	0.87	0.96
$\Gamma(\phi \to e^+e^-)$ [keV]	1.37 ± 0.05	1.24	4.5	1.50	2.06

Table 4.6: η, η' mixing parameters from BS norm (see eq.(2.31)) compared to data calculated from experimental J/Ψ decays [3]

Meson	mixing coefficient	J/Ψ decay	V1	V2	S
$\eta(547)$	$\lvert X_\eta \rvert$	0.63±0.06	0.71	0.71	0.70
	$\lvert Y_\eta \rvert$	0.83±0.13	0.70	0.70	0.72
$\eta'(958)$	$\lvert X_{\eta'} \rvert$	0.36±0.05	0.85	0.78	0.83
	$\lvert Y_{\eta'} \rvert$	0.72±0.12	0.52	0.63	0.55

model given by Rosner [59]. The physical mesons are expanded in a basis of three states $|N>= 1/\sqrt{2}\,|u\bar{u} + d\bar{d}>$, $|S>= |s\bar{s}>$ and $|G>= |Gluonium>$:

$$|\eta>= X_\eta|N> +Y_\eta|S> +Z_\eta|G> \tag{4.27}$$

The coefficients may be estimated from electromagnetic transitions [3]. We compared the results for the absolute values of X and Y in Tab.4.6 with the contributions of the nonstrange and strange part of the amplitude to the relativistic norm. The results agree well in the case of the η, but not for the η'. Experimental results indicate a larger gluonic component for the η', which could modify the results.

The leptonic decay widths for the vector mesons are also in good agreement with the data. This is essentially due to the small confinement slope, which determines the size of these mesons. We conclude that a consistent description of all the ground state pseudoscalar and vector mesons is possible in this framework. More observables like electromagnetic transitions or the pion form factor are calculated in ref.[37] to substantiate this statement.

The agreement with experimental data for model V2, which was designed

to reproduce the higher resonances and Regge trajectories, is only of a qualitative character (Tab.4.5). Decay constants and photon decay widths disagree by about 50%, which is essentially due to the large quark mass. The leptonic decay widths of the vector mesons are overestimated due to the steep confinement, which enlarges the amplitudes at the origin in coordinate space.

Comparing the two parameter sets for vector confinement we find: V1 with light quark masses gives a quantitative description for the vector and pseudoscalar ground states, but only a qualitative picture of the Regge behavior. For V2 with large quark masses the situation is opposite. This might be an indication that for large distances the mass of the quarks effectively should increase due to some additional contribution from the energy of a gluon string connecting the quarks.

For model S we find good agreement for the vector mesons, the description of the pseudoscalars being of moderate quality. Although it is possible to describe the latter with a smaller quark mass, we could not obtain a quantitative adjustment for both 0^- and 1^- mesons with a scalar confining kernel. This is mainly due to the strong influence of the instability for small quark masses discussed above.

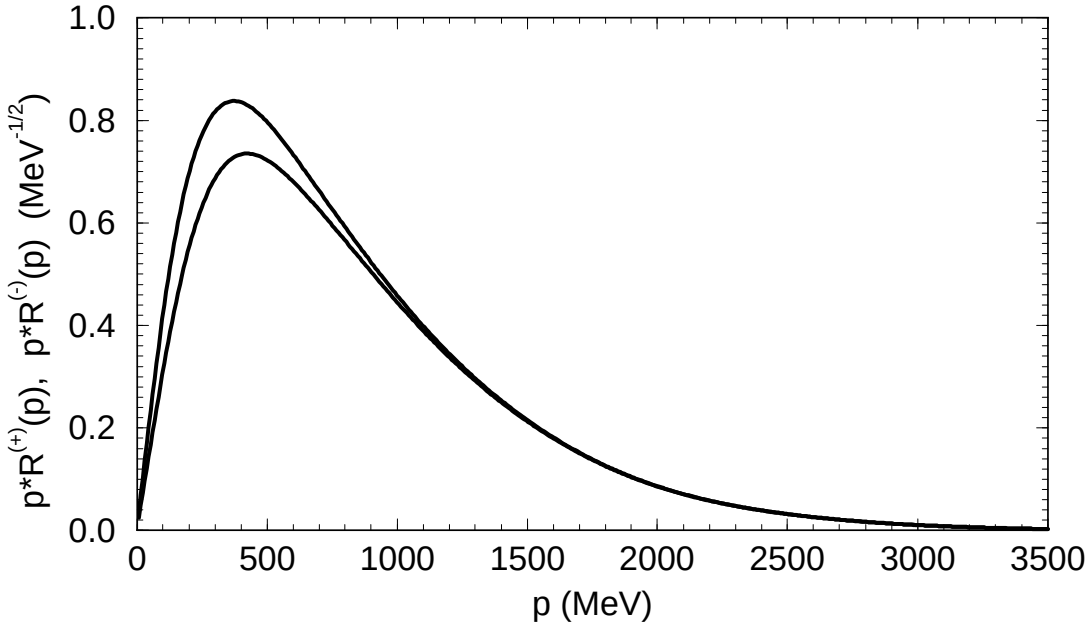

Figure 4.7: Radial Pion amplitudes $p\,\mathcal{R}_{00}^{(+)}(p)$ (upper component, upper curve) and $p\,\mathcal{R}_{00}^{(-)}(p)$ (lower component, lower curve) with the parameters of model V1

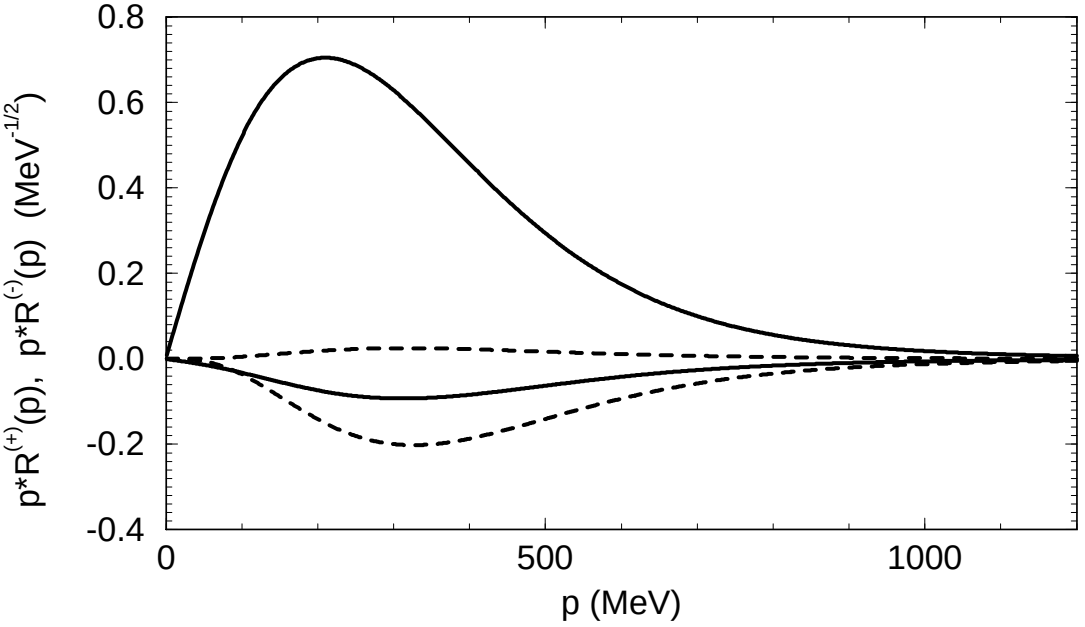

Figure 4.8: Radial Rho amplitudes $p\,\mathcal{R}_{01}^{(+)}(p)$ (upper s-wave component, upper solid curve), $p\,\mathcal{R}_{01}^{(-)}(p)$ (lower s-wave component, lower solid curve), $p\,\mathcal{R}_{21}^{(+)}(p)$ (upper d-wave component, upper dashed curve), $p\,\mathcal{R}_{21}^{(-)}(p)$ (lower d-wave component, lower dashed curve) with the parameters of model V1

4.3.4 Comparison with nonrelativistic results

In order to estimate the relevance of relativistic effects in our model it is useful to compare the results with the corresponding values computed in the nonrelativistic quark model. In the nonrelativistic limit the Salpeter equation reduces to the usual Schrödinger equation with the potential given by

$$V = a_c + b_c r + 8\, G_{f_2 f_1', f_1 f_2'}\, \delta^3(\vec{r}) \tag{4.28}$$

where the δ-function again has to be regularized according to eq.(4.26). The mass spectra for this hamiltonian have already been investigated in an earlier work [8] being in good agreement with experiment. In the following we will use the wave functions $\psi(\vec{r})$ of ref.[8] to calculate the decay observables using the well known formulas [5, 57, 28]

$$f_\pi = \frac{2\sqrt{3}}{\sqrt{M}} |\psi(0)| \tag{4.29}$$

$$\Gamma(1^- \to l^+ l^-) = \frac{16\,\pi\,\alpha^2\,\tilde{e}_q^2}{M^2} |\psi(0)|^2 \tag{4.30}$$

$$\Gamma(0^- \to \gamma\gamma) = \frac{12\,\pi\,\alpha^2\,\tilde{e}_q^4}{m_q^2} |\psi(0)|^2 \tag{4.31}$$

$$\tag{4.32}$$

Here M is the (experimental) meson mass, m_q is the quark mass, $\alpha = 1/137$ and $\tilde{e}_q$ gives the quark charge in units of the proton charge according to the flavor composition of the meson. The results for these decays are given in Tab.4.5. One finds that leptonic decays can already be described reasonably in a nonrelativistic framework. On the other hand the weak decay constants and especially the two photon decay widths are far away from the experimental data. This discrepancy cannot be cured by changing the parameters within reasonable limits. We therefore conclude that a relativistic treatment is essential for the description of pseudoscalar mesons.

4.3.5 Discussion of the gap equations

Due to the process of chiral symmetry breaking the 't Hooft interaction leads to relations for the effective constituent quark masses m_n, m_s and the coupling constants g, g' as given in eqs.(4.4),(4.8). In order to check if these relations are qualitatively compatible with the fitted parameter sets we use $\Lambda_{QCD} = 200\,MeV$, $m_n^0 = 9\,MeV$, $m_s^0 = 150\,MeV$, $\langle\bar{q}_n q_n\rangle = (-225\,MeV)^3$ and $\langle\bar{q}_s q_s\rangle = 0.8\,\langle\bar{q}_n q_n\rangle$ (compare ref.[51]) and plot m_n, m_s, g and g' as functions of the instanton size cutoff ρ_c as shown in Figs.4.9,4.10. Because of the delicate dependence on the condensate values and due to the regularization procedure in the 't Hooft kernel one should not expect quantitative agreement with the fitted parameter sets.

For $\rho_c = 0.408\,fm$ one finds e.g. $m_n = 170\,MeV$, $m_s = 270\,MeV$, $g = 79\,MeV\,fm^3$ and $g' = 58\,MeV\,fm^3$. Apart from the strange quark mass which comes out too small, the other parameters are quite close to the values of parameter set V1. Note that ρ_c is almost equal to the effective range Λ of the 't Hooft interaction. Furthermore we find that g' is smaller than g for all values of ρ_c as is the case for all three parameter sets.

4.4 Summary and conclusion

We investigated different models for light mesons as bound states of quark and antiquark within the Salpeter framework. As an important result we find that the masses, weak decay constants and two photon widths of the light pseudoscalar mesons (π, η, K) can be described even quantitatively. With the same parameters also the masses and leptonic decays of the vector mesons can be reproduced.

The pseudoscalar mesons are dominantly affected by an instanton induced interaction, which apart from the π, η splitting gives the correct $n\bar{n}-, s\bar{s}-$mixing for the η meson. The self energy corrections and coupling constants due to the resulting chiral symmetry breaking are compatible with the parameters we used for the quark antiquark interaction. In contrast to nonrelativistic calculations instanton effects appear also in the scalar sector.

Concerning the nature of the confinement kernel we find that a vector type interaction can reproduce the Regge trajectories, although with a larger quark mass than the one needed to describe the lowest lying mesons. This might be an indication that due to string effects the quark mass should increase with distance.

For a scalar kernel quasistable solutions exist only for relatively large quark masses and weak confinement. With these parameters, however, one cannot reproduce quantitatively the ground state mesons or the Regge trajectories. Nevertheless the spin orbit splitting indicates the existence of a scalar component in the interaction in order to cancel the large spin orbit splittings coming from the vector structure (compare also chapter 6).

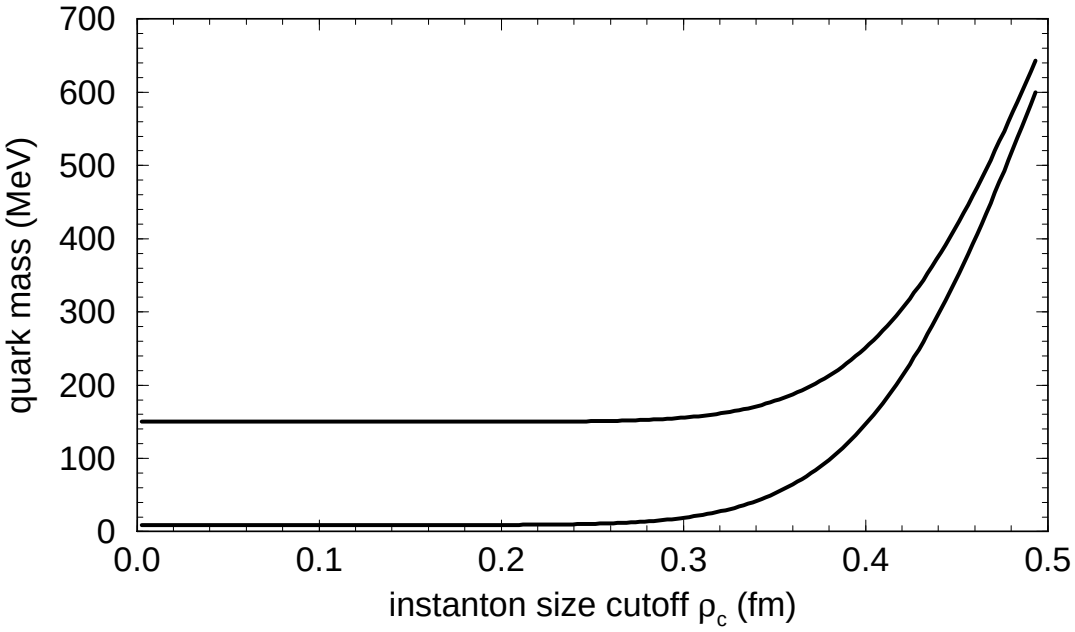

Figure 4.9: Effective mass dependence for the non strange (solid curve) and strange quark (dashed curve) on the instanton size cutoff ρ_c.

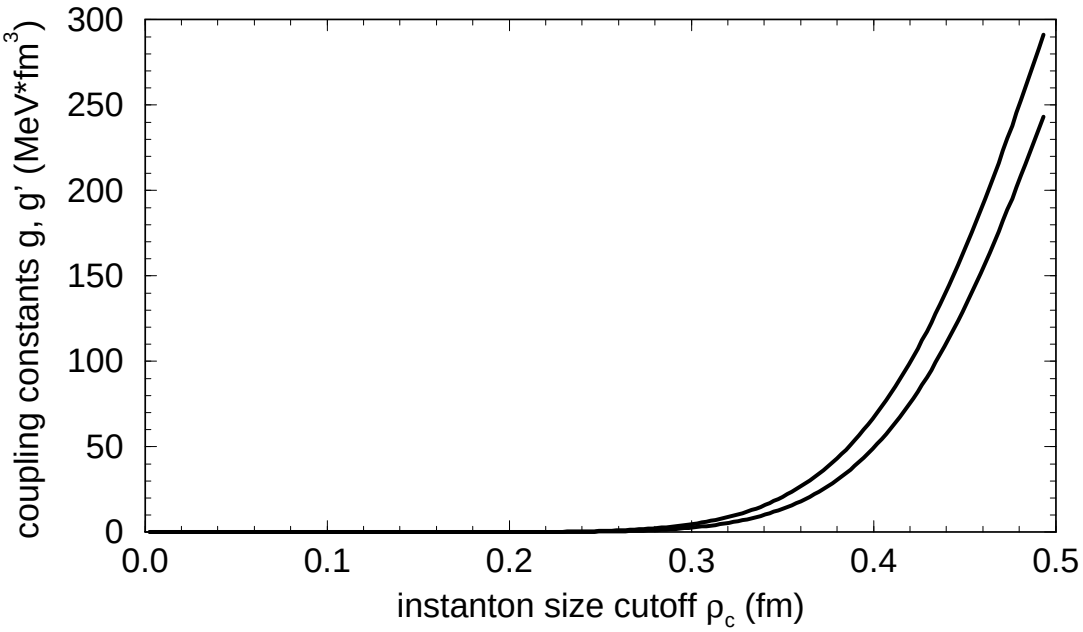

Figure 4.10: Effective coupling constants for the instanton induced non-strange quark interaction g (solid curve) and the strange non-strange quark interaction g' (dashed curve) as a function of the instanton size cutoff ρ_c, see eqs.(4.8, 4.20)

.

Chapter 5

Spectra and decays for heavy quarkonia

The heavy quarkonia (Charmonium $c\bar{c}$ and Bottomonium $b\bar{b}$) are investigated in the framework of the instantaneous BS-equation (Salpeter equation). We parametrize confinement alternatively by a linearly rizing scalar or a vector interaction kernel and take into account the one-gluon-exchange (OGE) interaction in the instantaneous approximation. We calculate mass spectra as well as leptonic and two-photon decay widths. Our results show that a reasonable description of the experimental data can be obtained with both spin structures for the confining kernel.

5.1 Introduction

In the past the heavy quarkonia have usually been investigated in the framework of the nonrelativistic quark model (we don't give a list of the many contributions here; see e.g. [5, 22, 32] and references therein). Because of the large masses of the c and b quark the nonrelativistic treatment of the bound state problem is expected to be a good first approximation. However in charmonium one still finds typical values of $v/c \approx 0.4$ (see e.g. ref.[23]), so that relativistic effects become important especially for electroweak decay properties, as has been shown in ref.[5].

Relativistic calculations for the heavy quarkonia have been given by Gara et.al. [17] in the framework of the reduced Salpeter equation, and by Murota [40] who uses the (full) Salpeter equation. Unfortunately, both references only give the mass spectra and do not calculate any decay widths, which should be most sensitive to relativistic effects.

In the present chapter we obtain the mass spectra as well as the leptonic and two-photon decay widths (taken from ref.[37], compare chapter 2.5 for the explicit formulas) in the framework of the (full) Salpeter equation. We parametrize

confinement by a linearly rizing scalar or a vector interaction kernel and take into account the one-gluon-exchange (OGE) interaction in the instantaneous approximation. Here the 't Hooft interaction used for the description of light mesons as shown in chapter 4 has been replaced by the instantaneous OGE. There are two reasons for this modification:

- The 't Hooft interaction is based on the assumption of massless quarks [24, 62] and therefore cannot easily be extended to heavy quarks. However one can show that in analogy to the η-mesons the 't Hooft interaction does not give first order contributions to the interaction between two charmed or bottom quarks because of the flavor antisymmetry of the interaction. Effects can only occur via flavor mixing in second order, but the large differences in the meson masses suppress such contributions. Furthermore there are no experimental indications for other flavors contributing signifficantly to $c\bar{c}$ and $b\bar{b}$ mesons.

- A good description for the mass spectra of the heavy quarkonia can already be obtained in the nonrelativistic quark model using a linear confinement potential plus the nonrelativistic reduction of the OGE interaction (i.e. the well-known Fermi-Breit potential). Therefore the OGE is the natural choice also for the Salpeter equation. For light quarks, however, the OGE leads to degenerate π and η masses in clear contradiction with experiment.

It should be noted that the instability of the Salpeter equation with a scalar confinement as discussed in chapter 4 is invisible here for any reasonable number of basis states (compare fig.5.3). We therefore think that it is legitimate to compare these (quasistable) solutions to the experimental meson masses.

The chapter is organized as follows: In Sec.5.2 the explicit form of the interaction kernel is given. The model parameters and results are discussed in Sec.5.3, and we give some concluding remarks in Sec.5.4.

5.2 The Bethe-Salpeter kernel

The interaction kernel is of the form

$$[V(\vec{p},\vec{p}\,')\,\Phi(\vec{p}\,')] = [V_C(\vec{p},\vec{p}\,')\,\Phi(\vec{p}\,')] + [V_G(\vec{p},\vec{p}\,')\,\Phi(\vec{p}\,')] \tag{5.1}$$

where the scalar or vector confining part is given by

$$\left[V_C^S(\vec{p},\vec{p}\,')\,\Phi(\vec{p}\,')\right] = \mathcal{V}_C((\vec{p}-\vec{p}\,')^2)\,\Phi(\vec{p}\,') \tag{5.2}$$

$$\left[V_C^V(\vec{p},\vec{p}\,')\,\Phi(\vec{p}\,')\right] = -\mathcal{V}_C((\vec{p}-\vec{p}\,')^2)\,\gamma^0\,\Phi(\vec{p}\,')\,\gamma^0 \tag{5.3}$$

Here $\mathcal{V}_C$ is a scalar function with a fourier transform $\mathcal{V}_C^F(r) = a_c + b_c r$.

For the OGE kernel V_G we have to note that it is not possible to formulate this term in a gauge-invariant way, since for a gauge-invariant kernel it is essential to take into account crossed gluon diagrams. However, for such diagrams the instantaneous approximation cannot be applied in a usefull way. Furthermore, also in a noninstantaneous treatment the incorporation of crossed diagrams is technically very difficult, so that it would be very hard to go beyond the gauge-dependent ladder approximation.

In view of the instantaneous treatment of the OGE the natural gauge for the gluon propagator is the Coulomb gauge, which will be applied in the following. The advantage of this gauge is the fact that the gluon propagator given by

$$\gamma^\mu \, D_{\mu\nu}(q) \, \gamma^\nu = 4\pi \, \left(\frac{\gamma^0\gamma^0}{\vec{q}^{\,2}} + \frac{\vec{\gamma}\vec{\gamma} - (\vec{\gamma}\hat{q})(\vec{\gamma}\hat{q})}{q^2 + i\epsilon} \right) \tag{5.4}$$

with $\hat{q} = \vec{q}/|\vec{q}|$ is already instantaneous in its component $D_{00}(q)$. In the instantaneous approximation we substitute q^2 by $-\vec{q}^{\,2}$. The OGE kernel (see fig.5.1) then reads [40, 66]

$$\begin{aligned} \left[V_G^C(\vec{p},\vec{p}\,') \, \Phi(\vec{p}\,') \right] &= \mathcal{V}_G((\vec{p}-\vec{p}\,')^2) \\ &\cdot \left[\gamma^0 \Phi(\vec{p}\,') \, \gamma^0 - \frac{1}{2} \, (\vec{\gamma}\Phi(\vec{p}\,')\,\vec{\gamma} + (\vec{\gamma}\hat{x})\Phi(\vec{p}\,')\,(\vec{\gamma}\hat{x}) \,) \right] \end{aligned} \tag{5.5}$$

We don't give the operator $\hat{x} = \vec{x}/|\vec{x}|$ explicitely in momentum space since the

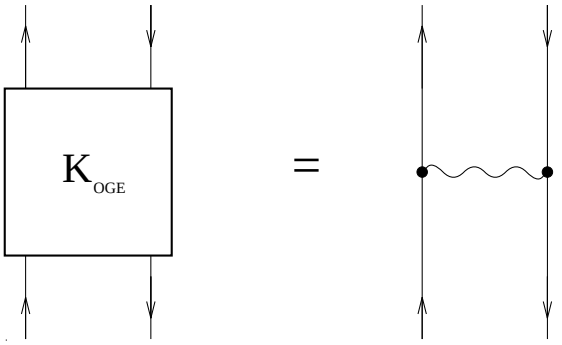

Figure 5.1: The One-Gluon-Exchange approximation to the interaction kernel

corresponding matrix elements will be evaluated in coordinate space, see appendix D.2.4. Also the matrix elements of the scalar function $\mathcal{V}_G(\vec{q}^{\,2})$ will be evaluated in coordinate space. For the numerical calculation we therefore use its Fourier transform $\mathcal{V}_G^F(r)$ which will be obtained in the following (the result is given in eq.(5.14)).

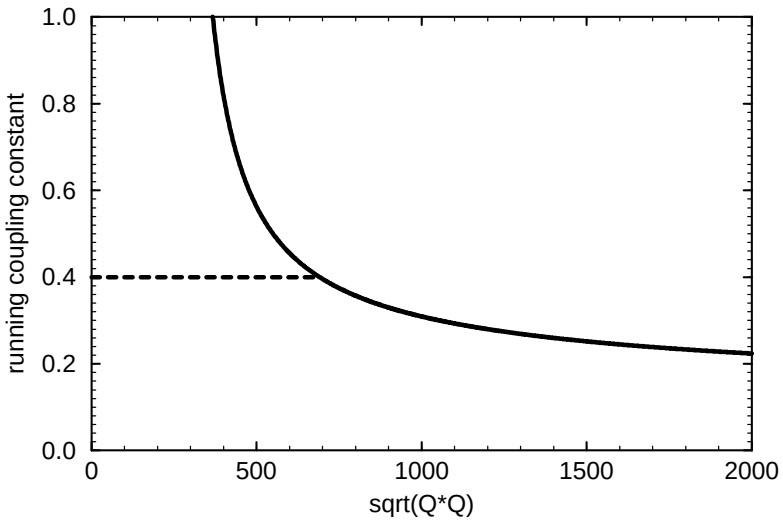

Figure 5.2: The running coupling constant α_s^{run} as given in eq.(5.7) with $\Lambda_{QCD} = 200\,MeV$ and $n_f = 3$. For small momenta it is assumed that α_s reaches a saturation value which is chosen to be $\alpha_{sat} = 0.4$ in this plot.

In momentum space $\mathcal{V}_G$ is given by

$$\mathcal{V}_G(\vec{q}^{\,2}) = 4\pi\,\frac{4}{3}\,\frac{\alpha_s(\vec{q}^{\,2})}{\vec{q}^{\,2}} \tag{5.6}$$

In QCD the running coupling constant for $Q^2 = -q^2 \gg \Lambda_{QCD}$ is given by [47]

$$\alpha_s^{run}(Q^2) = \frac{A}{\ln(Q^2/\Lambda^2_{QCD})}\left(1 - B\,\frac{\ln\left(\ln(Q^2/\Lambda^2_{QCD})\right)}{\ln(Q^2/\Lambda^2_{QCD})}\right) + \ldots \tag{5.7}$$

with

$$A = \frac{12\,\pi}{33 - 2\,n_f}\quad,\quad B = \frac{6\,(153 - 19\,n_f)}{(33 - 2\,n_f)^2} \tag{5.8}$$

where in the instantaneous approximation we set $Q^2 = \vec{q}^{\,2}$. We will now assume that $\alpha_s(\vec{q}^{\,2})$ behaves like $\alpha_s^{run}(\vec{q}^{\,2})$ for $\vec{q}^{\,2} > \vec{q}_0^{\,2} > \Lambda^2_{QCD}$ and reaches a saturation value α_{sat} for $\vec{q}^{\,2} \le \vec{q}_0^{\,2}$, where $\vec{q}_0^{\,2}$ is determined by the condition that $\alpha_s(\vec{q}^{\,2})$ is a continuous function (compare fig.5.2).

Unfortunately the Fourier transform of the OGE kernel given by

$$\begin{aligned}\mathcal{V}_G^F(r) &= \int \frac{d^3q}{(2\pi)^3}\,e^{i\vec{q}\vec{r}}\,\mathcal{V}_G(\vec{q}^{\,2}) \\ &= \frac{1}{2\pi^2 r}\int_0^\infty |\vec{q}|\,d|\vec{q}|\,\sin(|\vec{q}|r)\,\mathcal{V}_G(\vec{q}^{\,2})\end{aligned} \tag{5.9}$$

can only be calculated numerically. On the other hand, it is not really neccessary to use the exact $\mathcal{V}_G^F(r)$ as given above, since the form of $\alpha_s(\vec{q}^{\,2})$ is quite arbitrary

for intermediate values of $\vec{q}^2$. Therefore we will use eq.(5.9) to obtain analytic expressions for $\mathcal{V}_G^F(r)$ in the short and long distance region corresponding to $\vec{q}^2 \gg \Lambda_{QCD}^2$ and to $\vec{q}^2 \ll \Lambda_{QCD}^2$, and finally give an expression that has the correct limits for small and large r and gives a smooth interpolation in between.

For $r \gg \Lambda_{QCD}^{-1}$ only small $\vec{q}^2$ are important in the Fourier integral and we can set $\alpha_s(\vec{q}^2) = \alpha_{sat}$ so that

$$\mathcal{V}_G^F(r) = \frac{4}{3}\frac{\alpha_{sat}}{r} \quad \text{for} \quad r \gg \Lambda_{QCD}^{-1} \tag{5.10}$$

Analogously for $r \ll \Lambda_{QCD}^{-1}$ we set $\alpha_s(\vec{q}^2) = \alpha_s^{run}(\vec{q}^2)$. The corresponding Fourier integral can be performed analytically for small r as shown in appendix E. The result reads

$$\mathcal{V}_G^F(r) \approx \frac{4}{3}\frac{\alpha_s^{run}(r)}{r} \quad \text{for} \quad r \ll \Lambda_{QCD}^{-1} \quad \text{with} \tag{5.11}$$

$$\alpha_s^{run}(r) = \frac{A}{2\,\ln(e^{-\gamma}/a)}\left[1 - B\,\frac{\ln\left(2\,\ln(1/a)\right)}{2\,\ln(1/a)}\right] \quad \text{with} \quad a = \Lambda_{QCD}\,r \tag{5.12}$$

where $\gamma = 0.577215\ldots$ is the Euler-Mascheroni constant. A smooth interpolation between these two limiting cases is given by

$$\alpha_s(r) = \frac{A}{2\,\ln\left(e^{-(\gamma+\mu a)}/a + e^{A/(2\alpha_{sat})}\right)}\left[1 - B\,\frac{\ln\left(2\,\ln(e^{-\tilde{\mu}a}/a + e^{1/2})\right)}{2\,\ln(e^{-\mu a}/a + e^{B/2})}\right] \tag{5.13}$$

(see ref.[66] for the case $B = 0$), where we set $\mu = 4$ and $\tilde{\mu} = 20$ in order to obtain a good approximation of eq.(5.9) as shown in fig.5.4.

The Salpeter equation with $\mathcal{V}_G^F(r) = (-4/3)\,\alpha_s(r)/r$ is well defined. This is in contrast to the corresponding Schrödinger equation where the terms of order $\vec{p}^2/m^2$ like the spin-spin and spin-orbit interaction lead to a collaps of the wavefunction into the origin, i.e. the Fermi-Breit hamiltonian is unbound from below. This defect is usually cured by using first order perturbation theory or by regularizing the $1/r$ potential for small r.

For the Salpeter equation this problem disappears due to the relativistic treatment of the quark motion. However, most Salpeter amplitudes are divergent for $r \to 0$, as has been shown explicitely by Murota [40] for a fixed coupling constant. For a running coupling constant this divergence is less pronounced, but still present. The amplitudes are normalizable, but problems occur for decay observables like the leptonic decay widths, which depend on the value of the amplitudes at $r \to 0$. The easiest way to cure these divergencies is to regularize the OGE kernel for small r. We therefore will use the regularized potential

$$\begin{aligned} \mathcal{V}_G^F(r) &= -\frac{4}{3}\frac{\alpha_s(r)}{r} \quad \text{for} \quad r > r_0 \\ \mathcal{V}_G^F(r) &= a_G\,r^2 + b_G \quad \text{for} \quad r \le r_0 \end{aligned} \tag{5.14}$$

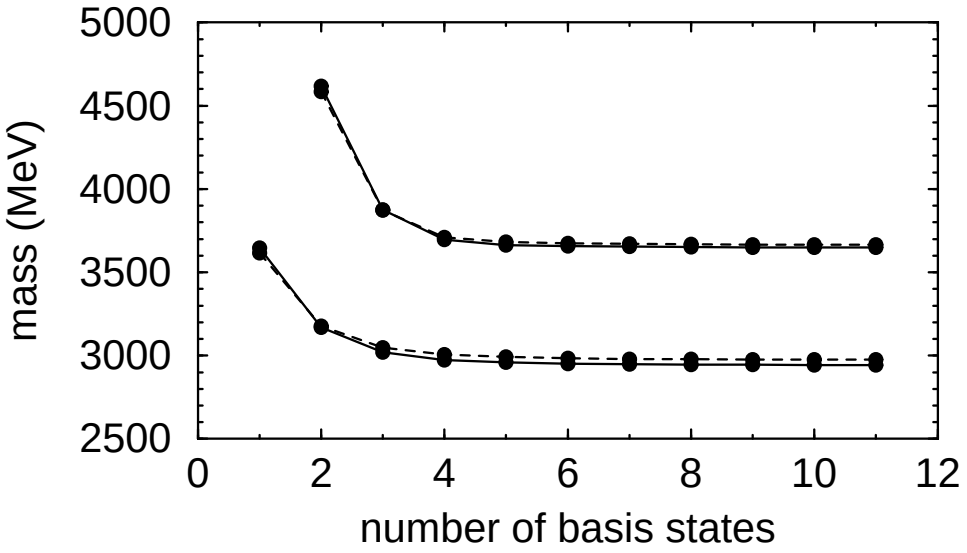

Figure 5.3: Dependence of the calculated Salpeter eigenvalues for the η_c ground state and first excited state on the number of basis states taken into account. The solid curves correspond to the scalar confinement, the dashed curves to the vector confinement. The parameters are given in tab.5.1. The radial part of the basis states in momentum space is given by $R_{nL}(y) = N_{nL}\, y^L\, L_n^{2L+2}(y)\, e^{-y/2}$ with $y = p\beta$ and $L_n^{2L+2}(y)$ being a Laguerre polynomial. We used $\beta = 2.0\, fm$ here.

with a_G and b_G determined by the condition that $\mathcal{V}_G^F(r)$ and its first derivative are continuous functions. The dependence of $\alpha_s(r)$ given by eq.(5.13) on Λ_{QCD} and n_f is not large and can be compensated for by modifying μ and α_{sat}. We will use $\Lambda_{QCD} = 200\, MeV$ and $n_f = 3$ for our calculation. A plot of $\mathcal{V}_G^F(r)$ is shown in fig.5.5. The dependence of the mass spectra on the regularization parameter r_0 is very weak as shown in fig.5.11, so that the differences in the mass spectra calculated with the regularized and unregularized potential are quite small. For our further calculation we will take $r_0 = 0.1\, fm$.

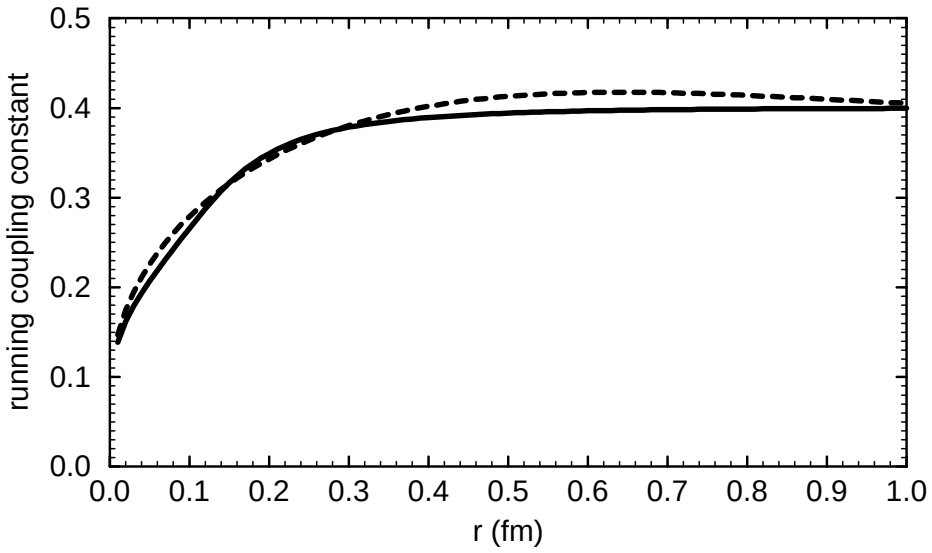

Figure 5.4: The running coupling constant $\alpha_s(r)$ (solid curve) as given in eq.(5.13). The dashed curve shows the result of the numerical Fourier transformation as given in eq.(5.9), i.e. $\mathcal{V}_G^F(r) \,/\, ((4/3)/r)$. In this plot $\alpha_{sat} = 0.4$ is used.

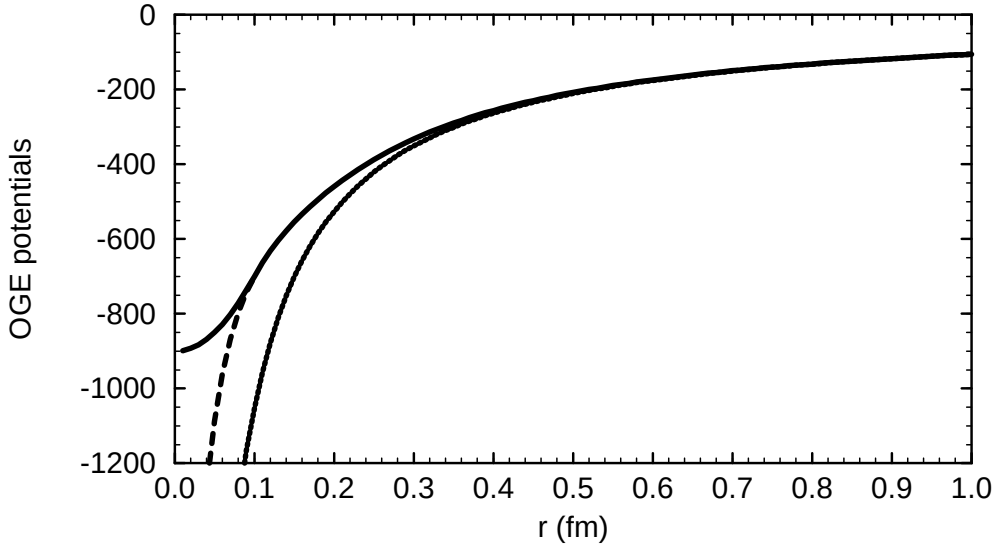

Figure 5.5: The regularized potential $\mathcal{V}_G^F(r)$ as given in eq.(5.14) (solid upper curve) compared to the unregularized potential (dashed curve) and the potential $(-4/3)\,\alpha_{sat}/r$ (lower curve) with $\alpha_{sat} = 0.4$.

5.3 Results and discussion

5.3.1 The model parameters

In order to obtain the best possible description for the mass spectra of the heavy quarkonia the model parameters have been determined independently from the parameter sets used for the light mesons in chapter 4. The reason for this procedure is the fact that the only two parameters common for heavy and light mesons (i.e. the confinement parameters a_c and b_c) are not well determined for the light mesons because of the difficulties to describe Regge trajectories and decay widths simultaneously. Note that for a scalar confinement it was generally not possible to describe the Regge trajectories, so that the value of b_c is quite arbitrary for this case.

The situation will be different in chapter 6, where also the heavy-light $q\bar{q}$-systems (D-mesons) are considered. Therefore only one parameter set will be used in chapter 6 to describe heavy, light and D-mesons simultaneously.

As in chapter 4 we investigate two different models of the confinement kernel: 1) a scalar $1 \otimes 1$- and 2) a vector $\gamma^0 \otimes \gamma^0$-structure.

The parameters used are the charm and bottom quark masses m_c and m_b, the offset a_c and slope b_c of the confinement interaction and the saturation value α_{sat} for $\alpha_s(r)$ used in eq.(5.13). These five parameters have been adjusted to the mass spectra by minimizing a χ^2 that incorporates all known charmonium and bottomonium ground states and first excited states. The obtained parameter sets are given in tab.5.1 for the scalar (S) and the vector (V) confinement.

It is remarkable that analogously to the light mesons the slope of the confining potential comes out much larger in than in nonrelativistic models, where a typical value is $b_c \approx 700$ MeV/fm [5]. The main difference between the two parameter sets is given by the larger value of α_{sat} for the scalar confinement. This can be easily understood from the nonrelativistic picture where the spin-orbit force coming from the scalar confinement conteracts the OGE spin-orbit force, whereas for the vector confinement both spin-orbit forces affect the mass spectra in the same way. Therefore, in order to compensate the reduced spin-orbit splitting of the χ-states in the scalar confining case, the strength of the OGE interaction has to be increased. Compared to nonrelativistic calculations (see e.g. [5]) we find smaller quark masses m_c, m_b and a larger confinement slope b_c.

5.3.2 Mass spectra

The mass spectra of Charmonium are given in figs.5.6,5.7, the mass spectra of Bottomonium are shown in figs.5.8,5.9. The experimental data are usually taken from the Particle Data Group [47]. For the recent measurement of the mass of the charmonium $^1P_1$ state ($J^{PC} = 1^{+-}$) in $p\bar{p}$ annihilations by the E760 collaboration at Fermilab see refs.[2, 22]. We find that both confinement spin structures give

Table 5.1: Model parameters for scalar and vector confinement

Parameter	scalar	vector
m_c [MeV]	1507	1631
m_b [MeV]	4857	5005
a_c [MeV]	-252	-640
b_c [MeV/fm]	1270	1291
α_{sat}	0.492	0.365

a reasonable overall description of the experimental mass spectra. The spin-spin and spin-orbit splittings are slightly better described for the vector confinement, whereas the radial excitations of the vector mesons are slightly better for the scalar confinement. However, we feel that these differences are not significant enough to decide wether the Lorentz nature of confinement should be of the scalar or vector type. This is in contrast to the nonrelativistic quark model where a scalar confinement gives the better results.

Allthough the description of the mass spectra can be considered quite satisfactory, there remain some characteristic deviations which indicate the relevance of retardation effects and higher order diagrams in the interaction kernel. We find that the binding of the η_c meson tends to be quite large. As a consequence it is not possible for a scalar confinement to simultaneously describe the hyperfine splitting $\eta_c \leftrightarrow J/\psi$ and the fine splitting $\chi_{c0} \leftrightarrow \chi_{c1} \leftrightarrow \chi_{c2}$ with higher accuracy. Furthermore the level spacing between the s-wave states of the vector mesons is overestimated for both spin structures, whereas the mass differences of s-waves and d-waves is underestimated, especially for higher radial excitations. It is interesting to note that deviations have also been found by Gara et.al [17] in the framework of the reduced Salpeter equation. They conclude that these difficulties are mainly due to the omission of the kinetic energy of the rotating flux tube connecting the quarks. The ommission of the rotating flux tube energy is also made responsible for the difficulties in describing the Regge trajectories of the light mesons, as found in their model. This is in qualitative agreement with our results.

We would like to mention that the use of the Feynman gauge given by

$$\left[V_G^F(\vec{p},\vec{p}\,')\,\Phi(\vec{p}\,')\right] = \mathcal{V}_G((\vec{p}-\vec{p}\,')^2)\,\gamma^\mu\Phi(\vec{p}\,')\,\gamma_\mu \tag{5.15}$$

does not give a satisfactory description of the mass spectra, since the binding energy of the η_c meson is overestimated, as can be seen in fig.5.10. It turns out that it is not possible to compensate for this effect in a satisfying way by readjusting the model parameters. The effect of the gauge on the other states is less important.

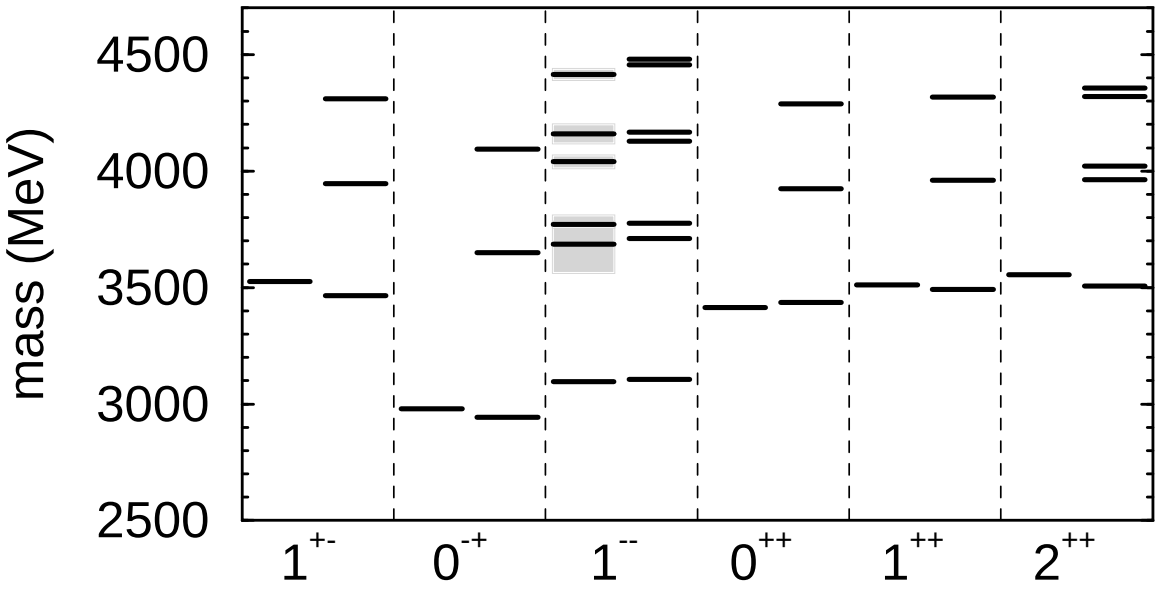

Figure 5.6: Charmonium mass spectrum for a scalar confinement with the parameters given in tab.5.1. The left column for each meson shows the experimental mass, where the shaded areas correspond to the full decay widths.

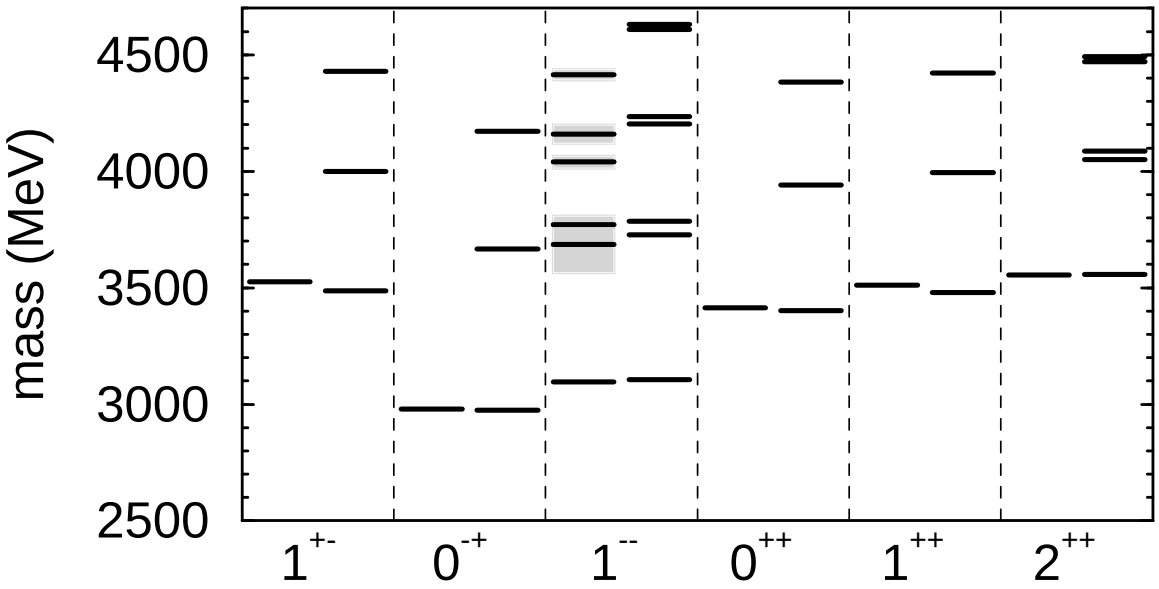

Figure 5.7: Same as fig.5.6 for a vector confinement.

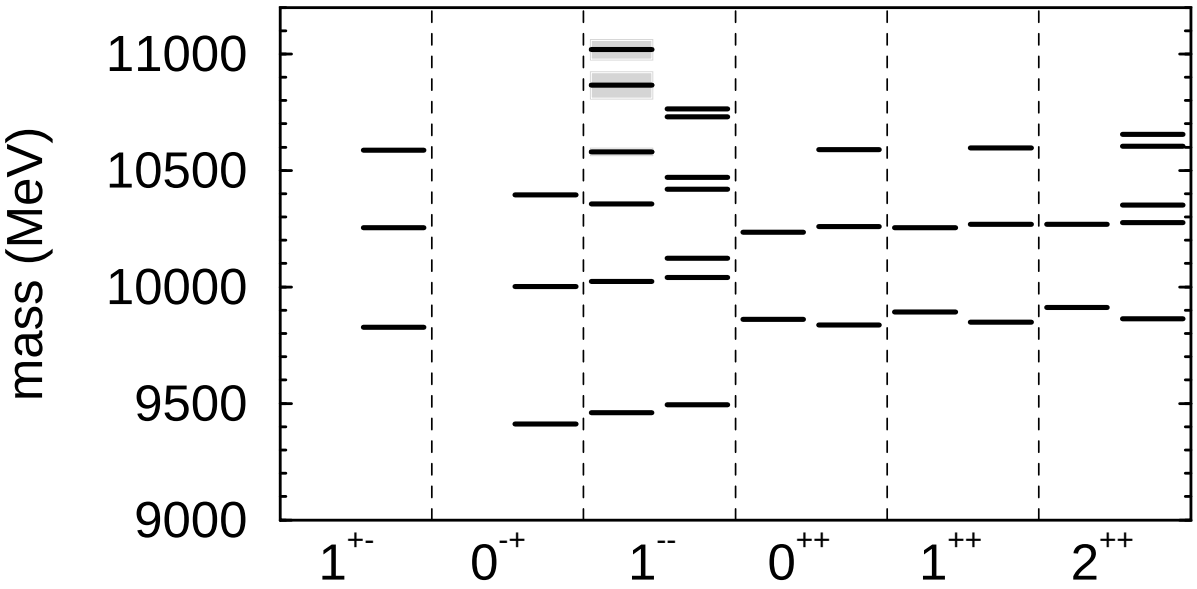

Figure 5.8: Bottomonium mass spectrum for a scalar confinement with the parameters given in tab.5.1. The left column for each meson shows the experimental mass, where the shaded areas correspond to the full decay widths.

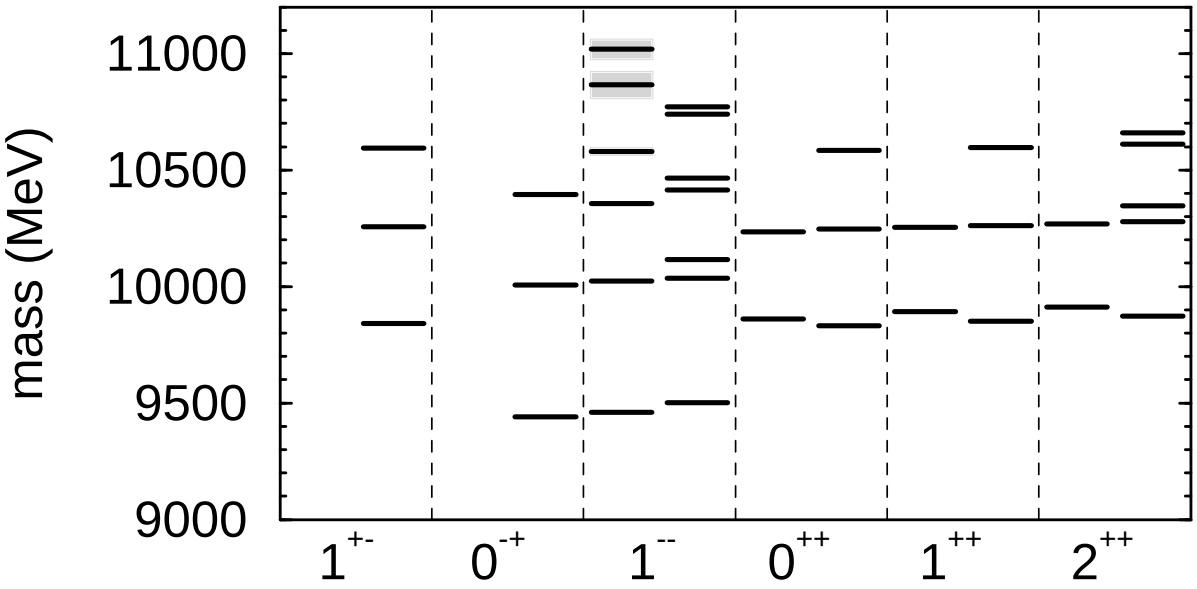

Figure 5.9: Same as fig.5.8 for a vector confinement.

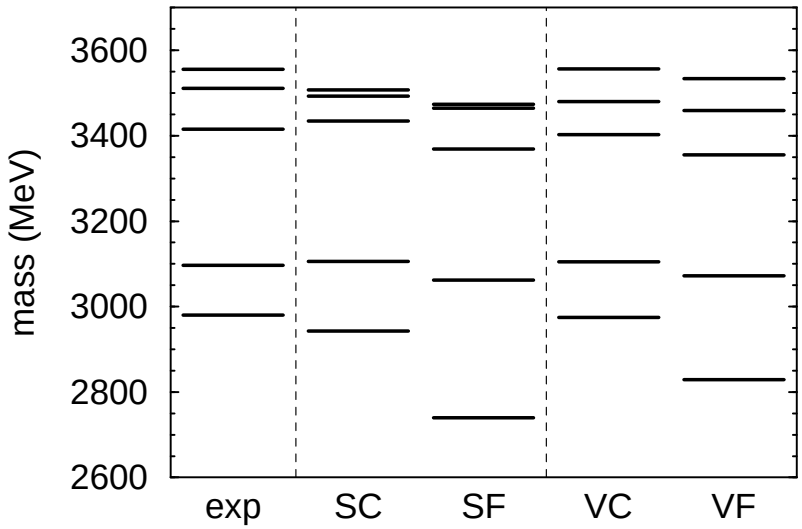

Figure 5.10: The charmonium ground states η_c, J/ψ, χ_{c0}, χ_{c1}, χ_{c2} (from bottom to top). The coloums correspond (from the left) to the experimental masses, the masses obtained with a scalar confinement using the Coulomb (SC) and the Feynman gauge (SF), and the same for a vector confinement, i.e. (VC) and (VF). For the Feynman gauge the same parameters have been used as for the corresponding Coulomb gauge, see tab.5.1.

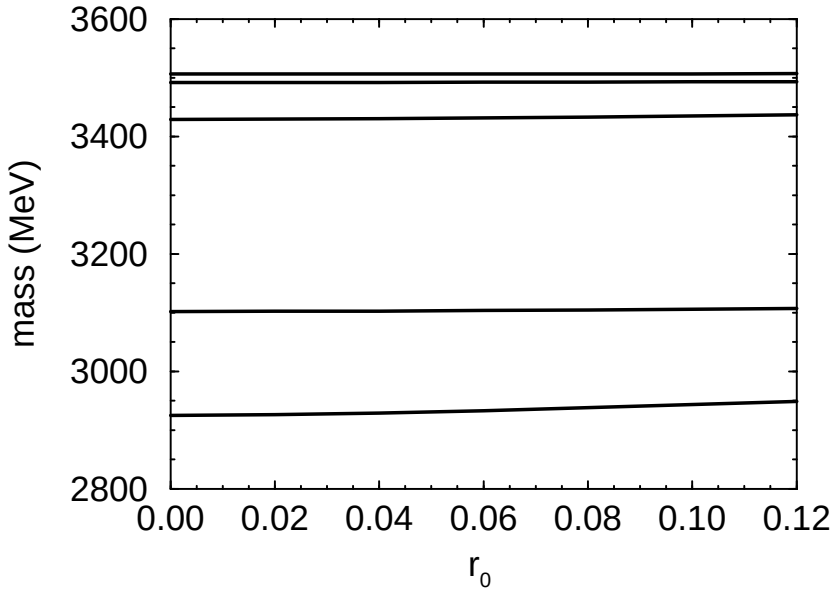

Figure 5.11: Dependence of the charmonium ground state masses η_c, J/ψ, χ_{c0}, χ_{c1} and χ_{c2} (from bottom to top) on the regularization parameter r_0 shown for a scalar confinement with the parameters given in tab.5.1.

Table 5.2: Comparison of experimental and calculated decay widths for scalar (S) and vector (V) confinement. The nonrelativistic results (NR) for the $c\bar{c}$ and $b\bar{b}$ leptonic decay widths are taken from [5] (version B of the model, nonrelativistic decay formula). The nonrelativistic results for $\eta_c(1S) \to \gamma\gamma$ are taken from ref.[53].

decay	experimental [47]	S	V	NR
$\Gamma(J/\psi(1S) \to e^+e^-)$ [keV]	5.36 ± 0.29	8.05	9.21	12.2
$\Gamma(\psi(2S) \to e^+e^-)$ [keV]	2.14 ± 0.21	4.30	5.87	4.63
$\Gamma(\psi(2D) \to e^+e^-)$ [keV]	0.26 ± 0.04	0.13	0.09	0.005
$\Gamma(\psi(3S) \to e^+e^-)$ [keV]	0.75 ± 0.15	3.05	4.81	3.20
$\Gamma(\psi(3D) \to e^+e^-)$ [keV]	0.77 ± 0.23	0.23	0.14	0.01
$\Gamma(\psi(4S) \to e^+e^-)$ [keV]	0.47 ± 0.10	2.16	3.95	2.41
$\Gamma(\Upsilon(1S) \to e^+e^-)$ [keV]	1.34 ± 0.04	0.80	0.84	1.49
$\Gamma(\Upsilon(2S) \to e^+e^-)$ [keV]	0.59 ± 0.03	0.54	0.57	0.61
$\Gamma(\Upsilon(3S) \to e^+e^-)$ [keV]	0.44 ± 0.03	0.44	0.47	0.39
$\Gamma(\Upsilon(4S) \to e^+e^-)$ [keV]	0.24 ± 0.05	0.40	0.49	0.33
$\Gamma(\eta_c(1S) \to 2\gamma)$ [keV]	6.6 ± 2.4	4.2	3.8	19.1

5.3.3 Decay observables

With the method outlined in chapter 4 leptonic decay widths for the vector mesons and the decay width for $\eta_c \to 2\,\gamma$ have been calculated with the parameters of the previous section (see ref.[37]). As shown in tab.5.2 there are only small differences between the two spin structures. The leptonic decay widths of the $c\bar{c}$ s-wave vector mesons are generally too large by a factor of ~ 1.5 for the $J/\psi(1S)$ and more for the higher radial excitations, whereas they are too small for the $\Upsilon(1S)$. We were not able to adjust the model parameters in order to find a better agreement with the experimental widths, since an increased leptonic width of the $\Upsilon(1S)$ is usually connected with an increased $J/\psi(1S)$ width. Furthermore the leptonic widths turned out to be quite insensitive to changes of the parameters. Note that the nonrelativistic results for the leptonic $b\bar{b}$ widths are quite good.

At this point we would like to note that the commonly used QCD correction factor $(1 - 16\,\alpha_s/(3\pi))$ [4] does obviously not improve these results, since the leptonic widths of the $J/\psi(1S)$ and the $\Upsilon(1S)$ would be changed in the same way.

The leptonic widths of the radially excited Υ states come out close to the experimental data. The same holds for the decay $\eta_c \to 2\gamma$, in contrast to nonrelativistic results. The leptonic widths of the charmonium d-wave states are too small by a factor ≥ 2.

5.4 Summary and conclusion

We investigated the heavy quarkonia in the framework of the Salpeter equation with a linear scalar or vector confinement plus the OGE interaction. For the mass spectra we obtained a reasonable agreement with the experimental meson masses both for a scalar as well as for a vector confining kernel. This is in contrast to the nonrelativistic quark model where a scalar confinement is prefered. However, the mass spectra show some moderate deviations which indicate the relevance of retardation effects and higher order diagrams beyond the OGE approximation.

For the leptonic widths we find too large values for the J/ψ and its radial excitation, whereas the leptonic width of the $\Upsilon(1S)$ is too small. The leptonic widths of the $\Upsilon(2S)$ and $\Upsilon(3S)$ and the two-photon width of the η_c are in good agreement with experiment.

Chapter 6

Simultaneous description of light, heavy and heavy-light mesons

In the framework of the instantaneous Bethe-Salpeter equation we give a simultaneous description of light, heavy and heavy-light mesons. The interaction kernel consists of a scalar plus vector linear confining potential and a residual $q\bar{q}$-interaction as shown in the previous chapters 4 and 5, i.e. for the light mesons we use the 't Hooft interaction, whereas for the heavy quarkonia ($c\bar{c}$ and $b\bar{b}$) and the heavy-light mesons ($c\bar{x}$ and $b\bar{x}$ with $x = u,\ d,\ s$) the OGE residual interaction is applied.

6.1 Introduction

In chapter 4 the framework of the Salpeter equation has been applied to calculate mass spectra and decay widths of light mesons, where the interaction kernel has been given by a combination of a linear (scalar or vector) confining potential and an Instanton-induced residual $q\bar{q}$-interaction ('t Hooft interaction). For the heavy quarkonia ($c\bar{c}$ and $b\bar{b}$) the mass spectra and decay widths have been calculated independently in chapter 5, where the 't Hooft interaction has been substituted by the residual One-Gluon-Exchange (OGE) in the BS-kernel.

In the present chapter we will investigate to what extent it is possible to describe light and heavy mesons simultaneously (i.e. with only one parameter set) using the interaction kernels given above, i.e. 't Hooft interaction for light quarks and OGE for heavy quarkonia.

Within this framework it is also possible to investigate the quarkonia consisting of one heavy and one light quark, i.e. the various D-mesons (and B-mesons; they will not always be adressed seperately in the following). These mesons have been of high interest in the recent years, especially in the context of the heavy quark effective theory (see e.g. [45] and references therein) which analyses the limit $m_c,\ m_b \to \infty$ in QCD. A detailed quark model calculation of D-meson mass

spectra as well as various weak decay widths and formfactors has recently been given by S.Resag and M.Beyer [52]. The Dirac equation has been applied to D-meson mass spectra e.g. by V.D.Mur et.al. [39], whereas P.C.Tiemeijer and J.A.Tjon [66] compare different quasipotential equations. In the present work we will focus on the mass spectra and the weak decay constants for the D-mesons. The Salpeter amplitudes obtained then provide a basis for the further investigation of other weak decay properties. Activities into this direction are planed for the future (see also refs.[37, 52]).

The chapter is organized as follows: In Sec.6.2 the form of the interaction kernel will be reviewed according to the chapters 4 and 5. The model parameters and results are discussed in Sec.6.3, and concluding remarks are made in Sec.6.4.

6.2 The Bethe-Salpeter kernel

The interaction kernel used in the following is given by

$$[V(\vec{p},\vec{p}\,')\,\Phi(\vec{p}\,')] = [V_C(\vec{p},\vec{p}\,')\,\Phi(\vec{p}\,')] + [V_{res}(\vec{p},\vec{p}\,')\,\Phi(\vec{p}\,')] \tag{6.1}$$

where the spin structure of the confining part is given by a combination of scalar plus vector confinement as

$$[V_C(\vec{p},\vec{p}\,')\,\Phi(\vec{p}\,')] = \mathcal{V}_C((\vec{p}-\vec{p}\,')^2)\,\left[(1-\epsilon)\,\Phi(\vec{p}\,') + \epsilon\,(-\gamma^0\,\Phi(\vec{p}\,')\,\gamma^0)\right] \tag{6.2}$$

Here $\mathcal{V}_C$ is a scalar function which has the fourier transform $\mathcal{V}_C^F(r) = a_c + b_c r$ (see also chapters 4 and 5). The determination of the confining spin structure is a delicate issue within the present framework. As shown in chapter 5 the results for the heavy quarkonia do not give clear indications in this context. From the light mesons (see chapter 4) we know that a pure scalar confinement ($\epsilon = 0$) leads to difficulties for higher angular momenta (Regge trajectories) and higher radial excitations. These difficulties were connected with an instability of the Salpeter equation.

In the framework presented in this chapter we find on the other hand that the observed splitting of the $D_1(2420)$ with $J^P = 1^+$ and $D_2^*(2460)$ with $J^P = 2^+$ cannot be described with a pure vector confinement ($\epsilon = 1$) since the 1^+ ground state then would have a much smaller mass than the 2^+ ground state, see fig.6.7. The same argument holds for the corresponding splittings of the light mesons $a_1 \leftrightarrow a_2$ and $K_1 \leftrightarrow K_2^*$ (see fig.6.2), as already mentioned in chapter 4. Therefore the appropriate choice within the presented framework is given by mixture of scalar plus vector confinement. We will take $\epsilon = 0.5$ for the mixing parameter in the following. For this choice one has

$$\frac{1}{2}\left(\Phi - \gamma^0\,\Phi\,\gamma^0\right) = \begin{pmatrix} 0 & \Phi^{++} \\ \Phi^{--} & 0 \end{pmatrix} \tag{6.3}$$

(compare eq.(2.12) for the notation), i.e. the confining kernel does not mix positive and negative energies. Note that generally the instability problem disappears for $\epsilon \geq 0.5$.

For the light mesons (i.e. no c or b quark) the residual interaction is given by the regularized 't Hooft interaction, which has already been studied in detail in chapter 4. We recall that $V_{res} = V_T$ with

$$[V_T(\vec{p},\vec{p}\,')\,\Phi(\vec{p}\,')]_{f_1 f_2} = 4 \sum_{f_1' f_2'} G_{f_2 f_1', f_1 f_2'}\; e^{-\frac{1}{4}\Lambda^2(\vec{p}-\vec{p}\,')^2}$$
$$\cdot \quad \left[1\,\mathrm{tr}\,\left(\Phi_{f_1' f_2'}(\vec{p}\,')\right) + \gamma^5\,\mathrm{tr}\,\left(\Phi_{f_1' f_2'}(\vec{p}\,')\,\gamma^5\right)\right] \tag{6.4}$$

with $f_i = u,\, d,\, s \equiv 1,\, 2,\, 3$ and the definition

$$G_{f_3 f_4, f_1 f_2} := \frac{3}{8} \sum_{f_5=1}^{3} g_{\mathrm{eff}}(f_5)\; \epsilon_{f_5 f_3 f_4}\, \epsilon_{f_5 f_1 f_2} \tag{6.5}$$

Since we assume $SU(2)$-flavor invariance of the interaction we set

$$g := \frac{3}{8} g_{\mathrm{eff}}(s) \quad , \quad g' := \frac{3}{8} g_{\mathrm{eff}}(n) \tag{6.6}$$

where s stands for strange and n stands for nonstrange (u,d) flavor. The results for $G_{f_2 f_3, f_1 f_4}$ have been given in Tab.4.2. The coupling constants g and g' are treated as free parameters in the following. As noted in chapter 4 the 't Hooft interaction only acts on the light scalar and pseudoscalar mesons $J^{\pi_P} = 0^{\pm}$.

For heavy quarkonia and D-mesons the OGE residual interaction in the Coulomb gauge is applied (compare chapter 5), i.e. $V_{res} = V_G^C$ with

$$\left[V_G^C\,(\vec{p},\vec{p}\,')\,\Phi(\vec{p}\,')\right] = \mathcal{V}_G((\vec{p}-\vec{p}\,')^2) \tag{6.7}$$
$$\cdot \quad \left[\gamma^0 \Phi(\vec{p}\,')\,\gamma^0 - \frac{1}{2}\,(\vec{\gamma}\Phi(\vec{p}\,')\,\vec{\gamma} + (\vec{\gamma}\hat{x})\Phi(\vec{p}\,')\,(\vec{\gamma}\hat{x})\,)\right] \tag{6.8}$$

where the regularized OGE potential $\mathcal{V}_G((\vec{p}-\vec{p}\,')^2)$ has the Fourier transform

$$\begin{aligned} \mathcal{V}_G^F(r) &= -\frac{4}{3}\frac{\alpha_s(r)}{r} \quad \text{for } r > r_0 \\ \mathcal{V}_G^F(r) &= a_G\, r^2 + b_G \quad \text{for } r \leq r_0 \end{aligned} \tag{6.9}$$

with a_G and b_G determined by the condition that $\mathcal{V}_G^F(r)$ and its first derivative are continuous functions and $r_0 = 0.1\,fm$. As shown in detail in chapter 5 the running coupling constant is given by

$$\alpha_s(r) = \frac{A}{2\,\ln\left(e^{-(\gamma+\mu a)}/a + e^{A/(2\alpha_{sat})}\right)}\left[1 - B\,\frac{\ln\left(2\,\ln(e^{-\tilde{\mu}a}/a + e^{1/2})\right)}{2\,\ln(e^{-\mu a}/a + e^{B/2})}\right] \tag{6.10}$$

with $a = \Lambda_{QCD}\, r$ and

$$A = \frac{12\,\pi}{33 - 2\,n_f} \quad , \quad B = \frac{6\,(153 - 19\,n_f)}{(33 - 2\,n_f)^2} \tag{6.11}$$

where we set $\mu = 4$, $\tilde{\mu} = 20$ and use $\Lambda_{QCD} = 200\,MeV$ and $n_f = 3$ for our calculation.

The reason for these special choices for the residual $q\bar{q}$ interactions have already been discussed in chapter 5 for heavy and light mesons. For D-mesons the situation is a priori not that clear since in principle the 't Hooft interaction can act on D-mesons in the same way as on K-mesons. However, there is the more practically motivated objection that the present form of the 't Hooft interaction is based on the assumption of massless quarks and thus cannot easily be extended to heavy quarks. Furthermore we expect that possible effects of the 't Hooft interaction on the D-mesons should be small in analogy to the K-meson which is already less affected than the π-meson. Therefore in the following we will assume that D-mesons are only affected by the OGE interaction.

There still is the possibility to apply the OGE also to the light mesons in addition to the 't Hooft interaction (as noted in chapters 4 and 5, the OGE alone cannot reproduce the observed $\pi \leftrightarrow \eta$ splitting). We did not make use of this possibility since it turnes out that the 't Hooft interaction alone is already sufficient to give good results for the light pseudoscalar mesons.

6.3 Results and discussion

6.3.1 The model parameters

The parameters of the model are the quark masses m_n, m_s, m_c, m_b (with $n = u,\, d$), the confinement slope b_c and offset a_c, the 't Hooft coupling constants g, g' and the OGE saturation value α_{sat} for the strong coupling constant. For the effective range Λ of the 't Hooft interaction the same value has been used as in chapter 4, i.e. $\Lambda = 0.42\,fm$. Therefore in total we have nine parameters that have to be adjusted to the experimental mass spectra. This has been done for the parameters except for g and g' by a χ^2 fitting procedure, where all known $c\bar{c}$, $b\bar{b}$ and D-meson ground and first excited states as well as the light meson ground states ρ and K^* were taken into account. The 't Hooft couplings g and g' have then been adjusted to the π and K meson masses. The parameter set obtained is given in tab.6.1.

6.3.2 Mass spectra

The resulting light meson mass spectra are shown in figs.6.1,6.2. For the heavy quarkonia the spectra are shown in figs.6.3,6.4 and the D-meson masses are given

in figs.6.5,6.6. Fig.6.8 shows the Regge trajectory for the light isovector mesons with $S = 1$, and fig.6.7 illustrates the dependence of the D-meson masses on the scalar-vector confinement mixing parameter ϵ.

The overall description of the mass spectra can be considered rather satisfying having in mind the large number of meson states taken into account. Note that also the η and η' masses can approximately be described due to the flavor structure of the 't Hooft interaction. The quality of the calculated mass spectra is comparable to results obtained in the nonrelativistic quark model [8, 10, 53], whereas the relativistic treatment of the quark dynamics leads to a large improvement for the calculated decay widths compared to nonrelativistic results (see tab.6.2 and the next section).

Some problems in describing certain features of the meson mass spectra have already been adresses in chapters 4 and 5. As shown in fig.6.8 the calculated slope of the shown Regge trajectory comes out too small, allthough the deviation is still moderate. Another problem is the calculated splitting of the a_0 and the f_0 meson due to the 't Hooft interaction, which is in contrast to the almost degenerate experimental masses of these two mesons (see fig.6.2). It is interesting to note that in typical nucleon-nucleon potentials an effective meson (usually called σ or σ' meson) with the quantum numbers of the f_0 and a mass of about $550\,MeV$ is needed to describe the experimental data [34, 16]. Allthough our calculation yields a scalar isoscalar state at 710 MeV, it seems more reasonable to identify this state with the experimentally found $f_0(975)$ meson. Note that in our calculated f_0 ground state the $s\bar{s}$ flavor admixture is about 25%, which might be interesting in view of the large experimental decay width $f_0 \to K\,\bar{K}$.

The description for the heavy quarkonia is approximately of the same quality as in the treatment of chapter 5. The spin-spin and spin-orbit splittings tend to be too small for $c\bar{c}$ and $b\bar{b}$ as well as for the D-mesons. This is a consequence of the small value for α_{sat} which is needed for the overall description of the meson

Table 6.1: Model parameters

m_n [MeV]	221
m_s [MeV]	492
m_c [MeV]	1863
m_b [MeV]	5235
a_c [MeV]	-1286
b_c [MeV/fm]	1475
g [MeV fm^3]	33.62
g' [MeV fm^3]	33.02
Λ [fm]	0.42
α_{sat}	0.244

mass spectra. Note that due to the large number of light, heavy and heavy-light meson states taken into account the overall quality of the meson mass spectrum depends on the parameters in a quite complex way.

6.3.3 Decay observables

With the Salpeter amplitudes obtained we have calculated weak decay constants, leptonic and two-photon decay widths using the formalism given in chapter 2 (see ref.[37] for a more detailed analysis of meson decay observables within the present model). The results are shown in tab.6.2, where they are compared to the experimental data and to nonrelativistic quark model results. We find good results for the π and K weak decay constants and for the two-photon decay widths. The comparision with the nonrelativistic results shows the importance of a relativistic treatment for these decays, even for heavy quarkonia (see $\eta_c \to \gamma\gamma$). The D-meson decay constants have not been measured so far, however our results are in quite good agreement with estimates obtained by J.Rosner [60] from data on the decays $\bar{B} \to D\, D_s^-$ and $\bar{B} \to D^*\, D_s^-$.

Problems occur for the leptonic decay widths, which are generally too large with the exception of the $b\bar{b}$ widths which come out too small.

6.4 Summary and conclusion

Within the framework of the Salpeter equation we obtain a reasonable overall description of light, heavy and D-mesons simultaneously. The interaction kernel consists of a linear scalar plus vector confinement and a residual $q\bar{q}$-interaction given by the instanton-induced 't Hooft interaction for light mesons and by the instantaneous OGE for heavy and heavy-light mesons. The quality of the calculated mass spectra is comparable with corresponding results in the nonrelativistic quark model.

The calculated weak decay constants and two-photon widths are in quite good agreement with experiment, whereas the obtained leptonic decay widths are not satisfying.

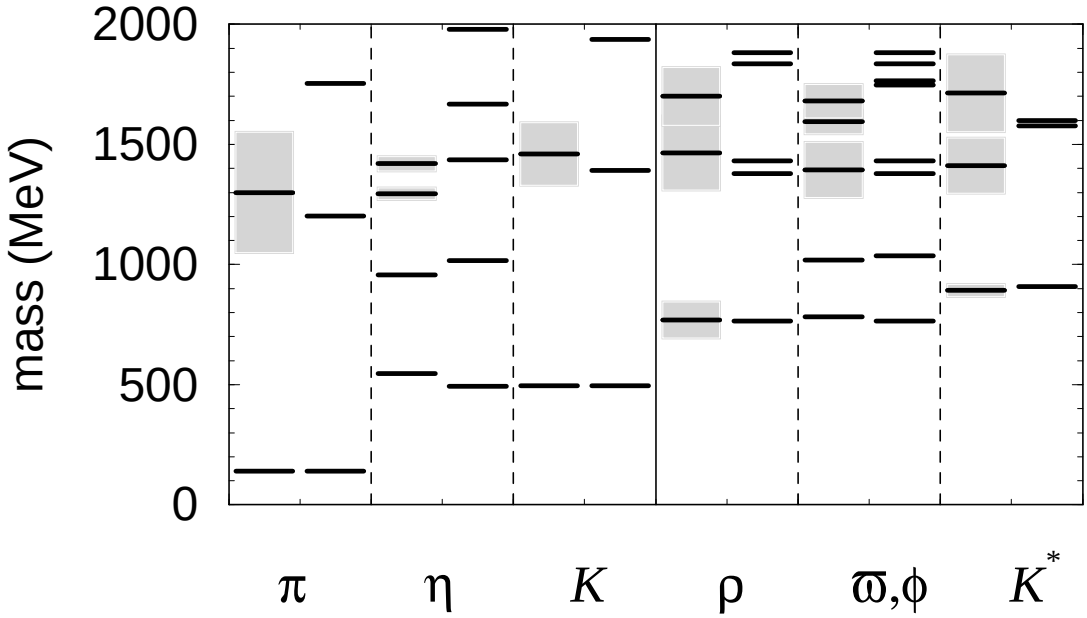

Figure 6.1: Mass spectra of the light pseudoscalar and vector mesons. The left column for each meson shows the experimental masses, where the shaded areas correspond to the full decay widths.

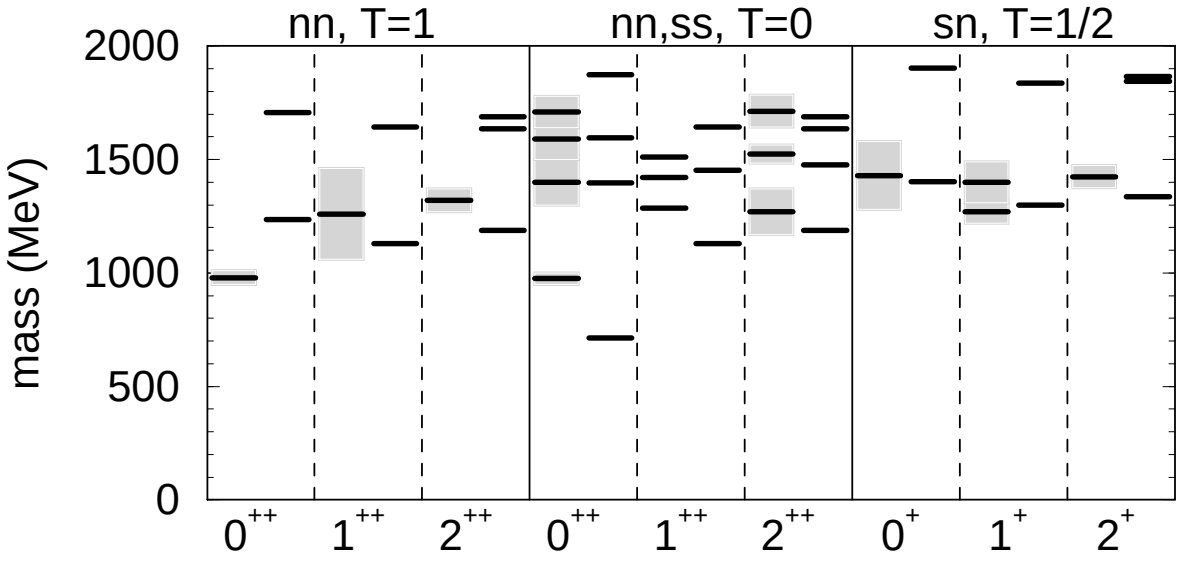

Figure 6.2: Mass spectra of the light mesons with positive parity, i.e. a_0, a_1, a_2, f_0, f_1, f_2, K_0^*, K_1, K_2^*; compare also fig.6.1. Note that each K_1 energy level corresponds to two degenerate states.

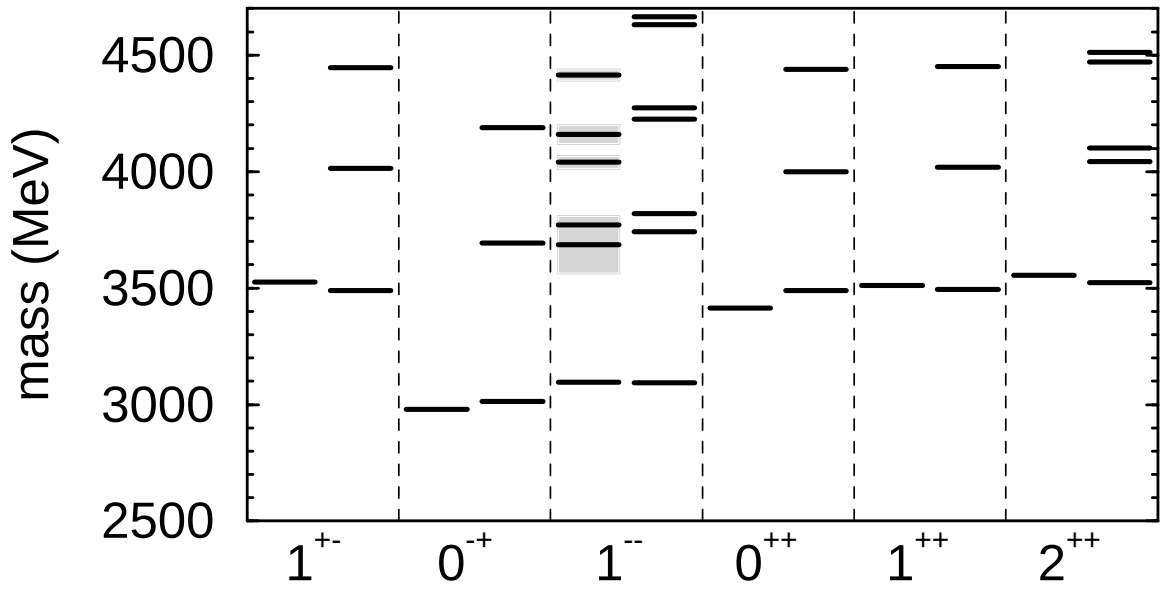

Figure 6.3: Charmonium mass spectrum. The left column for each meson shows the experimental masses, where the shaded areas correspond to the full decay widths.

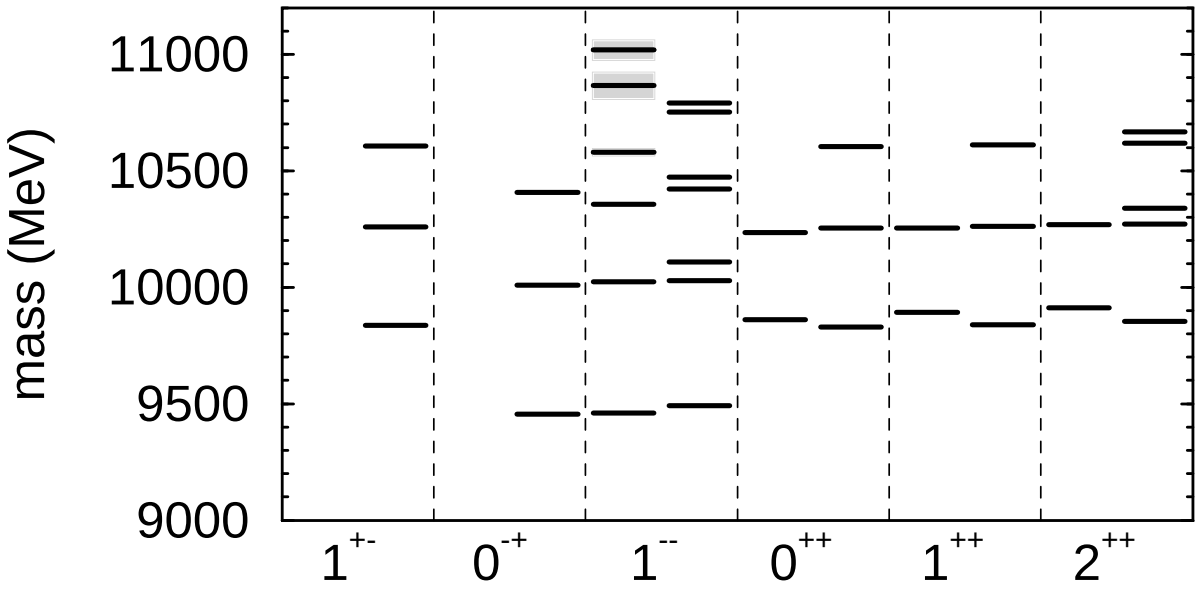

Figure 6.4: Same as fig.6.3 for Bottomonium.

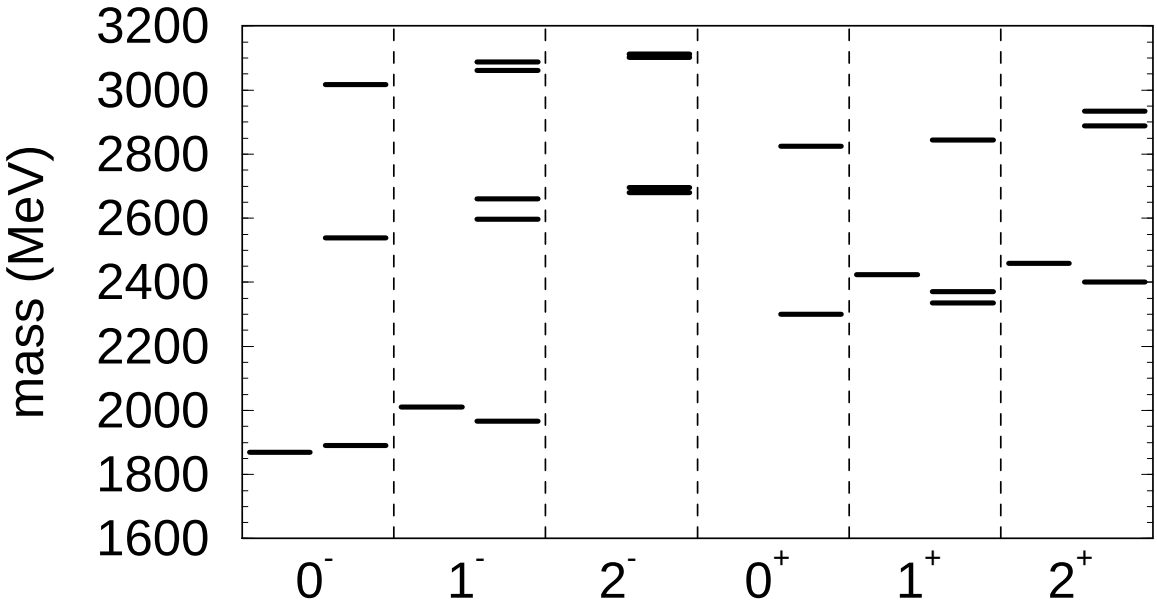

Figure 6.5: D-meson (i.e. $c\bar{n}$) mass spectrum. The left column for each meson shows the experimental masses.

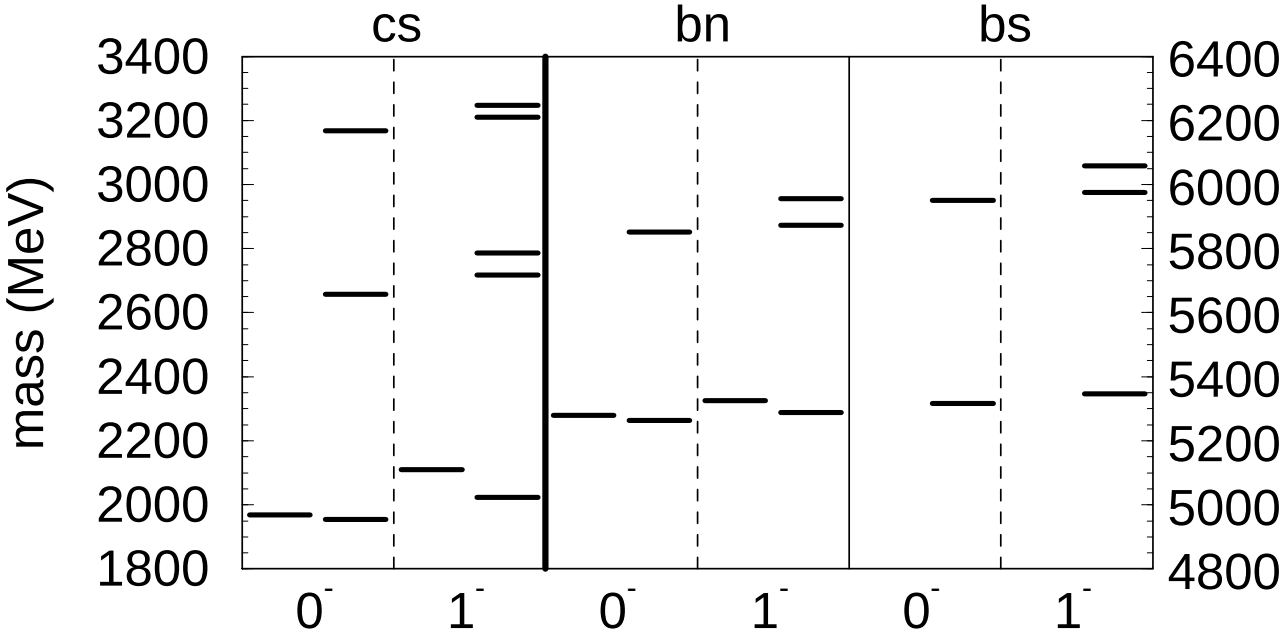

Figure 6.6: $c\bar{s}$, $b\bar{n}$ and $b\bar{s}$ mass spectra. The left column for each meson shows the experimental masses. The left mass scale corresponds to the $c\bar{s}$ states, whereas the right mass scale corresponds to the $b\bar{n}$ and $b\bar{s}$ states.

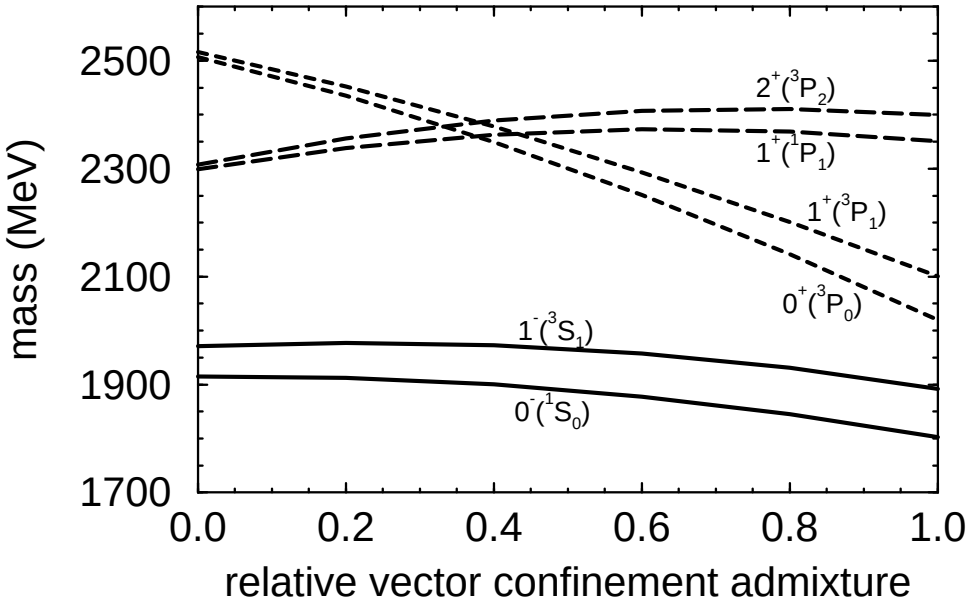

Figure 6.7: D meson ($c\bar{n}$) masses for a variable scalar/vector mixing in the confinement interaction. The x axis gives the relative vector admixture ϵ, i.e. the relative scalar admixture is given by $1-\epsilon$. In brackets the dominant partial wave is given for each state.

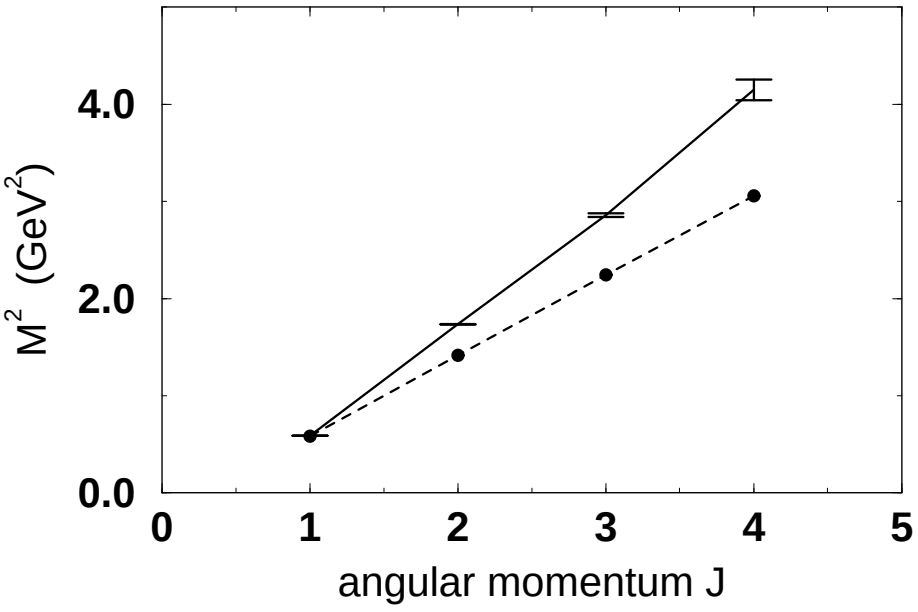

Figure 6.8: Regge trajectory for the isovector mesons with $S = 1$. The solid line shows the experimental masses for ρ, a_2, ρ_3, a_4 [47] where the errorbar gives the experimental error for the resonance position. The dashed line gives to the calculated masses.

Table 6.2: Comparison of experimental and calculated decay widths. Since experimental values for the D-meson decay constants are still missing, we give the results of J.L Rosner [60] who estimates the decay constants from experimental data on $\bar{B} \to D\, D_s^-$ and $\bar{B} \to D^*\, D_s^-$. The nonrelativistic results (NR) for the light mesons are taken from chapter 4, the nonrelativistic $c\bar{c}$ and $b\bar{b}$ leptonic decay widths are taken from [5] (version B of the model, nonrelativistic decay formula). The nonrelativistic results for $\eta_c(1S) \to \gamma\gamma$ and for the weak D-meson decay constants are taken from ref.[53].

decay	experimental [47]	calc	ref.[60]	NR
f_π [MeV]	131.7 ± 0.2	157		1440
f_K [MeV]	160.6 ± 1.4	211		730
f_D [MeV]	<290	259	207 ± 60	614
f_{D_s} [MeV]		314	259 ± 74	674
f_B [MeV]		208	140 ± 40	269
f_{B_s} [MeV]		258	175 ± 50	
$\Gamma(\pi^0 \to \gamma\gamma)$ [eV]	7.8 ± 0.5	6.2		30000
$\Gamma(\eta \to \gamma\gamma)$ [eV]	460 ± 5	377		18500
$\Gamma(\eta' \to \gamma\gamma)$ [eV]	4510 ± 260	2840		750
$\Gamma(\eta_c(1S) \to 2\gamma)$ [keV]	6.6 ± 2.4	2.3		19.1
$\Gamma(\rho \to e^+e^-)$ [keV]	6.8 ± 0.3	15.9		8.95
$\Gamma(\omega \to e^+e^-)$ [keV]	0.60 ± 0.02	1.73		0.96
$\Gamma(\phi \to e^+e^-)$ [keV]	1.37 ± 0.05	3.23		2.06
$\Gamma(J/\psi(1S) \to e^+e^-)$ [keV]	5.36 ± 0.29	8.01		12.2
$\Gamma(\psi(2S) \to e^+e^-)$ [keV]	2.14 ± 0.21	5.39		4.63
$\Gamma(\psi(2D) \to e^+e^-)$ [keV]	0.26 ± 0.04	0.04		0.005
$\Gamma(\psi(3S) \to e^+e^-)$ [keV]	0.75 ± 0.15	4.38		3.20
$\Gamma(\psi(3D) \to e^+e^-)$ [keV]	0.77 ± 0.23	0.05		0.01
$\Gamma(\psi(4S) \to e^+e^-)$ [keV]	0.47 ± 0.10	3.75		2.41
$\Gamma(\Upsilon(1S) \to e^+e^-)$ [keV]	1.34 ± 0.04	0.75		1.49
$\Gamma(\Upsilon(2S) \to e^+e^-)$ [keV]	0.59 ± 0.03	0.53		0.61
$\Gamma(\Upsilon(3S) \to e^+e^-)$ [keV]	0.44 ± 0.03	0.45		0.39
$\Gamma(\Upsilon(4S) \to e^+e^-)$ [keV]	0.24 ± 0.05	0.42		0.33

Chapter 7

Summary and Conclusion

The aim of the present thesis was to construct a relativistic extension of the nonrelativistic constituent quark model. Starting from the relativistic Bethe-Salpeter equation we applied two approximations in order to circumvent some principal and technical problems which are connected with the appearence of a relative energy variable p^0 in the BS-equation, i.e.

- the full quark propagator has been replaced by the free propagator with an effective constituent quark mass,
- retardation effects in the interaction are neglected (instantaneous or equal time approximation).

The resulting equation (called Salpeter equation) is independent of p^0, but still has the full Dirac structure including positive and negative energies for the quark and the antiquark. It can be regarded as an intermediate stage between the full BS equation and the nonrelativistic Schrödinger equation.

In chapter 2 we investigated the structure of the Salpeter equation for $q\bar{q}$-bound states in the general case of unequal quark masses and developed a numerical scheme for the calculation of mass spectra and Bethe-Salpeter amplitudes. Furthermore explicit formulas have been given to calculate some electroweak decays [37].

It turned out that the structure found for the Salpeter equation is very similar to the structure of the RPA (random phase approximation) equations, which are a common tool in nonrelativistic many particle theory. In chapter 3 it has been explicitely shown that Salpeter equation and RPA equations have the same form and can both be derived using the same approximations.

In chapter 4 the framework of the Salpeter equation has been used to derive an explicit quark model for light mesons. For the interaction kernel a combination of a scalar (or alternatively vector) linear confinement potential and an instanton induced residual interaction ('t Hooft interaction) has been chosen. It turned out that for a vector confinement the parameters can be chosen such that an

excellent description of the light pseudoscalar and vector ground state mesons can be achieved including weak decay constants, leptonic and two photon widths. A comparision with nonrelativistic results revealed the striking improvement for the weak decay constants and the two-photon widths due to the incorporation of the full relativistic Dirac structure and the negative energy components.

A scalar confinement did not give satisfying results due to an instability of the Salpeter equation, i.e. the bound state masses do not converge to real positive values if the number of basis states is increased, but finally become purely imaginary. For large enough quark masses, however, this instability is practically virtual and the numerical solutions aquire a quasistable character.

In chapter 5 the heavy quarkonia ($c\bar{c}$ and $b\bar{b}$) have been investigated, where confinement was parametrized in the same way as for the light mesons, and the 't Hooft interaction has been replaced by the one-gluon exchange (OGE) interaction. The instability of the Salpeter equation with a scalar confinement was completely invisible here, so that it should be legitimate to compare these (quasistable) solutions to the experimental meson masses. Reasonable fits to the experimental data could be obtained with a scalar as well as with a vector confinement. Some moderate deviations in the mass spectra and especially in the leptonic decay widths, however, indicated the relevance of retardation effects and higher order gluon diagrams in the interaction.

Finally the heavy-light (D and B -) mesons have been investigated in chapter 6 within a simultaneous fit of light and heavy mesons. Analogously to the previous chapters the interaction kernel was given by a combination of scalar plus vector confinement and a residual interaction, i.e. the 't Hooft interaction for light mesons and the OGE for heavy and heavy-light mesons. The resulting mass spectra had a quality similar to results found within the nonrelativistic quark model, whereas the results for the weak decay constants and the two-photon widths came out much better than the corresponding nonrelativistic results. The slightly too low Regge trajectory for the light mesons and the difficulties in describing the leptonic widths again indicated the relevance of retardation effects and higher order diagrams in the interaction as well as the possible relevance of additional contributions to the confining kernel.

Summarizing we found that the Salpeter equation indeed provides a usefull relativistic extension of the nonrelativistic constituent quark model. The present thesis therefore should provide an instructive step on the way to more involved treatments, which might include e.g. a selfconsistent determination of the quark propagators. Another challenge is the inclusion of retardation effects of the interaction, thus going beyond the instantaneous approximation applied in the present thesis.

Appendix A

Reduction to the Salpeter equation

For an instantaneous interaction kernel and free quark propagators the BS-equation (2.5) in the CMS is given by

$$\begin{aligned}\chi_P(p) &= \frac{\gamma(\eta_1 P + p) + m_1}{(\eta_1 P + p)^2 - m_1^2 + i\epsilon} \cdot \\ &\int \frac{d^4p'}{(2\pi)^4} \left[-i\, V(\vec{p},\vec{p}\,')\, \chi_P(p')\right] \frac{\gamma(\eta_2 P - p) - m_2}{(\eta_2 P - p)^2 - m_2^2 + i\epsilon} \end{aligned} \tag{A.1}$$

with $P = (M, \vec{0})$, where the notation of chapter 2 is used. The integral over $p^{0\,\prime}$ can now be performed. Integrating over p^0 in eq.(A.1) then leads to

$$\begin{aligned}\Phi(\vec{p}) &= -i \int \frac{dp^0}{2\pi} \frac{\gamma(\eta_1 P + p) + m_1}{(\eta_1 P + p)^2 - m_1^2 + i\epsilon} \cdot \\ &\cdot \int \frac{d^3p'}{(2\pi)^3} [(V(\vec{p},\vec{p}\,')\, \Phi(\vec{p}\,')] \frac{\gamma(\eta_2 P - p) - m_2}{(\eta_2 P - p)^2 - m_2^2 + i\epsilon} \end{aligned} \tag{A.2}$$

Note that only the propagators depend on p^0. It is now usefull to introduce

$$\Lambda_i^{\pm}(\vec{p}) = \frac{\omega_i \pm H_i(\vec{p})}{2\omega_i} = \frac{1}{2\omega_i} \begin{pmatrix} \omega_i \pm m_i & \pm\vec{\sigma}\vec{p} \\ \pm\vec{\sigma}\vec{p} & \omega_i \pm (-m_i) \end{pmatrix}$$

with $\omega_i = \sqrt{m_i^2 + \vec{p}^{\,2}}$ and $H_i(\vec{p}) = \gamma^0(\vec{\gamma}\vec{p} + m_i)$. The block matrix notation for $\Lambda_i^{\pm}$ refers to the standard Dirac representation for the γ-matrices. Since

$$H_i(\vec{p})\, \Lambda_i^{\pm}(\vec{p}) = \pm\omega_i\, \Lambda_i^{\pm}(\vec{p}) \tag{A.3}$$

$$\Lambda_i^{+}(\vec{p})\, \Lambda_i^{+}(\vec{p}) = \Lambda_i^{+}(\vec{p}) \tag{A.4}$$

$$\Lambda_i^{-}(\vec{p})\, \Lambda_i^{-}(\vec{p}) = \Lambda_i^{-}(\vec{p}) \tag{A.5}$$

$$\Lambda_i^{+}(\vec{p})\, \Lambda_i^{-}(\vec{p}) = 0 \tag{A.6}$$

the $\Lambda_i^{\pm}(\vec{p})$ can be interpreted as projectors on positive and negative energy states. With the help of these projectors the propagators can be written as

$$\frac{\gamma p_1 + m_1}{p_1^2 - m_1^2 + i\epsilon} = \left(\frac{\Lambda_1^+(\vec{p}_1)}{p_1^0 - \omega_1 + i\epsilon} + \frac{\Lambda_1^-(\vec{p}_1)}{p_1^0 + \omega_1 - i\epsilon} \right) \gamma^0 \tag{A.7}$$

$$\frac{\gamma p_2 - m_2}{p_2^2 - m_2^2 + i\epsilon} = \left(\frac{\Lambda_2^-(-\vec{p}_2)}{p_2^0 - \omega_2 + i\epsilon} + \frac{\Lambda_2^+(-\vec{p}_2)}{p_2^0 + \omega_2 - i\epsilon} \right) \gamma^0 \tag{A.8}$$

After inserting $p_1 = \eta_1 P + p,\ p_2 = \eta_2 P - p$ and $P = (M, \vec{0})$ we thus have four poles in p^0 given by

$$p_A^0 = -\eta_1 M + \omega_1 - i\epsilon \tag{A.9}$$

$$p_B^0 = -\eta_1 M - \omega_1 + i\epsilon \tag{A.10}$$

$$p_C^0 = +\eta_2 M - \omega_2 + i\epsilon \tag{A.11}$$

$$p_D^0 = +\eta_2 M + \omega_2 - i\epsilon \tag{A.12}$$

(compare figure (A.1)). The p^0 integral may now be computed using the residue

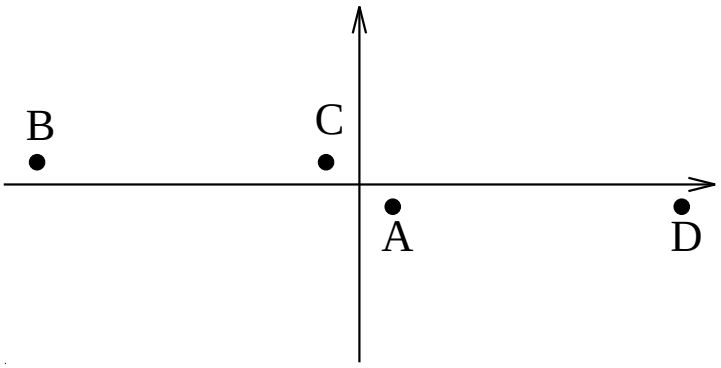

Figure A.1: Position of the poles in the complex p^0 plane for the low binding case with small p/m

theorem by closing the contour in the upper half plane encountering the poles $p_B^0,\ p_C^0$. Making use of $\Lambda_2^{\pm}(\vec{p})\,\gamma^0 = \gamma^0\,\Lambda_2^{\pm}(-\vec{p})$ one obtains the (full) Salpeter equation as given in eq.(2.9), i.e.

$$\begin{aligned} \Phi(\vec{p}) &= \int \frac{d^3p'}{(2\pi)^3} \frac{\Lambda_1^-(\vec{p})\,\gamma^0\,[(V(\vec{p},\vec{p}\,')\,\Phi(\vec{p}\,')]\,\gamma^0\,\Lambda_2^+(-\vec{p})}{M + \omega_1 + \omega_2} \\ &- \int \frac{d^3p'}{(2\pi)^3} \frac{\Lambda_1^+(\vec{p})\,\gamma^0\,[(V(\vec{p},\vec{p}\,')\,\Phi(\vec{p}\,')]\,\gamma^0\,\Lambda_2^-(-\vec{p})}{M - \omega_1 - \omega_2} \end{aligned} \tag{A.13}$$

which is independant of the choice for $\eta_1,\ \eta_2$.

Appendix B

Lorentz transformation properties

B.1 Special Lorentz transformations

Let Λ be a special Lorentz transformation and g be the corresponding element of the covering group $SL(2,C)$, given by

$$g\,\sigma(x)\,g^{\dagger} = \sigma(\Lambda x) \tag{B.1}$$

with $\sigma(x) = x^{\mu}\sigma_{\mu}$ and $(\sigma_{\mu}) = (1, \vec{\sigma})$. The transformation matrix S_g for Dirac spinors in the Weyl representation is then given by

$$S_g = \begin{pmatrix} g & 0 \\ 0 & (g^{\dagger})^{-1} \end{pmatrix} \tag{B.2}$$

With the transformation matrix

$$B = \frac{1}{\sqrt{2}} \begin{pmatrix} 1 & 1 \\ 1 & -1 \end{pmatrix} \tag{B.3}$$

we can use $S_g^D = B\,S_g^W\,B^{-1}$ to transform S_g into the standard Dirac basis employed in this work. The result reads

$$S_g = \frac{1}{2} \begin{pmatrix} g + (g^{\dagger})^{-1} & g - (g^{\dagger})^{-1} \\ g - (g^{\dagger})^{-1} & g + (g^{\dagger})^{-1} \end{pmatrix} \tag{B.4}$$

Note that the relation $\Lambda^{\mu}_{\ \nu}\,\gamma^{\nu} = S_g^{-1}\,\gamma^{\mu}\,S_g$ is automatically fulfilled. For a boost Λ with $\Lambda\,(M,\vec{0}) = P$ and $P^2 = M^2$ one has explicitely

$$g = \left[\sigma\left(\frac{P}{M}\right)\right]^{\frac{1}{2}} = \sqrt{\frac{M}{2(M+P^0)}}\left(1 + \sigma\left(\frac{P}{M}\right)\right) \tag{B.5}$$

and for a 3-dimensional rotation $\Lambda = R$ one has $g = u \in SU(2)$ and therefore

$$S_u = \begin{pmatrix} u & 0 \\ 0 & u \end{pmatrix} \tag{B.6}$$

in the Weyl basis as well as in the standard Dirac basis.

The transformation of a Dirac field operator $\Psi(x)$ is given by

$$U_g\,\Psi(x)\,U_g^{-1} = S_g^{-1}\,\Psi(\Lambda x) \tag{B.7}$$

$$U_g\,\bar{\Psi}(x)\,U_g^{-1} = \bar{\Psi}(\Lambda x)\,S_g \tag{B.8}$$

with U_g being a unitary operator. Consider a state with momentum P and $P^2 = M^2$, total angular momentum J and 3-component M_J normalized as $\langle P', J', M_J'|\, P, J, M_J\rangle = (2\pi)^3\, 2P^0\, \delta^3(\vec{P}\,' - \vec{P})\, \delta_{J'J}\, \delta_{M_J' M_J}$. Then the action of U_g on this state is given by

$$U_g\,|P, J, M_J\rangle = \sum_{M_J'} |\Lambda P, J, M_J'\rangle\, D^J_{M_J'\,M_J}(u) \tag{B.9}$$

where $D^J_{M_J'\,M_J}(u)$ is a Wigner D-function with $D^{1/2}_{M_J'\,M_J}(u) = u_{M_J'\,M_J}$ and $u = [\sigma(\Lambda P/M)]^{1/2}\, g\, [\sigma(P/M)]^{1/2}$ is the Wigner rotation.

From the definition of the BS-amplitude in chapter 2 one can see by inserting the unity operator $1 = U_g^{-1}\, U_g$ that the BS-amplitude transforms as

$$\chi_P^{JM_J}(p) = \sum_{M_J'} S_g^{-1}\, \chi_{\Lambda P}^{JM_J'}(\Lambda p)\, S_g\; D^J_{M_J'\,M_J}(u) \tag{B.10}$$

The BS-equation is compatible with this transformation law for covariant kernels.

B.2 Angular decomposition of the 2×2-amplitudes

Let $\Lambda = R$ be a 3-dimensional rotation and $g = u$ be the corresponding matrix $\in SU(2)$. With eq.(B.10) and the block matrix structure of Φ given in eq.(2.12) as well as the relation $(-i\sigma_2)\, u^{-1}\, i\sigma_2 = {}^t u$ we find

$$\begin{aligned} &[\Phi^{++}(\vec{p})]_{JM_J}\, i\sigma_2 \\ &\quad = \sum_{M_J'} [u \times u]\, \{[\Phi^{++}(R^{-1}\vec{p})]_{JM_J'}\, i\sigma_2\}\; D^J_{M_J'M_J}(u^{-1}) \end{aligned} \tag{B.11}$$

and the same for the other amplitudes, where we use the tensor notation $\{[u \times u]\,(\Phi^{++}\, i\sigma_2)\}_{m_1 m_2} = \sum_{m_1' m_2'} u_{m_1 m_1'}\, u_{m_2 m_2'}\, (\Phi^{++}\, i\sigma_2)_{m_1' m_2'}$. Therefore one can identify the indices m_1, m_2 of the matrix elements $[\Phi^{++}\, i\sigma_2]_{m_1 m_2}$ with the 3-components of the spin of the quark and the antiquark. Let $(\chi_{SM_S})_{m_1 m_2} = \langle 1/2\, m_1\, 1/2\, m_2 | S M_S\rangle$

be the spin matrix of the two quarks coupled to the total spin S. Define $\varphi_{S\,q}\, i\sigma_2 := \chi_{S\,q}$, i.e.

$$\varphi_{0\,0} = \frac{1}{\sqrt{2}}\, 1 \quad , \quad \varphi_{1\,q} = \frac{1}{\sqrt{2}}\, \sigma_q \tag{B.12}$$

or explicitely

$$\varphi_{0\,0} = \frac{1}{\sqrt{2}} \begin{pmatrix} 1 & 0 \\ 0 & 1 \end{pmatrix} \quad ; \quad \varphi_{1\,1} = \begin{pmatrix} 0 & -1 \\ 0 & 0 \end{pmatrix} \tag{B.13}$$

$$\varphi_{1\,0} = \frac{1}{\sqrt{2}} \begin{pmatrix} 1 & 0 \\ 0 & -1 \end{pmatrix} \quad ; \quad \varphi_{1\,-1} = \begin{pmatrix} 0 & 0 \\ 1 & 0 \end{pmatrix} \tag{B.14}$$

Then eq.(B.11) implies that we can decompose Φ^{++}, Φ^{--} as

$$\begin{aligned} \Phi^{++}(\vec{p}) &= \sum_{L\,S} \mathcal{R}^{(+)}_{LS}(p)\; [Y_L(\Omega_p) \otimes \varphi_S]^J \\ \Phi^{--}(\vec{p}) &= \sum_{L\,S} \mathcal{R}^{(-)}_{LS}(p)\; [Y_L(\Omega_p) \otimes \varphi_S]^J \end{aligned} \tag{B.15}$$

with the spin S and the orbital angular momentum L coupled to J. We assume that the BS-kernel allows choosing $\mathcal{R}^{(+)}_{LS}(p)$ to be a real function. The sum goes over all values L, S that are compatible with parity and charge parity of the bound state, see below.

B.3 Parity transformation

The Dirac field operator $\Psi(x)$ and the bound state with parity number $\pi_P = \pm 1$ transform under parity transformation $\hat{P}$ as

$$U_P\, \Psi(x)\, U_P^{-1} = \gamma^0\, \Psi(\hat{P}x) \tag{B.16}$$

$$U_P\, \bar{\Psi}(x)\, U_P^{-1} = \bar{\Psi}(\hat{P}x)\, \gamma^0 \tag{B.17}$$

$$U_P\, |K, J, M_J, \pi_P\rangle = \pi_P\, |K, J, M_J, \pi_P\rangle \tag{B.18}$$

where K is the momentum of the bound state and $\hat{P}\, x = (x^0, -\vec{x})$. For the BS-amplitude this implies

$$\chi_K(p) = \pi_P\, \gamma^0\, \chi_{\hat{P}K}(\hat{P}p)\, \gamma^0 \tag{B.19}$$

For the block matrix structure one finds

$$\begin{pmatrix} \Phi^{+-}(\vec{p}) & \Phi^{++}(\vec{p}) \\ \Phi^{--}(\vec{p}) & \Phi^{-+}(\vec{p}) \end{pmatrix} = \pi_P \begin{pmatrix} \Phi^{+-}(-\vec{p}) & -\Phi^{++}(-\vec{p}) \\ -\Phi^{--}(-\vec{p}) & \Phi^{-+}(-\vec{p}) \end{pmatrix} \tag{B.20}$$

To be compatible with the angular decomposition eq.(B.15) we find the well-known condition $\pi_P = (-1)^{L+1}$.

B.4 Charge conjugation

Let $|f_1\bar{f}_2,\, P\rangle$ be a $q\bar{q}$-bound state with flavors f_1 and f_2 and momentum P. The charge conjugation then acts like

$$U_C\,\Psi_\alpha(x)\,U_C^{-1} = \sum_\beta (S_C)_{\alpha\beta}\,{}^t\Psi^+_\beta(x) \tag{B.21}$$

$$U_C\,{}^t\Psi^+_\alpha(x)\,U_C^{-1} = \sum_\beta (S_C)_{\alpha\beta}\,\Psi_\beta(x) \tag{B.22}$$

$$U_C\,|f_1\bar{f}_2,\, P\rangle = |f_2\bar{f}_1,\, P\rangle \tag{B.23}$$

and we find for the BS-amplitude

$$\chi^P_{f_1f_2}(p) = -(S_C\gamma_0)\,{}^t\chi^P_{f_2f_1}(-p)\,(S_C\gamma^0) \tag{B.24}$$

with the matrix $S_C\gamma^0$ given in the standard basis as

$$S_C\gamma^0 = \begin{pmatrix} 0 & -i\sigma_2 \\ -i\sigma_2 & 0 \end{pmatrix} \tag{B.25}$$

Making the choice $\eta_1 = \eta_2 = 1/2$ implies

$$\begin{pmatrix} \Phi^{+-}_{f_1f_2}(\vec{p}) & \Phi^{++}_{f_1f_2}(\vec{p}) \\ \Phi^{--}_{f_1f_2}(\vec{p}) & \Phi^{-+}_{f_1f_2}(\vec{p}) \end{pmatrix} = \begin{pmatrix} \tilde{\Phi}^{-+}_{f_2f_1}(-\vec{p}) & \tilde{\Phi}^{++}_{f_2f_1}(-\vec{p}) \\ \tilde{\Phi}^{--}_{f_2f_1}(-\vec{p}) & \tilde{\Phi}^{+-}_{f_2f_1}(-\vec{p}) \end{pmatrix} \tag{B.26}$$

with $\tilde{\Phi}^{++} = -i\sigma_2\,({}^t\Phi^{++})\,i\sigma_2$. With the angular decomposition eq.(B.15) and $\tilde{\varphi}_{S\,q} = (-1)^S\,\varphi_{S\,q}$ one finds

$$\left[\mathcal{R}^{(\pm)}_{LS}(p)\right]_{f_1f_2} = (-1)^{L+S}\,\left[\mathcal{R}^{(\pm)}_{LS}(p)\right]_{f_2f_1} \tag{B.27}$$

For an eigenstate $|P,\,\pi_C\rangle$ of the charge conjugation we have $f_1 = f_2$ and $U_C\,|P,\,\pi_C\rangle = \pi_C\,|P,\,\pi_C\rangle$ which implies the well-known condition $\pi_C = (-1)^{L+S}$.

To investigate the compatibility of eq.(B.24) with the BS-equation we use the relation $S^F_{f_i}(p_i) = -(S_C\gamma^0)\,{}^tS^F_{f_i}(-p_i)\,(S_C\gamma^0)$ for the fermion propagator. Let $\chi_{f_1f_2}(p)$ be a solution of the BS-equation with f_1 being the quark flavor and f_2 being the antiquark flavor. It is straightforward to show that $\chi_{f_2f_1}(p)$ as given in eq.(B.24) is a solution of the BS-equation with interchanged flavors, if the interaction kernel transforms appropriately under charge conjugation. For the Salpeter equation this implies that the solution $\psi_{f_1f_2}$ and the solution of the equation with flavors interchanged $\psi_{f_2f_1}$ are connected by

$$\psi_{f_1f_2}(\vec{p}) = -S_C\,{}^t\psi_{f_2f_1}(-\vec{p})\,S_C \tag{B.28}$$

Appendix C

The 't Hooft interaction

C.1 The Lagrangian

As shown by Shifman, Vainshtein and Zakharov [62] the contribution of an instanton-antiinstanton configuration to the effective quark Lagrangian for three quark flavors u, d, s is given by

$$\begin{aligned}
\Delta\mathcal{L} = \int d\rho \frac{d_0(\rho)}{\rho^5} \Bigg\{ & \left[\prod_{i=1}^{3} \left(m_i^0 \rho - \frac{4}{3}\pi^2\rho^3(\bar{q}_{iR}q_{iL}) \right) \right. \\
& + \frac{3}{32}\left(\frac{4}{3}\pi^2\rho^3\right)^2 \left[\left\{ (\bar{q}_{1R}\lambda^a q_{1L})(\bar{q}_{2R}\lambda^a q_{2L}) \right. \right. \\
& \left. - \frac{3}{4}(\bar{q}_{1R}\sigma_{\mu\nu}\lambda^a q_{1L})(\bar{q}_{2R}\sigma^{\mu\nu}\lambda^a q_{2L}) \right\} \left(m_3^0 \rho - \frac{4}{3}\pi^2\rho^3(\bar{q}_{3R}q_{3L}) \right) \\
& + \frac{9}{40}\left(\frac{4}{3}\pi^2\rho^3\right) d^{abc} (\bar{q}_{1R}\sigma_{\mu\nu}\lambda^a q_{1L}) (\bar{q}_{2R}\sigma^{\mu\nu}\lambda^b q_{2L}) (\bar{q}_{3R}\lambda^c q_{3L}) \\
& \left. + \text{cycl. perm. of (123)} \right] \qquad \text{(C.1)} \\
& + \frac{9}{256} i \left(\frac{4}{3}\pi^2\rho^3\right)^3 f^{abc} (\bar{q}_{1R}\sigma_\mu{}^\nu \lambda^a q_{1L}) (\bar{q}_{2R}\sigma_\nu{}^\tau \lambda^b q_{2L}) (\bar{q}_{3R}\sigma_\tau{}^\mu \lambda^c q_{3L}) \\
& + \frac{9}{320}\left(\frac{4}{3}\pi^2\rho^3\right)^3 d^{abc} (\bar{q}_{1R}\lambda^a q_{1L})(\bar{q}_{2R}\lambda^b q_{2L}) (\bar{q}_{3R}\lambda^c q_{3L}) \Bigg] \\
& + (R \leftrightarrow L) \Bigg\}
\end{aligned}$$

with $\sigma_{\mu\nu} := [\gamma_\mu, \gamma_\nu]/2$ and $q_{iL} := \frac{1}{2}(1+\gamma_5)q_i$, $q_{iR} := \frac{1}{2}(1-\gamma_5)q_i$ being the projections of the quark Dirac operators q_i onto left and right handed components. Furthermore $i = 1,2,3 = u,d,s$ denotes the flavor degrees of freedom, m_i^0 the corresponding current quark masses, λ^a $(a = 1,\ldots,8)$ are the color matrices and f^{abc}, d^{abc} are the standard $SU(3)$ structure constants defined by the commutator $[\lambda^a,\lambda^b]_- = 2i\, f^{abc}\lambda^c$ and the anticommutator $[\lambda^a,\lambda^b]_+ = \frac{4}{3}\delta^{ab} + 2\, d^{abc}\lambda^c$. For the other notations compare chapter 4.2.2. The 't Hooft interaction leads to spontaneous chiral symmetry breaking as can be seen by normal ordering $\mathcal{L} =$

$\mathcal{L}_0+\Delta\mathcal{L}$ with respect to the physical QCD vacuum, where $\mathcal{L}_0 = \sum_{j=1}^{3} (i\bar{q}_j\gamma^\mu\partial_\mu q_j - m_j^0\,\bar{q}q)$ is the free quark Lagrangian. Using the Wick theorem one finally obtains eq.(4.3), i.e.

$$\mathcal{L} = k + \sum_{j=1}^{3} :(i\bar{q}_j\gamma^\mu\partial_\mu q_j - m_j\,\bar{q}q): + \Delta\mathcal{L}(2) + \Delta\mathcal{L}(3) \tag{C.2}$$

with the different terms given in chapter 4.2.2. The two-body term $\Delta\mathcal{L}(2)$ will be investigated in more detail also in the following section.

C.2 The interaction between two quarks

After normal ordering the two body interaction term is given by

$$\begin{aligned}
\Delta\mathcal{L}(2) \;=\; & g_{\rm eff}(3)\Big\{ :(\bar{q}_{1R}q_{1L}\bar{q}_{2R}q_{2L}): \\
& + \frac{3}{32} :\Big[(\bar{q}_{1R}\lambda^a q_{1L})(\bar{q}_{2R}\lambda^a q_{2L}) \\
& - \frac{3}{4}(\bar{q}_{1R}\sigma_{\mu\nu}\lambda^a q_{1L})(\bar{q}_{2R}\sigma^{\mu\nu}\lambda^a q_{2L})\Big]: \\
& + (R \leftrightarrow L)\Big\} + \text{cycl. perm. of (123)}
\end{aligned} \tag{C.3}$$

with $g_{\rm eff}(i)$ given in eq.(4.8). One can transform the two body force into a more transparent form using the notation $\varepsilon_{ijk}, i = u,d,s$ with $\varepsilon_{uds} = 1$. Insert $q_{i\,L,R} = (1 \pm \gamma_5)/2\, q_i$ and use the relations

$$\sigma_{\mu\nu}\cdot\sigma^{\mu\nu} + \sigma_{\mu\nu}\gamma_5\cdot\sigma^{\mu\nu}\gamma_5 = -4\,\left(\Sigma^i\cdot\Sigma^i + \gamma_5\Sigma^i\cdot\gamma_5\Sigma^i\right) \tag{C.4}$$

with $\Sigma = diag(\sigma,\sigma)$ where the notation $(A\cdot B)_{ij,kl} = A_{ik}\,B_{jl}$ has been used. Furthermore

$$\begin{aligned}
\Sigma^k\cdot\Sigma^k &= 2\,\Pi^S - 1^S \\
\lambda^a\cdot\lambda^a &= 2\,\Pi^C - \frac{2}{3}1^C
\end{aligned} \tag{C.5}$$

with Π^S, Π^F and Π^C being exchange operators in spin, flavor and color defined as $\Pi_{ij,kl} = \delta_{il}\,\delta_{jk}$. On the antisymmetric tensors one has $\Pi^S\,\Pi^F\,\Pi^C = -1$ which can be used to eliminate the spin dependence leading to eq.(4.7), i.e.

$$\begin{aligned}
\Delta\mathcal{L}(2) = & -\frac{3}{16}\sum_i\sum_{kl}\sum_{mn} g_{\rm eff}(i)\,\varepsilon_{ikl}\varepsilon_{imn} \\
& \Big\{ :q_k^\dagger q_l^\dagger\,[\gamma_0\cdot\gamma_0 + \gamma_0\gamma_5\cdot\gamma_0\gamma_5]\,(2\mathcal{P}_{\bar{3}}^C + \mathcal{P}_6^C)\,q_m q_n : \Big\}
\end{aligned} \tag{C.6}$$

C.3 The 't Hooft vertex

The two-body 't Hooft interaction vertex in lowest order is determined by the first order term of the 4-point Green's function [12]

$$\mathcal{G}^{(4)}_{1\,2\,3\,4} = (-i) \int d^4y \left\langle 0 \left| T\, \Psi_1 \Psi_2 \bar{\Psi}_3 \bar{\Psi}_4 \left(-\Delta\mathcal{L}(2)(y)\right) \right| 0 \right\rangle \tag{C.7}$$

where the notation

$$\begin{aligned} \Psi_i &= [\Psi(x_i)]_{s_i,c_i,f_i} \quad \text{for } i = 1,2,3,4 \\ \Psi_i &= [\Psi(y)]_{s_i,c_i,f_i} \quad \text{for } i = 5,6,7,8 \end{aligned}$$

has been used (for $i \leq 4$ up to now). Here s_i denotes Dirac indices, c_i and f_i stand for color and flavor indices. We use the Wick theorem and the notation

$$\left\langle 0 \left| T\, \Psi_i \bar{\Psi}_j \right| 0 \right\rangle = -\left\langle 0 \left| T\, \bar{\Psi}_j \Psi_i \right| 0 \right\rangle = i\, S^F_{ij}$$

to obtain

$$\begin{aligned} &\left\langle 0 \left| T\, \Psi_1 \Psi_2 \bar{\Psi}_3 \bar{\Psi}_4 \,:\bar{\Psi}_5 \bar{\Psi}_6 \Psi_7 \Psi_8 : \right| 0 \right\rangle = \\ &= S^F_{15}\, S^F_{26}\, S^F_{73}\, S^F_{84} - S^F_{15}\, S^F_{26}\, S^F_{83}\, S^F_{74} \\ &- S^F_{16}\, S^F_{25}\, S^F_{73}\, S^F_{84} + S^F_{16}\, S^F_{25}\, S^F_{83}\, S^F_{74} \end{aligned}$$

Insert this equation into eq.(C.7) and rename the summation indices for the second term as $8 \leftrightarrow 7$, for the third term as $5 \leftrightarrow 6$ and for the fourth term as $5 \leftrightarrow 6,\ 8 \leftrightarrow 7$ to find

$$\begin{aligned} \mathcal{G}^{(4)}_{1\,2\,3\,4} &= (-i) \int d^4y \sum_{1,2} \sum_{3,4} S^F_{15}\, S^F_{26}\, S^F_{73}\, S^F_{84} \sum_{f_9} \frac{3}{16}\, g_{\text{eff}}(f_9) \cdot \\ &\cdot (\epsilon_{f_9 f_5 f_6}\, \epsilon_{f_9 f_7 f_8}\, A^D_{s_5 s_6, s_7 s_8}\, A^C_{c_5 c_6, c_7 c_8} + \\ &- \ (8 \leftrightarrow 7) - \ (5 \leftrightarrow 6) \ + \\ &+ \ (8 \leftrightarrow 7), (5 \leftrightarrow 6) \ ) \end{aligned} \tag{C.8}$$

with $A^D = 1 \otimes 1 + \gamma^5 \otimes \gamma^5$ and $A^C = P^C_6 + 2\, P^C_{\bar{3}}$. The matrix tensor products are of the general form $A_{5\,6,7\,8} = B_{5\,7}\, B_{6\,8}$ with matrices B. Therefore

$$\begin{aligned} A_{6\,5,7\,8} &= B_{6\,7}\, B_{5\,8} = B_{5\,8}\, B_{6\,7} = A_{5\,6,8\,7} \\ A_{6\,5,8\,7} &= B_{6\,8}\, B_{5\,7} = B_{5\,7}\, B_{6\,8} = A_{5\,6,7\,8} \end{aligned}$$

and we find that the fourth term in eq.(C.8) is equal to the first term and the same for the second and the third term. Let

$$G_{f_5 f_6, f_7 f_8} := \frac{3}{8} \sum_{f_9} g_{\text{eff}}(f_9)\, \epsilon_{f_9 f_5 f_6}\, \epsilon_{f_9 f_7 f_8}$$

to obtain

$$\mathcal{G}^{(4)}_{1\,2\,3\,4} = (-i) \int d^4y \sum_{1,2} \sum_{3,4} S^F_{15}\, S^F_{26}\, S^F_{73}\, S^F_{84} \tag{C.9}$$

$$\left[G_{f_5 f_6, f_7 f_8} \left(1_{s_5 s_7} 1_{s_6 s_8} + \gamma^5_{s_5 s_7} \gamma^5_{s_6 s_8} \right) \left(\frac{4}{3}\, 1_{c_5 c_7}\, 1_{c_6 c_8} - \frac{1}{4}\, \vec{\lambda}_{c_5 c_7} \vec{\lambda}_{c_6 c_8} \right) \; - \; (5 \leftrightarrow 6) \right]$$

Therefore the 't Hooft vertex is given by

$$(-i)\, G_{f_3 f_4, f_1 f_2} \left(1_{s_3 s_1} 1_{s_4 s_2} + \gamma^5_{s_3 s_1} \gamma^5_{s_4 s_2} \right) \left(\frac{4}{3} \left(1_{c_3 c_1}\, 1_{c_4 c_2} - \frac{1}{4}\, \vec{\lambda}_{c_3 c_1} \vec{\lambda}_{c_4 c_2} \right) \right. \tag{C.10}$$

(see also Fig.4.1). The two terms in eq.(C.9) represent the direct and the crossed diagram. For quarks and antiquarks one has to consider the 4-point function

$$\begin{aligned} (\mathcal{G}')^{(4)}_{1\,2\,3\,4} &= (-i) \int d^4y \left\langle 0 \left| T\, \Psi_1 \bar{\Psi}_2 \bar{\Psi}_3 \Psi_4 \left(-\mathcal{L}_{\rm tho}(y) \right) \right| 0 \right\rangle \\ &= -\mathcal{G}^{(4)}_{1\,4\,3\,2} \end{aligned}$$

i.e. the quark-antiquark diagramms are obtained from the quark-quark diagramms by exchanging $2 \leftrightarrow 4$ and by changing the sign appropriately (see Fig.4.2).

Appendix D

Calculation of the matrix elements

D.1 Expectation values

In order to compute the matrix elements present in eq.(2.58) it is useful to rewrite $\langle\psi|\psi\rangle$ and $\langle\psi|\mathcal{H}\psi\rangle$ in terms of Φ^{++} and Φ^{--} using eq.(2.14). We find

$$\langle\psi|\psi\rangle = \int \frac{2\,\omega_1\,\omega_2}{\omega_1\,m_2+\omega_2\,m_1}\,\mathrm{tr}\,\left((\Phi^{++})^\dagger\Phi^{++}-(\Phi^{--})^\dagger\Phi^{--}\right) \tag{D.1}$$

for the norm. The matrix elements of $\mathcal{H}$ can be split as

$$\langle\psi|\mathcal{H}\psi\rangle = \langle\psi|\mathcal{T}\psi\rangle+\langle\psi|\mathcal{V}\psi\rangle \tag{D.2}$$

$$\langle\psi|\mathcal{T}\psi\rangle = \int(\omega_1+\omega_2)\,\mathrm{tr}\left[\Phi^\dagger\,\Phi\right] \tag{D.3}$$

$$\langle\psi|\mathcal{V}\psi\rangle = -\int\!\!\int' \mathrm{tr}\left[\Phi^\dagger\,\gamma^0\,(V\Phi')\,\gamma^0\right] \tag{D.4}$$

with $\int = \int d^3p/(2\pi)^3$. The basic formula for the calculation of the kinetic energy and confinement matrix elements is given by

$$\begin{aligned}
&\mathrm{tr}\,(\Phi^\dagger\Phi') = \qquad\qquad (D.5)\\
&= \mathrm{tr}\ \ [(\Phi^{++})^\dagger(\Phi^{++})'+(\Phi^{--})^\dagger(\Phi^{--})'+\\
&\qquad +(\Phi^{+-})^\dagger(\Phi^{+-})'+(\Phi^{-+})^\dagger(\Phi^{-+})']=\\
&= \mathrm{tr}\ \ [(\Phi^{++})^\dagger(\Phi^{++})'+(\Phi^{--})^\dagger(\Phi^{--})'+\\
&\qquad +c_1c_1'\,(\Phi^{++})^\dagger(\Phi^{++})'s's-c_1c_2'\,(\Phi^{++})^\dagger\,s'(\Phi^{--})'s-\\
&\qquad -c_2c_1'\,(\Phi^{--})^\dagger\,s(\Phi^{++})'\,s'+c_2c_2'\,(\Phi^{--})^\dagger\,ss'(\Phi^{--})'+\\
&\qquad +c_1c_1'\,(\Phi^{--})^\dagger(\Phi^{--})'s's-c_1c_2'\,(\Phi^{--})^\dagger\,s'(\Phi^{++})'s-\\
&\qquad -c_2c_1'\,(\Phi^{++})^\dagger\,s(\Phi^{--})'\,s'+c_2c_2'\,(\Phi^{++})^\dagger\,ss'(\Phi^{++})']
\end{aligned}$$

where the prime indicates the dependence on $\vec{p}\,'$. To compute the kinetic energy term eq.(D.3) set $\vec{p}\,'=\vec{p}$ in this equation.

For the interaction term eq.(D.4) we investigate the following contributions:

D.1.1 Scalar confinement

From the scalar confining kernel eq.(4.2) one has

$$\langle\psi|\mathcal{V}_C^S\,\psi\rangle = -\int\!\!\int' \mathcal{V}_C\,\mathrm{tr}\,\left[\Phi^\dagger\,\gamma^0\,\Phi'\,\gamma^0\right] \tag{D.6}$$

with $\mathcal{V}_C = \mathcal{V}_C((\vec{p}-\vec{p}\,')^2)$. Since

$$\gamma^0\,\Phi\,\gamma^0 = \begin{pmatrix} \Phi^{+-} & -\Phi^{++} \\ -\Phi^{--} & \Phi^{-+} \end{pmatrix} \tag{D.7}$$

the expression for $\mathrm{tr}\,\left[\Phi^\dagger\,\gamma^0\,\Phi'\,\gamma^0\right]$ is obtained by changing the sign of the first two terms $(\Phi^{++})^\dagger(\Phi^{++})'$ and $(\Phi^{--})^\dagger(\Phi^{--})'$ in eq.(D.5).

D.1.2 Vector confinement

From the vector confining kernel eq.(4.1) one has

$$\langle\psi|\mathcal{V}_C^V\,\psi\rangle = \int\!\!\int' \mathcal{V}_C\,\mathrm{tr}\,\left[\Phi^\dagger\Phi'\right] \tag{D.8}$$

and eq.(D.5) can be applied directly. Note that a covariant form to write the vector confinement kernel is

$$\begin{aligned}[K(P,p,p')\,\chi(p')] = & \qquad (D.9)\\ = \quad & -\mathcal{V}_C((p_\perp - p'_\perp)^2)\,\frac{1}{P^2}\,P^\mu\gamma_\mu\,\chi(p')\,P^\nu\gamma_\nu\end{aligned}$$

with $p_\perp = p - (Pp)/P^2$, so that the relation

$$P^\mu\frac{d}{dP^\mu}\,[K(P,p,p')] = 0 \tag{D.10}$$

holds as is required to rewrite the normalization condition for Φ.

D.1.3 One Gluon Exchange

From the OGE-kernel in the Feynman gauge eq.(5.15) one has

$$\begin{aligned}\langle\psi|\mathcal{V}_G^F\,\psi\rangle \;&=\; \int\!\!\int' \mathcal{V}_G\,\mathrm{tr}\,\left[\Phi^\dagger\,\gamma^0\gamma^\mu\,\Phi'\,\gamma_\mu\gamma^0\,\right] \qquad (D.11)\\ &=\; \int\!\!\int' \mathcal{V}_G\,\mathrm{tr}\,\left[\Phi^\dagger\Phi'\right] - \int\!\!\int' \mathcal{V}_G\,\mathrm{tr}\,\left[\Phi^\dagger\,\gamma^0\vec{\gamma}\,\Phi'\,\vec{\gamma}\gamma^0\,\right]\end{aligned}$$

The first term has already been investigated in Sec.D.1.2. For the second term we calculate

$$
\begin{aligned}
&-\mathrm{tr}\,(\Phi^\dagger\,\gamma^0\vec{\gamma}\,\Phi'\,\vec{\gamma}\gamma^0) = \\
&\quad = \ \mathrm{tr}\ \ [\,(\Phi^{++})^\dagger\vec{\sigma}(\Phi^{++})'\vec{\sigma} + \\
&\qquad\quad +c_1c_2'\,(\Phi^{++})^\dagger\vec{\sigma}s'\,(\Phi^{++})'\,\vec{\sigma}s + c_2c_1'\,(\Phi^{--})^\dagger\,s\vec{\sigma}\,(\Phi^{--})'s'\vec{\sigma} \\
&\qquad\quad -c_1c_1'\,(\Phi^{++})^\dagger\,\vec{\sigma}\,(\Phi^{--})'\,s'\vec{\sigma}s - c_2c_2'\,(\Phi^{--})^\dagger\,s\vec{\sigma}s'\,(\Phi^{++})'\,\vec{\sigma} \\
&\qquad\quad +\ \ (\Phi^{++}\leftrightarrow\Phi^{--})\,]
\end{aligned}
\tag{D.12}
$$

In the Coulomb gauge (see eq.(5.5)) one has to replace $\gamma^\mu\otimes\gamma_\mu$ in eq.(D.11) by

$$
\gamma^0\otimes\gamma^0 - \frac{1}{2}\,[\,\vec{\gamma}\otimes\vec{\gamma} + (\vec{\gamma}\hat{x})\otimes(\vec{\gamma}\hat{x})\,]
$$

with $\hat{x} = \vec{x}/|\vec{x}|$ (we don't specify the operator $\hat{x}$ in momentum space since the corresponding matrix elements will be evaluated in coordinate space). The only new term to be considered here is the third one. Then $-\mathrm{tr}\,[\Phi^\dagger\,\gamma^0\,(\vec{\gamma}\hat{x})\,\Phi'\,(\vec{\gamma}\hat{x})\,\gamma^0]$ is obtained by replacing $\vec{\sigma}$ with $\vec{\sigma}\hat{x}$ in eq.(D.12).

D.1.4 't Hooft interaction

From the 't Hooft kernel eq.(4.24) we find (omitting flavor indices)

$$
\begin{aligned}
&\langle\psi|\mathcal{V}_T\,\psi\rangle = \\
&\quad = \ -4G\int\!\!\int'\,\mathrm{tr}\,\left[\Phi^\dagger\,\gamma^0\,\left(1_4\,\mathrm{tr}\,\Phi' + \gamma^5\,\mathrm{tr}\,(\Phi'\,\gamma^5)\right)\,\gamma^0\right] = \\
&\quad = \ -4G\int\!\!\int'\,\left[(\mathrm{tr}\,\Phi)^*\ (\mathrm{tr}\,\Phi') - \left(\mathrm{tr}\,\Phi\,\gamma^5\right)^*\,\left(\mathrm{tr}\,\Phi'\,\gamma^5\right)\right]
\end{aligned}
\tag{D.13}
$$

with

$$
\begin{aligned}
\mathrm{tr}\,\Phi &= \mathrm{tr}\,(\Phi^{+-} + \Phi^{-+}) \\
\mathrm{tr}\,(\Phi\gamma^5) &= \mathrm{tr}\,(\Phi^{++} + \Phi^{--})
\end{aligned}
\tag{D.14}
$$

Using the decomposition eq.(B.15) and $\mathrm{tr}\,\varphi_{S\,q} = \sqrt{2}\,\delta_{S\,0}$ one obtains

$$
\mathrm{tr}\,\Phi^{++}_{JM_J}(\vec{p}) = \sqrt{2}\,\mathcal{R}^{(+)}_{NJ0}(p)\,Y_{JM_J}(\Omega_p)\,\delta_{S\,0} \tag{D.15}
$$

$$
\mathrm{tr}\,\Phi^{--}_{JM_J}(\vec{p}) = \sqrt{2}\,\mathcal{R}^{(-)}_{NJ0}(p)\,Y_{JM_J}(\Omega_p)\,\delta_{S\,0} \tag{D.16}
$$

We further see that

$$
\mathrm{tr}\,(\varphi_{S\,q}\,\vec{\sigma}\vec{p}) = \mathrm{tr}\,(\vec{\sigma}\vec{p}\,\varphi_{S\,q}) = \sqrt{2}\,\delta_{S\,1}\,p_q \tag{D.17}
$$

with the spherical components $p_q = \sqrt{4\pi/3}\, p\, Y_{1\,q}(\Omega_p)$. We find

$$\int d\Omega_p \,\mathrm{tr}\,(\Phi\gamma^5) = \tag{D.18}$$
$$= \sqrt{2}\,\sqrt{4\pi}\,(\mathcal{R}^{(+)}_{NJ0}(p) + \mathcal{R}^{(-)}_{NJ0}(p))\,\delta_{S\,0}\,\delta_{L\,0}\,\delta_{J\,0}$$
$$\int d\Omega_p \,\mathrm{tr}\,\Phi = \tag{D.19}$$
$$= -\sqrt{2}\,\sqrt{4\pi}\,p\,(c_1+c_2)\,(\mathcal{R}^{(+)}_{NJ0}(p) - \mathcal{R}^{(-)}_{NJ0}(p))\,\delta_{S\,1}\,\delta_{L\,1}\,\delta_{J\,0}$$

D.2 Matrix elements

The expressions obtained above can now be used to compute the required matrix elements. In order to calculate e.g. $N^{++}_{ij} = \langle e^{(+)}_i | e^{(+)}_j \rangle$ one has to replace in eq.(D.1) $(\Phi^{++})^\dagger$ by $E^\dagger_i$ and Φ^{++} by E_j setting $(\Phi^{--})^\dagger = 0$ and $\Phi^{--} = 0$. In the following we will use the notation

$$(i|f(p)|j) = \int \frac{p^2\,dp}{(2\pi)^3}\, R_{n_i L_i}(p)\, R_{n_j L_j}(p)\, f(p) \tag{D.20}$$

for the radial integrals between the basis states. These integrals can be effectively computed numerically using e.g. Gauss quadrature routines. According to eq.(D.2) we write $H^{ss'}_{ij} = T^{ss'}_{ij} + V^{ss'}_{ij}$ with $V^{ss'}_{ij} = (V_C)^{ss'}_{ij} + (V_T)^{ss'}_{ij}$.

D.2.1 Normalization matrix elements

For the normalization matrix elements we find from eq.(D.1)

$$N^{++}_{ij} = -N^{--}_{ij} = \left(i \left| \frac{2\omega_1\omega_2}{\omega_1 m_2 + \omega_2 m_1} \right| j\right) \tag{D.21}$$
$$N^{+-}_{ij} = N^{-+}_{ij} = 0 \tag{D.22}$$

D.2.2 Kinetic energy matrix elements

In order to evaluate the angular momentum structure of matrix elements the relation $(-i\sigma_2)\,\vec{\sigma}\,(i\sigma_2) = -{}^t\vec{\sigma}$ is quite useful. Define the $q\bar{q}$ spin matrix as $\chi_{S\,q} = \varphi_{S\,q}\, i\sigma_2$ and use $s = \vec{\sigma}\vec{p}$. Then one can write e.g.

$$\mathrm{tr}\,(\varphi^\dagger_{S_i\,M_i}\, s\, \varphi_{S_j\,M_j}\, s)$$
$$= -\mathrm{tr}\,(\chi^\dagger_{S_i\,M_i}\,(s_1 \otimes s_2)\,\chi_{S_j\,M_j}) =$$
$$=: -\langle S_i M_i\,|s_1 \otimes s_2|\, S_j M_j\rangle \tag{D.23}$$

with $s_i = 2\vec{S}_i\vec{p}$ where $\vec{S}_1$ is the spin operator acting on the first quark and $\vec{S}_2$ on the second quark. It is useful to define

$$\begin{aligned} S_1(L',S',L,S,J) &:= \left\langle [L'\otimes S']^J \, |s_1/p| \, [L\otimes S]^J \right\rangle \\ S_2(L',S',L,S,J) &:= \left\langle [L'\otimes S']^J \, |s_2/p| \, [L\otimes S]^J \right\rangle \\ S_{12}(L',S',L,S,J) &:= \left\langle [L'\otimes S']^J \, \left|(s_1\otimes s_2)/p^2\right| \, [L\otimes S]^J \right\rangle \end{aligned} \tag{D.24}$$

Using the Wigner-Eckart theorem and the notation $\hat{L} = \sqrt{2L+1}$ one has

$$\begin{aligned} &S_1(L',S',L,S,J) = (-1)^{S+S'}\, S_2(L',S',L,S,J) = \\ &= (-1)^{L'+1}\, \hat{J}\hat{L}'\hat{L}\hat{S}'\hat{S}\,\sqrt{9}\sqrt{12} \begin{pmatrix} L' & 1 & L \\ 0 & 0 & 0 \end{pmatrix} \\ &\quad \cdot \begin{Bmatrix} L' & S' & J \\ L & S & J \\ 1 & 1 & 0 \end{Bmatrix} \begin{Bmatrix} 1/2 & 1/2 & S' \\ 1/2 & 1/2 & S \\ 1 & 0 & 1 \end{Bmatrix} \end{aligned} \tag{D.25}$$

$$\begin{aligned} &S_{12}(L',S',L,S,J) = \\ &= \sum_{L_k\, S_k} S_1(L',S',L_k,S_k,J)\; S_2(L_k,S_k,L,S,J) \end{aligned} \tag{D.26}$$

The kinetic energy matrix elements are now given by

$$\begin{aligned} T_{ij}^{++} &= T_{ij}^{--} = \\ &= (i|(\omega_1+\omega_2)\,(1+p^2(c_1^2+c_2^2))\,|j)\,\delta_{L_iL_j}\,\delta_{S_iS_j} \\ T_{ij}^{+-} &= T_{ij}^{-+} = \\ &= (i|(\omega_1+\omega_2)\,2\,p^2\,c_1\,c_2|j)\,S_{12}(i,j) \end{aligned} \tag{D.27}$$

with $S_{12}(i,j) = S_{12}(L_i,S_i,L_j,S_j,J)$.

D.2.3 Scalar and vector confinement matrix elements

The confinement matrix elements can be computed by inserting two complete sets of basis functions like

$$\begin{aligned} &\langle i|f_1(\vec{p})\,V(r)\,f_2(\vec{p}\,')|j\rangle = \\ &= \sum_{g,h} \langle i|f_1(\vec{p})|g\rangle\,\langle g|V(r)|h\rangle\,\langle h|f_2(\vec{p}\,')|j\rangle \end{aligned} \tag{D.28}$$

where the matrix element of V can be evaluated in coordinate space. One finds for the scalar confinement matrix elements

$$\begin{aligned} (V_C^S)_{ij}^{++} = (V_C^S)_{ij}^{--} &= (i|\mathcal{V}_C|j) - \sum_{g,h}\delta_{L_gL_h}\,\delta_{S_gS_h} \\ &\Big\{ (i|pc_1|g)\,S_2(i,g)\;(g|\mathcal{V}_C|h)\;(h|pc_1|j)\,S_2(h,j) \\ &+(i|pc_2|g)\,S_1(i,g)\;(g|\mathcal{V}_C|h)\;(h|pc_2|j)\,S_1(h,j)\;\Big\} \end{aligned} \tag{D.29}$$

and

$$(V_C^S)_{ij}^{+-} = (V_C^S)_{ij}^{-+} = -\sum_{g,h} \delta_{L_g L_h}\, \delta_{S_g S_h} \tag{D.30}$$
$$\Big\{ (i|pc_1|g)\, S_2(i,g)\, (g|\mathcal{V}_C|h)\, (h|pc_2|j)\, S_1(h,j)$$
$$+(i|pc_2|g)\, S_1(i,g)\, (g|\mathcal{V}_C|h)\, (h|pc_1|j)\, S_2(h,j) \Big\}$$

with $(g|\mathcal{V}_C|h) = \int r^2\, dr\, R^F_{n_i L_i}(r)\, R^F_{n_j L_j}(r)\, \mathcal{V}_C^F(r)$ where R^F denotes the Fourier transformed basis functions and $\mathcal{V}_C^F(r) = a_c + b_c r$.

For the vector confinement matrix elements one only has to change the sign of $\sum_{g,h}$ in the two equations above.

D.2.4 OGE matrix elements

Analogously to the confinement matrix elements one can evaluate the OGE matrix elements by inserting complete sets of basis functions. One finds for the $\vec{\gamma} \otimes \vec{\gamma}$ -term

$$(V_G^{\vec{\gamma}})_{ij}^{++} = (V_G^{\vec{\gamma}})_{ij}^{--} = \sum_{g,h} \delta_{L_g L_h}\, \delta_{S_g S_h} \tag{D.31}$$
$$\Big\{ (i|pc_1|g)\, S_2(i,g)\, (g|\mathcal{V}_G|h)\, (2S_g(S_g+1)-3)\, (h|pc_2|j)\, S_1(h,j)$$
$$+(i|pc_2|g)\, S_1(i,g)\, (g|\mathcal{V}_G|h)\, (2S_g(S_g+1)-3)\, (h|pc_1|j)\, S_2(h,j) \Big\}$$

and

$$(V_G^{\vec{\gamma}})_{ij}^{+-} = (V_G^{\vec{\gamma}})_{ij}^{-+} = \tag{D.32}$$
$$= -(i|\mathcal{V}_G|j)\, (2S_i(S_i+1)-3)\, \delta_{L_i L_j}\, \delta_{S_i S_j} + \sum_{g,h} \delta_{L_g L_h}\, \delta_{S_g S_h}$$
$$\Big\{ (i|pc_1|g)\, S_2(i,g)\, (g|\mathcal{V}_G|h)\, (2S_g(S_g+1)-3)\, (h|pc_1|j)\, S_2(h,j)$$
$$+(i|pc_2|g)\, S_1(i,g)\, (g|\mathcal{V}_G|h)\, (2S_g(S_g+1)-3)\, (h|pc_2|j)\, S_1(h,j) \Big\}$$

with $(g|\mathcal{V}_G|h) = \int r^2\, dr\, R^F_{n_i L_i}(r)\, R^F_{n_j L_j}(r)\, \mathcal{V}_G^F(r)$ where (up to the regularization) $\mathcal{V}_G^F(r) = -4/3\, \alpha_s(r)/r$. For the $\vec{\gamma}\hat{x}$ -terms $(V_G^{\vec{\gamma}\hat{x}})_{ij}^{\pm\pm}$ one only has to replace the factors $(2S_g(S_g+1)-3)\, \delta_{L_g L_h}\, \delta_{S_g S_h}$ by $S_{12}(g,h)$ and the same for the index pair (i,j). With the terms given above we find for the OGE matrix elements in the Feynman and the Coulomb gauge

$$(V_G^F)_{ij}^{\pm\pm} = (V_G^{\gamma^0})_{ij}^{\pm\pm} + (V_G^{\vec{\gamma}})_{ij}^{\pm\pm} \tag{D.33}$$
$$(V_G^C)_{ij}^{\pm\pm} = (V_G^{\gamma^0})_{ij}^{\pm\pm} + \frac{1}{2}\left[(V_G^{\vec{\gamma}})_{ij}^{\pm\pm} + (V_G^{\vec{\gamma}\hat{x}})_{ij}^{\pm\pm}\right] \tag{D.34}$$

where $(V_G^{\gamma^0})_{ij}^{\pm\pm}$ is of the same form as the vector confinement matrix elements.

D.2.5 't Hooft matrix elements

The 't Hooft matrix elements with the regularizing potential can be computed analogously to the confinement matrix elements. In the unregularized case $\Lambda \to 0$ corresponding to $\mathcal{V}^F_{\rm reg}(r) \to \delta(\vec{r})$ only $L = 0$ basis states contribute to $(g|\mathcal{V}_{\rm reg}|h)$. Consistently only $L = 0$ states will be taken into account for $(g|\mathcal{V}_{\rm reg}|h)$ also for $\Lambda > 0$ so that the angular selection rules are not changed by the regularization. The result for $L = S = 0$ reads

$$\begin{aligned}(V_T^{++})_{ij}^{S=0} &= (V_T^{--})_{ij}^{S=0} = (V_T^{+-})_{ij}^{S=0} = (V_T^{-+})_{ij}^{S=0} \\ &= 8G\,(i|\mathcal{V}_{\rm reg}|j)\;\delta_{S_i\,0}\,\delta_{S_j\,0}\,\delta_{L_i\,0}\,\delta_{L_j\,0}\,\delta_{J\,0}\end{aligned} \tag{D.35}$$

and for $L = S = 1$

$$\begin{aligned}(V_T^{++})_{ij}^{S=1} &= (V_T^{--})_{ij}^{S=1} = -(V_T^{+-})_{ij}^{S=1} = -(V_T^{-+})_{ij}^{S=1} \\ &= -8G \sum_{g,h} (i|p\,(c_1+c_2)|g)\,(g|\mathcal{V}_{\rm reg}|h)(h|p\,(c_1+c_2)|j) \\ &\quad \delta_{S_i\,1}\,\delta_{S_j\,1}\,\delta_{L_i\,1}\,\delta_{L_j\,1}\,\delta_{J\,0}\end{aligned} \tag{D.36}$$

This result shows that the 't Hooft interactions affects only mesons with $J = 0$ and $L = S = 0$ (i.e. pseudoscalar mesons with $J^{\pi_P} = 0^-$) or $L = S = 1$ (i.e. scalar mesons with $J^{\pi_P} = 0^+$). In the nonrelativistic limit the contributions to the scalar mesons vanish.

Appendix E

The OGE potential for small distances

In this section we will analytically perform the Fourier transformation of the OGE kernel into coordinate space for $r \ll \Lambda_{QCD}^{-1}$ as given by

$$\begin{aligned} \mathcal{V}_G^F(r) &= \frac{1}{2\pi^2 r} \int_{|\vec{q}_{low}|}^{|\vec{q}_{high}|} |\vec{q}|\, d|\vec{q}|\, \sin(|\vec{q}|r)\, 4\pi\, \frac{4}{3}\, \frac{1}{\vec{q}^2} \\ &\cdot \frac{A}{\ln(\vec{q}^2/\Lambda_{QCD}^2)} \left(1 - B\, \frac{\ln\left(\ln(\vec{q}^2/\Lambda_{QCD}^2)\right)}{\ln(\vec{q}^2/\Lambda_{QCD}^2)}\right) \end{aligned} \tag{E.1}$$

The cutoff $|\vec{q}_{low}| \gg \Lambda_{QCD}$ has been introduced to keep the variable $|\vec{q}|$ in the high momentum range where the QCD formula for the running coupling constant is approximately valid. The other cutoff $|\vec{q}_{high}|$ has been introduced for formal reasons as shown below. It is chosen according to the condition $|\vec{q}_{high}|\, r \ll 1/(\Lambda_{QCD}\, r)$. We mainly follow the way outlined by Lucha et.al. [32] who treated the first order case, i.e. $B = 0$. Using $x = |\vec{q}|\, r$ and $a = \Lambda_{QCD}\, r \ll 1$ we can write

$$\mathcal{V}_G^F(r) = \frac{4}{3r}\, \frac{2\,A}{\pi} \int_{x_{low}}^{x_{high}} dx\, \frac{\sin(x)}{x}\, \frac{1}{\ln(x/a)^2} \left(1 - B\, \frac{\ln\left(\ln(x/a)^2\right)}{\ln(x/a)^2}\right) \tag{E.2}$$

with $x_{low} = |\vec{q}_{low}|\, r \gg a$ and $x_{high} = |\vec{q}_{high}|\, r \ll 1/a$. Rewrite

$$\frac{1}{\ln(x/a)^2} = \frac{1}{2\,(\ln x - \ln a)} = \frac{1}{2\ln a\,(\ln x/\ln a - 1)} =: (*) \tag{E.3}$$

Since $x \geq x_{low} \gg a$ and $x < x_{high} \ll 1/a$ we have $|\ln x/\ln a| \ll 1$ so that

$$(*) \approx \frac{(-1)}{2\ln a} \left(1 + \frac{\ln x}{\ln a}\right) \tag{E.4}$$

For the $\ln\ln$ -term we further use

$$\ln\left(\ln(x/a)^2\right) = \ln\left(2\ln x - 2\ln a\right) \approx \ln(-2\ln a) - \ln x/\ln a \tag{E.5}$$

so that we can write

$$\begin{aligned}\mathcal{V}_G^F(r) &= \frac{4}{3r}\,\frac{2\,A}{\pi}\int_{x_{low}}^{x_{high}} dx\,\frac{\sin(x)}{x}\,\frac{(-1)}{2\ln a}\left(1+\frac{\ln x}{\ln a}\right)\\ &\cdot\ \left(1-B\,\frac{(-1)}{2\ln a}\left(1+\frac{\ln x}{\ln a}\right)\left(\ln(-2\ln a)-\frac{ln x}{\ln a}\right)\right)\end{aligned}\tag{E.6}$$

It is a good approximation to neglect terms $\sim(\ln x/\ln a)^2$ in the following, so that

$$\begin{aligned}\mathcal{V}_G^F(r) &= \frac{4}{3r}\,\frac{2\,A}{\pi}\,\frac{(-1)}{2\ln a}\int_{x_{low}}^{x_{high}} dx\,\frac{\sin(x)}{x}\left[1+\frac{\ln x}{\ln a}\right.\\ &\left.+\left(1+2\,\frac{\ln x}{\ln a}\right)\,B\,\frac{\ln(-2\ln a)}{2\ln a}-\frac{\ln x}{\ln a}\,\frac{B}{2\ln a}\right]\end{aligned}\tag{E.7}$$

In the limit $r\to 0$ one has $a\to 0$, so that the limits $x_{low}\to 0$ and $x_{high}\to\infty$ can be performed. Using the integrals

$$\int_0^\infty dx\,\frac{\sin x}{x}=\frac{\pi}{2}\ ;\quad \int_0^\infty dx\,\frac{\sin x}{x}\,\ln x=-\frac{\pi}{2}\,\gamma\tag{E.8}$$

with the Euler-Mascheroni constant $\gamma=0.577215\ldots$ and using

$$\frac{1}{\ln a}\left(1-\frac{\gamma}{\ln a}\right)\approx\frac{1}{\ln a\,(1+\gamma/\ln a)}=\frac{1}{\ln a+\gamma}=\frac{1}{\ln(e^\gamma\,a)}\tag{E.9}$$

we find

$$\begin{aligned}\mathcal{V}_G^F(r) &\approx \frac{4}{3r}\left[\frac{-A}{2\ln(e^\gamma\,a)}\left(1+B\,\frac{\ln(-2\ln a)}{2\ln a}\right)\right.\\ &\left.+\frac{\gamma\,A\,B}{4\,(\ln a)^3}\left(\ln(-2\ln a)-\frac{1}{\ln a}\right)\right]\end{aligned}\tag{E.10}$$

The term $\sim 1/(\ln a)^3$ can be neglected to a good approximation and we finally obtain eq.(5.12), i.e.

$$\mathcal{V}_G^F(r)\ \approx\ \frac{4}{3}\,\frac{\alpha_s^{run}(r)}{r}\quad\text{for}\ \ r\ll\Lambda_{QCD}^{-1}\quad\text{with}\tag{E.11}$$

$$\alpha_s^{run}(r)\ =\ \frac{A}{2\,\ln(e^{-\gamma}/a)}\left[1-B\,\frac{\ln\left(2\,\ln(1/a)\right)}{2\,\ln(1/a)}\right]\quad\text{with}\ \ a=\Lambda_{QCD}\,r\tag{E.12}$$

Bibliography

[1] S.L.Adler: Phys.Rev. 177,2426 (1969)
J.S.Bell,R.Jackiv: Nuovo Cimento 60A, 47 (1969)

[2] T.A.Armstrong et.al., Phys.Rev.Lett. 69, 2337 (1992)

[3] R.M.Baltrusaitis et al.: Phys.Rev. D32, 2883 (1985)

[4] R.Barbieri, R.Gatto, R.Kögerler, Z.Kunszt, Phys.Lett. 57B, 455 (1975)

[5] M.Beyer, U.Bohn, M.G.Huber, B.C.Metsch, J.Resag: Z.Phys.C-Particles and Fields 55, 307 (1992)

[6] S.N.Biwas, S.R.Choudhury, K.Datta, A.Goyal: Phys.Rev. D26, 1983 (1982)

[7] R.Blankenbecler, R.Sugar, Phys.Rev. 142, 1051 (1966);
A.A.Logunov, A.N.Tavkhelidze, Nuovo Cim. 29, 380 (1963)

[8] W.H.Blask, U.Bohn, M.G.Huber, B.C.Metsch, H.R.Petry: Z.Phys.A 337, 327 (1990)

[9] M.Böhm, Nucl.Phys. B91, 494 (1975)

[10] U.Bohn, Diploma Thesis, Bonn TK-89-08 (unpublished)

[11] B.E.Chi, Nucl.Phys. A146, 449 (1970)

[12] Ta-Pei Cheng, Ling-Fong Li, Gauge theory of elementary particle physics (Oxford University Press, 1984)

[13] R.E.Cutkosky, Phys.Rev. Vol.96, 1135 (1954)

[14] R.E.Cutkosky, M.Leon, Phys.Rev. 135 B, 1445 (1964)

[15] A.L.Fetter, J.D.Walecka, Quantum Theory of Many Particle Systems (McGraw-Hill, New York, 1971)

[16] M.Fuchs, PhD thesis, Univ.Bonn (1993), TK-93-06

[17] A.Gara, B.Durand, L.Durand, L.J.Nickisch: Phys.Rev. D40, 843 (1989)
A.Gara, B.Durand, L.Durand: Phys.Rev. D42, 1651 (1990)

[18] M.Gell-Mann, F.Low: Phys.Rev. 84, 350 (1951)

[19] S.Godfrey, N.Isgur: Phys.Rev. D32, 189 (1985)

[20] D.Gromes: Z.Phys.C-Particles and Fields 26, 401 (1984)

[21] F.Gross, J.Milana, CEBAF preprint (1990), CEBAF-TH-90-09

[22] S.N.Gupta, J.M.Johnson, W.W.Repko, C.J.Suchyta, hep-ph/9312205 (1993)

[23] G.Hardekopf, J.Sucher, Phys.Rev. D33, 2035 (1986)

[24] G.'t Hooft: Phys.Rev. D14, 3432 (1976)

[25] C.Itzykson, J.-B.Zuber: Quantum Field Theory (McGraw-Hill, New York 1985)

[26] Yu.L.Kalinowski, C.Weiss, preprint Univ. Tübingen, UNITUE-THEP-17/93, hep-ph/9402236

[27] S.Klimt et.al., Nucl.Phys. A516, 429 (1990)

[28] W.Kwong, J.L.Rosner, C.Quigg: Ann.Rev.Nucl.Part.Sci. 37, 325 (1987)

[29] J.F.Lagaë: Phys.Rev. D45, 305, 317 (1992)

[30] C.H. Llewellyn Smith, Nuovo Cim. 60A, 348 (1969)

[31] C.H. Llewellyn Smith, Ann.Phys. 53, 521 (1969)

[32] W.Lucha, F.F.Schöberl, D.Gromes: Phys.Rep. 200, No.4, 127 (1991)

[33] D.Lurie: Particles and Fields, (Interscience Publishers, New York 1968)

[34] R.Machleidt, K.Holinde, Ch.Elster, Phys.Rep. 149 No.1, 1 (1987)

[35] S.Mandelstam, Proc. Roy. Soc. 233, 248 (1955)

[36] A.N.Mitra, A.Pagnamenta, N.N.Singh, Phys.Rev.Lett. 59, 2408 (1987)

[37] C.R.Münz, PhD thesis, Univ. Bonn (1994)

[38] C.R.Münz, J.Resag, B.C.Metsch, H.R.Petry, Bonn TK-93-14, Nucl.Phys. A (in print)

[39] V.D.Mur, V.S.Popov, Yu.A.Simonov, V.P.Yurow, preprint ITEP 83-92, hep-ph/9401203

[40] T.Murota, Progr.Theor.Phys. 69, 181 (1983), ibid. 1498

[41] O.Nachtmann: Elementarteilchenphysik Phänomene und Konzepte, (Vieweg, Braunschweig 1986)

[42] N.Nakanishi: Suppl.Theor.Phys., No.43, 1 (1969)

[43] N.Nakanishi: Progr.Theor.Phys., Suppl. No.95, 1 (1988)

[44] Y.Nambu, G.Jona-Lasinio: Phys.Rev. 122, 345 (1961)

[45] M.Neubert, SLAC-PUB-6263, June 1993

[46] K.Nishijima, Prog.Theor.Phys. 10, 549 (1953); 12, 279 (1954); 13, 305 (1955)

[47] Particle Data Group, Phys.Rev. D45 Part II (1992)

[48] J.Parramore, J.Piekarewicz, preprint of the Florida State University 1994, FSU-SCRI-94-15, nucl-th/9402019

[49] H.R.Petry et.al., Phys.Lett 159B, 363 (1985)

[50] J.Piekarewicz, Revista Mexicana de Física 39, No.4, (1993) 542

[51] L.J.Reinders, H.Rubinstein, S.Yazaki: Phys.Rep.Vol.127, 1 (1985)

[52] S.Resag, M.Beyer, Bonn TK-93-18, hep-ph/9312298, Z.Phys. C (1994), in print

[53] J.Resag, Diploma Thesis, Bonn TK-91-04 (unpublished)

[54] J.Resag, C.R.Münz, B.C.Metsch, H.R.Petry, Bonn TK-93-13, Nucl.Phys. A (in print)

[55] J.Resag, D.Schütte, nucl-th/9312013, Bonn TK-93-19

[56] P.Ring, P.Schuck: The Nuclear Many-Body Problem, Berlin: Springer-Verlag 1980

[57] R.van Royen, V.F.Weisskopf: Nuov.Cim. 50,2 A, 617 (1967)

[58] E.E.Salpeter, H.A.Bethe: Phys.Rev. 84, 132 (1951)

[59] J.L.Rosner, Phys.Rev. D27 1101 (1983)

[60] J.L.Rosner, Phys.Rev. D42 3732 (1990)

[61] E.E.Salpeter, Phys.Rev. 87, 328 (1952)

[62] M.A.Shifman, A.I.Vainshtein, V.I.Zakharov: Nucl.Phys. B163, 46 (1980)

[63] E.V.Shuryak: Nucl.Phys. B203, 93 (1982)

[64] B.Silvestre-Brac, C.Gignoux: Preprint, Institut des Sciences Nucléaires, Grenoble 1989

[65] D.J.Thouless, Nucl.Phys. 21, 225 (1960), Nucl.Phys. 22, 78 (1961)

[66] P.C.Tiemeijer, J.A.Tjon: Phys.Lett. B277, 38 (1992); Utrecht preprint THU-92/31 (1992); Utrecht preprint THU-93/12 (1993)

[67] N.Ullah, D.J.Rowe, Nucl.Phys. A163, 257 (1971)

[68] S.J.Wallace, V.B.Mandelzweig, Nucl.Phys. A503, 673(1989)

[69] Progress in particle and nuclear physics, Vol.27, editor: A.Faessler, pergamom press 1991, chapter 4 by U.Vogl, W.Weise, 195

[70] G.C.Wick, Phys.Rev. Vol.96, 1124 (1954)

[71] A.Le Yaouanc, L.Oliver, S.Ono, O.Pene, J.C.Raynal, Phys.Rev. D31, 137 (1985)